Improving Network Reductions for Power System Analysis

by

Yujia Zhu

A Dissertation Presented in Partial Fulfillment
of the Requirements for the Degree
Doctor of Philosophy

Approved January 2017 by the
Graduate Supervisory Committee:

Daniel Tylavsky, Chair
Kory Hedman
Vijay Vittal
Raja Ayyanar

ARIZONA STATE UNIVERSITY

May 2017

ABSTRACT

The power system is the largest man-made physical network in the world. Performing analysis of a large bulk system is computationally complex, especially when the study involves engineering, economic and environmental considerations. For instance, running a unit-commitment (UC) over a large system involves a huge number of constraints and integer variables. One way to reduce the computational expense is to perform the analysis on a small equivalent (reduced) model instead on the original (full) model.

The research reported here focuses on improving the network reduction methods so that the calculated results obtained from the reduced model better approximate the performance of the original model. An optimization-based Ward reduction (OP-Ward) and two new generator placement methods in network reduction are introduced and numerical test results on large systems provide proof of concept.

In addition to dc-type reductions (ignoring reactive power, resistance elements in the network, etc.), the new methods applicable to ac domain are introduced. For conventional reduction methods (Ward-type methods, REI-type methods), eliminating external generator buses (PV buses) is a tough problem, because it is difficult to accurately approximate the external reactive support in the reduced model. Recently, the holomorphic embedding (HE) based load-flow method (HELM) was proposed, which theoretically guarantees convergence given that the power flow equations are structure in accordance with Stahl's theory requirements. In this work, a holomorphic embedding based network reduction (HE reduction) method is proposed which takes advantage of the HELM technique. Test results shows that the HE reduction method can approximate the original system performance very accurately even when the operating condition changes.

TABLE OF CONTENTS

LIST OF FIGURES

ix

LIST OF TABLES

NOMENCLATURE

| | |
|---|---|
| $B_{bus}$, $B_{branch}$ | Bus and branch admittance matrix including variables of equivalent line admittance |
| $B_j, j \in J$ | Line admittance of branch $j$ |
| $b_i$ | The partial column in the branch susceptance matrix corresponding to the $i$th retained bus and retained branches |
| $C_f$, $C_r$ | Node-branch incidence matrix of the full and reduced model |
| $D_z$ | Set of the coefficients of the terms whose combined degrees of $\alpha$ and $\beta$ is $z$ ($m+n=z$) |
| $E_i(\alpha), E_{i,r}(\alpha),$ | Voltage power series of the germ solution of the full and reduced models |
| $E_i[n]$, $E_{i,r}[n]$ | Complex-valued coefficient of the $n$th term in the power series $E_i(\alpha)$ and $E_{i,r}(\alpha)$ |
| $F_i(\alpha), F_{i,r}(\alpha)$ | Reciprocal power series of $E_i(\alpha)$ of the full and reduced models |
| $F_i[n]$, $F_{i,r}[n]$ | Complex-valued coefficient of the $n$th term in the power series $F_i(\alpha)$ and $F_{i,r}(\alpha)$ |
| $G$ | Set of generator indices |
| $G_E, G_I$ ($G = G_I \cup G_E$) | Set of external and internal generator indices |
| $I_e(\alpha)$ | Power series of the current injected at bus $e$ |
| $I_a^{ex}(\alpha)$ | Power series of external current injection of bus $a$ |
| $J, J_{reduced}$ | Set of branch indices in the full and reduced model |
| $J_r$ | Set of indices of the retained congested branches, $J_r \subseteq J$ |
| $K$ | Set of all buses in the full model |

| | |
|---|---|
| $K_E, K_I$ | Set of external and retained buses |
| $K_B$ | Set of boundary bus indices, $I_B \subseteq I_I$ |
| $K_{Bi}, i \in K_E, K_{Bi} \in K_B,$ | Set of boundary bus indices adjacent to external bus $i$ |
| $K_{pv}, K_{pq}$ | Set of all PV buses and set of all PQ buses |
| $L_r, U_r$ | Partially factored lower and upper triangular matrices of $Y_{bus}$ |
| $\hat{l}_{ij}$ | Splitting factor which defines the size of the proportion of injected power of external bus $j$ split to the boundary bus $i$ |
| $P_i^g, g \in G_I, i \in K_I$ | MW Generation of generator $g$ on bus $i$ |
| $P_{i_e,i}^{g_e}, g_e \in G_E, i_e \in K_E, i \in K_I$ | MW Generation of external generator $g_e$ moved from external bus $i_e$ to retained bus $i$ |
| $P_i^l, i \in K_I$ | MW Load on retained bus $i$ |
| $P_{i_e,i}^l, i_e \in K_E, i \in K_I$ | MW Load on external bus $i_e$ moved to retained bus $i$ |
| $P_j^f, j \in J$ | MW Line flow on branch $j$ |
| $P_{j_r}^f, j_r \in J_r$ | MW Line flow on branch $j_r$ |
| $P_{inj_i}, i \in K$ | Power injection at bus $i$ |
| $P_{inj_{ik}}, i \in K_E, k \in K_B$ | Fractional power injection of external bus $i$ distributed to bus $k$ during Ward reduction |
| $P_{inj_i}, i \in K$ | Vector of power injection with all elements equal to zero except the $i$th element equal to power injection at bus $i$ |
| $P_{inj_{ik}}, i \in K_E, k \in K_B$ | Vector of power injection with all elements equal to zero except the $k$th element equals to fractional power injection split from bus $i$ to bus $k$ ($= P_{inj_{ik}}$) |

| | |
|---|---|
| $P_{full,i}^{f}, P_{reduced,i}^{f}, i \in K$ | Vector of branch flow with the only non-zero power injection at bus $i$ |
| $V_i(\alpha), V_{i,r}(\alpha)$ | Power series of bus $i$ voltage of the full and reduced model |
| $Q_i^{g}(\alpha)$ | Power series of the reactive power generation of bus $i$ |
| $Q_i^{g}[n]$ | Coefficient of the $n$th term in the power series $Q_i^{g}(\alpha)$ |
| $S_a^{ex}(\alpha)$ | Power series of external power injection of bus $a$ |
| $V_i[n], V_{i,r}[n]$ | Complex-valued coefficient of the $n$th term in the power series $V_i(\alpha)$ and $V_{i,r}(\alpha)$ |
| $V_{slack}$ | Slack bus voltage |
| $V_k(\alpha, \beta)$ | Bivariate voltage power series of bus $k$ |
| $V[m,n]$ | Coefficient of the term $\alpha^m \beta^n$ |
| $|V_i^{sp}|$ | The specified voltage magnitude of a PV bus $i$ |
| $W_k(\alpha, \beta)$ | Reciprocal of power series $V_k(\alpha, \beta)$ |
| $W_i(\alpha), W_{i,r}(\alpha)$ | Reciprocal of the voltage power series of bus $i$ of the full and reduced model |
| $W_i[n], W_{i,r}[n]$ | Complex-valued coefficient of the $n$th term in the power series $W_i(\alpha)$ and $W_{i,r}(\alpha)$ |
| $x_{i_e,i}, i_e \in K_E, i \in K_I$ | Binary variable indicates if load on external bus $i_e$ is moved to retained bus $i$ |
| $x_{g_e,i}, g_e \in G_E, i \in K_I$ | Binary variable indicates if generator $g_e$ to retained bus $k$ |
| $Y_{bus}, Y_{bus}^{reduced}$ | Bus admittance matrices of the full and reduced model |
| $\alpha_1, \alpha_2$ | Type 1 and Type 2 equivalent $\alpha$ |
| $\theta_i, i \in K_I$ | Bus voltage angle (deg) of retained bus $i$ |

$\Phi_{full}, \Phi_{reduced}$   Full and reduced-model PTDF matrices

$\Phi_{i,j}^{i_{ref}}, i, i_{ref} \in K_I, j \in J$   Element in the PTDF matrix correspond to bus $i$ and branch $j$ with reference bus $i_{ref}$

$\Psi$   Set of all equivalent branches to be eliminated from the reduced model in the OP-Ward reduction

# 1  INTRODUCTION

## 1.1  Overview

Power system planning and operation on a large network is a complicated engineering problem. Recently, the growing concerns about economics and the environment have made the problem interdisciplinary and more complicated. For example, the Engineering, Economic, and Environmental Electricity Simulation Tool (E4ST) group of Cornell is focusing on the power system planning problem which not only considers the grid reliability but also pricing of the energy and emission of the NOx and SOx gases. Such problems, are complex to solve for a large-scale bulk system and require exponentially increasing large amounts of memory and computation time. Thus there exist the need to reduce the computational burden.

Two main paths to reducing the computational burden are to 1) generate small equivalent networks to replace the original large networks (network reduction) and 2) simplify the problem by making assumptions or improving the algorithms. The first path is the focus of the dissertation. The second path is also a subject of ongoing research but is beyond the scope of this work. One of the most popular approaches of the second path is the dc approximation to the ac problem which simplifies the complex nonlinear power flow problem to a linear problem.

## 1.2  Literature Review

Network reduction methods are widely used in different studies. In this work, we focus on the reduction methods used in static analysis. Three major categories of network

reduction methods have been historically used: 1) the Ward-type methods, 2) the REI-type methods and 3) the PTDF-based methods.

The Ward reduction was first proposed by J.B. Ward [1]. A Ward-type reduced network is generated by performing partial matrix factorization. During partial matrix factorization, the external buses are eliminated by Gauss elimination [2]. The equivalent model thus produced is often very dense and with high impedance branches. This is because the non-zero fills in the factorized matrix create fictitious (or equivalent) branches in the reduced model and the value of the fills are equal to the branch admittances. Some of the fills have extremely small values, which implies that the corresponding equivalent branches have extremely high impedances. These high-impedance branches can be discarded with minimal impact on accuracy in order to reduce the density of the equivalent model proved the impedance threshold selected is sufficiently high. When PV buses are eliminated from the model, the predictions of the Ward equivalent may deviate far from the original model when the operating point changes. This is mainly due to the elimination of external PV buses. The voltage magnitude of the PV buses are given in the power-flow formulation and constrained in the calculations. To maintain the voltage magnitude at the specified value, reactive power is generated to support the bus voltage. When the operating point changes, the reactive power support from the PV buses is hard to approximate accurately which leads to the degradation in performance of the models produced by Ward-type and other conventional reduction methods. Two improved reduction methods were proposed to deal with the problem. The first improvement was the Ward-PV method, [3], [4], which retains all the external PV buses and eliminates the external load buses (PQ buses) only. This method bypasses all of the problems of eliminating PV buses and can accurately

approximate the original model performance over a broader range of operating conditions. However, when the number of PV buses is large, the reduced model is not small enough to reduce the computational burden significantly. Another method, the extended-Ward method, [3], [5]-[7], was derived to approximate the Ward-PV method. The main idea is to make the incremental response of VAr support close to the Ward PV method. This method adds one fictitious PV bus to every boundary PQ bus to provide reactive support. The fictitious PV buses are radially connected to the boundary PQ buses.

Though Ward reduction can be performed in a relative simple way, one drawback is that it has to split the external generators and distribute them across the boundary buses. Two problems arise. First, for a boundary PQ bus, if fractions of external generators (PV buses) are distributed to it, the bus type is strictly neither PV nor PQ. Second, for optimal power-flow (OPF) studies, the generator fractions make the equivalents unusable. One way to solve the problems is to use to the REI reduction method and the other way is to keep the generators whole and to move/place the external generators at "appropriate" boundary buses.

The REI (radial equivalent independent) was first introduced by P. Dimo [8] in 1975. It has been implemented and improved by many researchers [7], [9]-[13]. The REI equivalence is a bus-aggregation-based equivalencing technique. The general steps of REI require one to:

1. Define the essential buses and non-essential buses. The non-essential buses are to be equivalenced.

2. Group the non-essential buses into different study areas.

3. Create a zero power balance network for each study area.

4. Eliminate all zero injection buses in all zero-power-balance networks via Gaussian elimination.

The REI method groups the external buses instead of splitting them by constructing the zero-power balance network. It can avoid the problem of assigning boundary bus types.

Unlike the Ward reduction, which generates a reduced network (topology and branch reactances) independent to the different operating conditions. The REI method is a hot start method, which needs the power-flow solution of the base case. As a result, the REI reduction has following two properties:

1. The REI reduction is case dependent. The equivalent is created based on the base-case power-flow solution.

2. At the base case the REI equivalent can perform exactly the same as the original system; however when the operating condition changes, the predictions become approximate, with the approximation growing worse the further the operating point moves from the base case.

The property 2 above motivated researchers to develop the online calibrating methods so as to make the REI equivalent perform as close to the original system as possible in different operating conditions [9], [10]. An X-REI method was proposed in [10] and an S-REI method was proposed in [9]. Both X-REI and S-REI methods enable online calibrating. The X-REI adds one calibrating bus to each of the zero–power-balance networks which updates the boundary bus power injection in accordance with the changes of the operating condition. The S-REI method solves an overdetermined problem (obtained from redundant real-time measurements, i.e., state estimation) to update the boundary power injections and applies system identification techniques to update the equivalent network parameters.

In addition, a critical factor of the REI method is the criteria used for grouping the external buses. In [9] and [11], theoretical studies were performed and strict criteria on bus grouping were proposed. However, the theoretical criteria are too strict and hard to implement in practical analysis. Some heuristic criteria are purposed in [10] and [13].

One new group of reduction methods, strictly applicable to only dc models, was proposed which are based on the power transfer distribution factors (PTDF) [14]-[16]. These methods focus on approximating the original system's interactions between areas and generate the network equivalents using the following steps:

1. Group all buses into different areas.

2. Calculate the area PTDF of the original system.

3. Represent each area as a fictitious bus and connect the adjacent areas with fictitious branches. Calculate the fictitious branch admittance.

This method has proved to be useful in planning studies. However, several challenges need to be dealt with in the implementation. First, calculating the fictitious branch admittances involves solving an overdetermined homogeneous system. One can always find the trivial "all zeros" solution to the problem. To find a non-trivial solution, some techniques must be applied. In [14], the author iteratively found the cut nodes of the system and divided the original large system into several sub-systems. Then the problem was formulated based on the subsystems and each individual subsystem was solved separately. In [15], the author used the QR factorization method to solve the problem. It turns out the QR factorization is an effective way which not only can find the non-trivial solution but also reduces the computational memory requirements because it can find the most linearly independent rows and columns in the original problem.

5

For the studies based on dc-modeling assumptions, all three groups of equivalent methods can be applied. However, for ac-type studies, the fundamental assumptions in the derivation of the PTDF-based methods are violated. The reason is simple: in the ac scenario, the PTDF matrix is a function of operating point which means that at different operating points the PTDF matrices are different. This is due to the changes in the line losses.

## 1.3    The Need for ac Model Reductions

As introduced earlier, it is impractical to solve the complicated planning problem over a large system due to the high computational demand. Though the dc-assumption-based network reduction is desirable in many applications because of its simplicity [17], [18], a nonlinear ac model reduction, which is more computationally complex and more accurately models the system, is needed when the nonlinear features of the power system become important, such as for reactive power planning (RPP). For the RPP problem, which studies the placement and size of reactive power sources in the network to maintain voltage levels within appropriate ranges, the dc assumption, which assumes all voltage to be 1.0 pu, renders the formulation useless. Further, an RPP problem is a mixed-integer nonlinear programming (MINLP) problem which is of high computational complexity when applied to a large system; thus a reduced ac model is typically necessary. For example, in [21], and [22], a 17-bus equivalent model of the New Zealand power system was used to solve the RPP problem while incorporating the voltage stability constraints. In [23], the New England 39-bus system and a 2069-bus equivalent of the eastern-interconnection were used. Reduced-order ac models are also found to be useful for investment studies. For example, in [19], [20] a 46-bus and an 87-bus ac equivalent model of the Brazilian power system

were applied to the optimal investment problem. In [24], the authors show that the ac reduced model is also applied in online operations when the data of the external network is not available.

## 1.4    Objective

The network reduction work reported here focuses on three objectives: 1) Improve flexibility, 2) Improve robustness and 3) Improve accuracy.

To improve flexibility, an optimization-based network reduction method (OPNR) is proposed. This method formulates an optimization problem which can be treated as a framework for a class of PTDF-based reductions. The objective function and constraints can be modified to generate different equivalents for different studies. It is shown in this work that OPNR can replicate the Ward reduction on large test systems (IEEE 118-bus system, IEEE 300-bus system). In addition, the method can improve the accuracy and sparsity pattern of the Ward reduction by appropriately compensating for the elimination of high impedance equivalent branches.

Planning studies require running OPFs. Ward reduction splits the external generators into fractions and distributes them across (typically) a large fraction of the boundary buses, which adds computational complexity to OPF-type algorithms, which already have a high order of complexity. One way to solve the problem (albeit an approximate technique) is to move each of the external generators to one "appropriate" boundary buses. In this work, different generator placement methods are investigated. An important metric which can be used to evaluate a generator method is its robustness (defined more precisely later.) After placing the external generators in the reduced network, the reduced-model OPF may not

7

be feasible under certain operating conditions for which the full model OPF is feasible. The robustness is measured by the frequency of the occurrence of infeasibility on the reduced model. Compared to finding the optimal solution, achieving a feasible solution is more fundamental. Naturally, a basic requirement of the equivalent model is that a feasible solution exists when the original model has a feasible solution. It is shown in this work that the generator placement in the network reduction process can significantly affect power-flow robustness. Three generator placement methods are proposed and: 1) the shortest-electrical–distance-based method (SED), 2) the optimization-based generator placement method (OGP), 3) the minimum-shift-factor-change-based method (MIN-SF). Results of tests on large and existing systems (IEEE 118, ERCOT, WECC) are shown and discussed.

One of the most fundamental and critical problems in power system analysis is solving the ac power-flow problem using reduced network equivalents. It is shown that the traditional reduction methods (e.g., Ward, REI) fail to yield accurate results when the operating condition changes. This is mainly due to two reasons. One is that the approximation to real and reactive power losses is inaccurate and the other one is that the external controlled reactive power generation is hard to approximate. In this work, a novel network reduction method, taking advantage of the holomorphic embedding (HE) technique is proposed. Results show that the HE equivalent yields superior results compared to the Ward-type or the REI-type methods.

# 2 GENERATOR PLACEMENT METHODS IN NETWORK REDUCTION

## 2.1 Introduction

In network reduction, after generating the reduced network, the next step is to place the external power injections: generators and loads. In this work, the goal is to find a generator placement method which can be integrated in the network-reduction process and yield good accuracy in terms of matching the full-model dc OPF results. In this work, the metrics used for accessing accuracy of matching the full-model dc OPF results are bus LMP, generation dispatch and the total cost.

Placing external load is less complex than placing generators since a load does not have an "identity," unlike generators which have individual real and reactive power limits and production cost curves. One can split the load and distribute the fractional load across the reduced network in order to match the branch flows in reduced model to those in the full model. A brief introduction of one method to distribute the load will be given in Section 2.5.

For planning or market studies conducted by the (E4ST) application, formerly known as the SuperOPF, generators need to be moved whole. It is impractical to use fractions of the external generators, which are generated in the traditional Ward reduction for at least two reasons. First, Ward reduction distributes the external generators to all boundary buses. This process will generate a huge number of fictitious generators in the reduced model. Consequently, in a large system where significant bus reduction takes place, there will be a large number of variables related to the splitting of the generators. Second, for each external generator, the power output of each fraction may not be scheduled independently

in the planning study. Outputs of fractions of one external generator must always hold a fixed proportional relationship and their sum must be constrained to operate within the generator's capability. Consequently, there will be a large number of constraints involved in the dc OPF study related to the generator fractions. Thus a reduced model with generator fractions may be more complex the than the original model, defeating the purpose of network reduction.

## 2.2 Shortest Electrical Distance (SED) Based Method

One method for moving generators whole is known as the shortest electrical distance (SED) method. The SED method, [26], [30], moves each external generator to a boundary bus via the shortest path in terms of electrical distance. There are many definitions of electrical distance. Here the electrical distance of a path between two buses is the sum of impedances (reactance with dc assumptions) in that path.
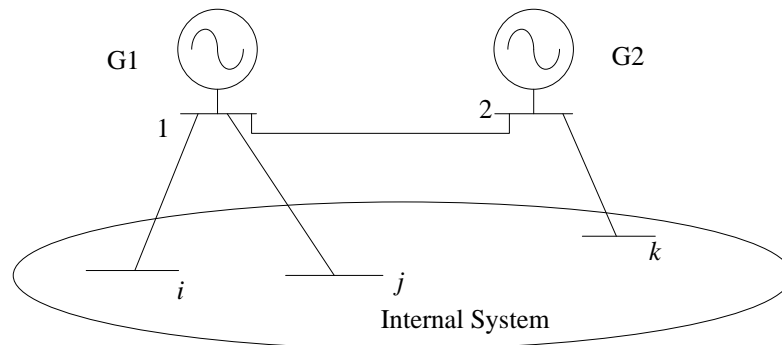


Fig. 2-1 Example to show electrical distance

As shown in Fig. 2-1, for generator G1 there are three possible paths to boundary buses: path 1 is from bus 1 to bus $i$, path 2 is from bus 1 to bus $j$ and path 3 is from bus 1 to bus $k$ via bus 2. The distance of path 1 and path 2 are same as reactance values of the lines connecting the two buses. For path 3, the path distance is the sum of the reactances of the

line connecting bus 1 and 2 and the line connecting bus 2 and $k$. The shortest path can be found using Dijkstra's algorithm [33].

The SED method is an optimal method in terms of finding the minimum electrical distance. Its accuracy in terms of approximating the full-model dc OPF results will be studied and discussed in the following.

2.3    Optimization Based Generator Placement (OGP) Method

2.3.1    Formulation

The OGP method places external generators on retained buses by solving an optimization problem. The formulation of the problem shares aspects of the dc OPF formulation as it is applied to the reduced model.

Recall that for the dc OPF formulation, the LMP is influenced by two system features: the marginal energy cost, which is a function of the generation mix, and marginal congestion cost, which is a function of generator location (which may be thought of as a feature characterized by topology and branch parameters.) When producing a reduced equivalent the generation mix is fixed. Given that the topology and branch parameters of a network equivalent are also determined by Ward reduction, the only remaining free variables available to match the marginal congestion cost component of the LMP's are the placement of generators, placement of the loads, or both, so that congestion in the full and reduced models is maintained.

With the strategy mentioned above, formulation of the generator placement problem can be made by somewhat generalizing the dc OPF formulation applied to the reduced

model with binary variables added to specify generator placement. A set of new variables are introduced.

$$x_{g_e,k} = \begin{cases} 1, \text{if external generator } g_e \text{ is placed at internal bus } k \\ 0, \text{otherwise} \end{cases}$$

To balance power generation and consumption, the external load should be moved to a retained bus. In the OGP problem, each external load is also moved to one "appropriate" retained bus. Similar to moving generators, a set of binary variables is introduced:

$$x_{k_e,k} = \begin{cases} 1, \text{if load on external bus } k_e \text{ is moved to retained bus } k \\ 0, \text{otherwise} \end{cases}$$

Since the new set of variables are binary, the optimization problem becomes a mixed integer programming (MIP) problem. The objective function can be written as

$$\min \sum_{g \in G_I, g_e \in G_E} c_g \left( P_k^g + P_{k_e,k}^{g_e} \right) + \sum_{j \in Jr} W_j \left\| P_{j,full}^f - P_{j,reduced}^f \right\|, \forall k_e \in K_E, \forall k \in K_I \qquad (2\text{-}1)$$

Two components are included in the objective function. The first component minimizes generation cost which maintains similarity between the OGP solution and the reduced-model dc OPF solution. The second component minimizes the flow error on the retained congested lines between the full-model dc OPF solution and the OGP solution. In the second component, $P_{j,full}^f$ is the line flow (MW) on branch $j$ which is assumed to be *a priori* knowledge. Since line $j$ is congested, the line flow is actually the same as the limit. As formulated, the OGP benefits from knowledge of the full model dc OPF results or the congestion profile in the full system.

In the second component of (2-1), the parameter $W_j$ is the weight of line-flow error of the congested line $j$. It is important to assign an appropriate value to $W_j$. The effects of

12

different weight assignments will be discussed later in this chapter and a tentative strategy will be proposed.

The constraints of the OGP formulation can be divided into four groups. The first group is the modified reduced-model dc OPF formulation:

$$\sum_{g(i)\in G_I}\left(P_k^g\right)-P_k^l-P_{k_e,i}^l k +\left(\sum_{\forall j(.,i)\in J}P_j^f - \sum_{\forall j(i,.)\in J}P_j^f\right)+ \sum_{g_e \in G_E}\left(P_{k_e,k}^{g_e}\right)=0, \forall k \in K_I, \forall k_e \in K_E \qquad (2\text{-}2)$$

$$P_{g\,\min}^k \leq P_g^k \leq P_{g\,\max}^k, \forall g \in G_I, \forall k \in K_I \qquad (2\text{-}3)$$

$$-P_{j\,\max}^f \leq P_j^f \leq P_{j\,\max}^f, \forall j \in J \qquad (2\text{-}4)$$

$$P_j^f = B_j\left(\theta_{j_f} - \theta_{j_t}\right), \forall j \in J, \qquad (2\text{-}5)$$

where $K_I$ and $K_E$ are the sets of internal and external buses respectively and $j_f$ and $j_t$ are the indices of the from and to end buses.

The second group of the constraints are configured to assign external generators to retained buses:

$$P_{k_e,k}^{g_e} \leq P_{k_e\,\max}^{g_e} x_{g_e,k}, \forall k \in K_I, \forall k_e \in K_E, \forall g_e \in G_E \qquad (2\text{-}6)$$

$$P_{k_e,k}^{g_e} \geq P_{k_e\,\min}^{g_e} x_{g_e,k}, \forall k \in K_I, \forall k_e \in K_E, \forall g_e \in G_E \qquad (2\text{-}7)$$

$$\sum_{k\in K_I} x_{g_e,k} =1, \forall g_e \in G_E \qquad (2\text{-}8)$$

$$x_{g_e,k} = \{0,1\}, g_e \in G_E, k \in K_I \qquad (2\text{-}9)$$

Constraint sets (2-6) and (2-7) impose limits on the external generators. Constraint set (2-8) ensures that each external generator is moved to one and only one retained bus.

A third group of the constraints assigns each external load to a retained bus:

$$P_{k_e,k}^l = P_{k_e}^l \cdot x_{k_e,k}, \forall k \in K_I, \forall k_e \in K_E \qquad (2\text{-}10)$$

$$\sum_{k \in K_I} x_{k_e,k} = 1, \forall i_e \in K_E \qquad (2\text{-}11)$$

$$x_{k_e,k} = \{0,1\}, \forall k_e \in K_E \qquad (2\text{-}12)$$

Constraint set (2-10) guarantees that the load at each external bus is moved to an "appropriate" retained bus. Note that after placing the external generators and loads by the OGP method, the load will be redistributed by running the inverse power flow illustrated in Section 2.5.

In the objective function, (2-1), the second component involves calculation of the absolute value of line-flow errors. Calculation of the absolute value can be reformulated into linear expressions. The reformulation involves a set of variables $t$ and also a group of constraints:

$$t_{j_r} \geq P_{j_r,full}^f - P_{j_r,reduced}^f, \forall j_r \in J_r \qquad (2\text{-}13)$$

$$t_{j_r} \geq -P_{j_r,full}^f + P_{j_r,reduced}^f, \forall j_r \in J_r \qquad (2\text{-}14)$$

Constraint sets (2-13) and (2-14) indicates that $t_j$ is greater or equal to the absolute value of the line flow error. The objective function can be updated as:

$$\min \sum_{g \in G_I, g_e \in G_E} c_g \left( P_k^g + P_{k_e,k}^{g_e} \right) + \sum_{j \in Jr} W_j t_j, \forall k \in K_I, \forall k_e \in K_E \qquad (2\text{-}15)$$

As shown in (2-15), the OGP problem is a minimization problem and the weights are all positive. In the process of solving the problem, $t_j$ will be equal to the absolute value of the flow error.

Consequently, the OGP problem formulation includes the objective function (2-15) and constraints (2-2)-(2-14).

## 2.3.2 Discussion on the OGP method

### 2.3.2.1 Calculation complexity

The number of binary variables needed in the formulation is equal to the number of external generators multiplied by the number of retained buses. As the system size grows, the number of binary variables will grow rapidly. Solving optimization problems on large scale power systems involves a large number of binary variables and constraints combining binary and non-integer variables. In these situations, common techniques like Lagrangian Relaxation [31] and Benders Decomposition [32] can be applied to reduce execution time. In the problem formulation, constraints (2-6)-(2-9) are imposed on every external generator individually and constraints (2-10)-(2-12) are imposed on every external load or buses individually. Only constraint (2-2) is imposed on all binary variables. A practical way to apply Lagrangian Relaxation and enable parallel computation is to dualize constraint (2-2) and then the problem can be solved by parallel computing with every sub-problem involving only one external generator or load bus.

### 2.3.2.2 Weights of line flow error of congested lines

In (2-15), value of weights $W_j$ can significantly affect the accuracy. Tests presented in [30] show that large weights will make the OGP tend to focus more on minimizing the congested line flow error. This may result in small bus LMP errors but large generation dispatch errors [30].

One strategy for assigning these weights is to use the value of the optimized Lagrange multiplier of the line-flow limit constraint (marginal flow gate price) for every congested line on the full model. In this way the weights on the congested lines will depend on the significance of the congested lines.

## 2.4    The Minimum Shift Factor Change (Min-SF) Based Method

In addition to the OGP method proposed in the previous section, a second generator placement strategy, the Min-SF, method is proposed. The Min-SF method assigns each external generator to a bus whose shift factor is closest to the shift factor of the external bus at which the external generator initially resided. The shift factor associate with a bus is defined as the vector of branch flows occurring due to an injection of 1 pu MW at that bus. Each column of a PTDF matrix is a shift factor. Fig. 2-2 shows the PTDF matrix and the column of shift factor of bus $i$ inside the PTDF matrix.

$$\mathbf{\Phi} = \begin{bmatrix} \varphi_{11} & \cdots & \boxed{\varphi_{1i}} & \cdots & \varphi_{1n} \\ \vdots & \ddots & \vdots & \ddots & \vdots \\ \varphi_{j1} & \cdots & \varphi_{ji} & \cdots & \varphi_{jn} \\ \vdots & \ddots & \vdots & \ddots & \vdots \\ \varphi_{m1} & \cdots & \varphi_{mi} & \cdots & \varphi_{mn} \end{bmatrix}$$

$$SF_i$$

Fig. 2-2 Shift factor and PTDF matrix

The reasoning for using this approach is that, after moving the external generator to the retained bus, the change in the line flows on all branches in the reduced model is minimal.

16

If multiple generators share the same bus assignment in the original model, they will be moved to the same retained bus since these generators have the same shift factor.

The Min-SF method requires three distinct steps in its implementation. The first step is to generate the full model PTDF matrix while being careful to select the reference bus $i_{ref}$ as one of the external buses. The variable $\Phi_i^{r,i_{ref}}$ represesnts a column in the PTDF matrix corresponding to the chosen generator bus. The second step is to calculate the shift factor change between, $\Phi_{k_e}^{r,k_{ref}}$ and all other columns corresponding to retained buses, $\Phi_k^{r,k_{ref}}, k \in K_I$:

$$\Delta\Phi_{k,k_e}^{r,k_{ref}} = \left\| \Phi_k^{r,k_{ref}} - \Phi_{k_e}^{r,k_{ref}} \right\|_1 \tag{2-16}$$

In this step, the superscript $r$ indicates that the comparison only involves the rows that correspond to the retained lines. This second step needs to be repeated for each external generator bus. The third step is to find, for each external generator bus, the retained bus that has the minimum shift factor change. The generator will then be placed at that bus.

## 2.5 Load Redistribution

After placing external generators on retained buses, the load needs to be redistributed in order to match the full-model line flow solution. In this work, the load is redistributed by solving the inverse power flow [29].

For the dc power-flow problem, bus injections of the reduce model can be calculated as:

$$P^g - P^l = B_{bus,reduced} \cdot \theta_{reduced} \tag{2-17}$$

where $P^g$ and $P^l$ are vectors of real-power generation (after placing the external generators) and load on all buses, respectively, $B_{bus,reduced}$ is the bus susceptance matrix of the reduced model and $\theta_{reduced}$ is the vector of bus voltage angles.

The redistributed load can be calculated as:

$$P^l = P^g - B_{bus,reduced} \cdot \theta^r_{full} \tag{2-18}$$

In (2-18), $\theta^r_{full}$ is the vector of bus angles of retained buses given in the full model solution.

## 2.6    Numerical Test Results

The three aforementioned generator placement methods were tested on the IEEE 118-bus system. The SED method and the Min-SF method were tested on the ERCOT and WECC system. The OGP method was not tested on the ERCOT and WECC system. The reason is explained in Section 2.6.2.

### 2.6.1    Measurements of accuracy and robustness

A good generator placement should lead to a reduced model that produces accurate LMP values and is robust in the sense that the reduced model has a feasible solution when the full model has a feasible solution. Three test metrics were chosen to measure accuracy and robustness in the numerical tests performed. The combined metrics show how well the reduced-model dc OPF results match the full-model dc OPF results.  The metrics chosen are as follows:

18

### 2.6.1.1  Error measurement

Reduced model accuracy is measured in terms of the average bus LMP error ($/MWh) and the average energy cost (AEC, $/MWh) error.

The average bus LMP error ($/MWh) is calculated as:

$$Error_{LMP} = \frac{\sum_{i \in K}\left| LMP_i^f - LMP_i^r \right|}{N} \tag{2-19}$$

The AEC error ($/MWh) is calculated as:

$$Error_{AEC} = \frac{\left| AEC_{full} - AEC_{reduced} \right|}{\sum_{i \in K} P_i^l} \tag{2-20}$$

where $LMP_i^f$ and $LMP_i^r$ are the LMP value of bus $i$ in the full and reduced model respectively; $K$ is the set of all buses; $AEC_{full}$ and $AEC_{reduced}$ are the AEC obtained from the full and reduced-model dc OPF results, respectively.

### 2.6.1.2  Robustness

Since the load is redistributed after generator placement for all three methods, the reduced-model dc OPF is always feasible under the base case. However, when the operating point shifts, the reduced-model dc OPF may become infeasible. Tests will be conducted under different operating conditions to determine robustness. The robustness of each method is measured by counting and comparing the number of infeasible cases under varied loading conditions. A method with fewer infeasible cases will be regarded as more robust.

## 2.6.2 IEEE 118-bus system

The IEEE 118-bus system was reduced to a 35 bus system in the test. Fig. 2-3 and Fig.

2-4 show the diagrams of the original system and the reduced system respectively.
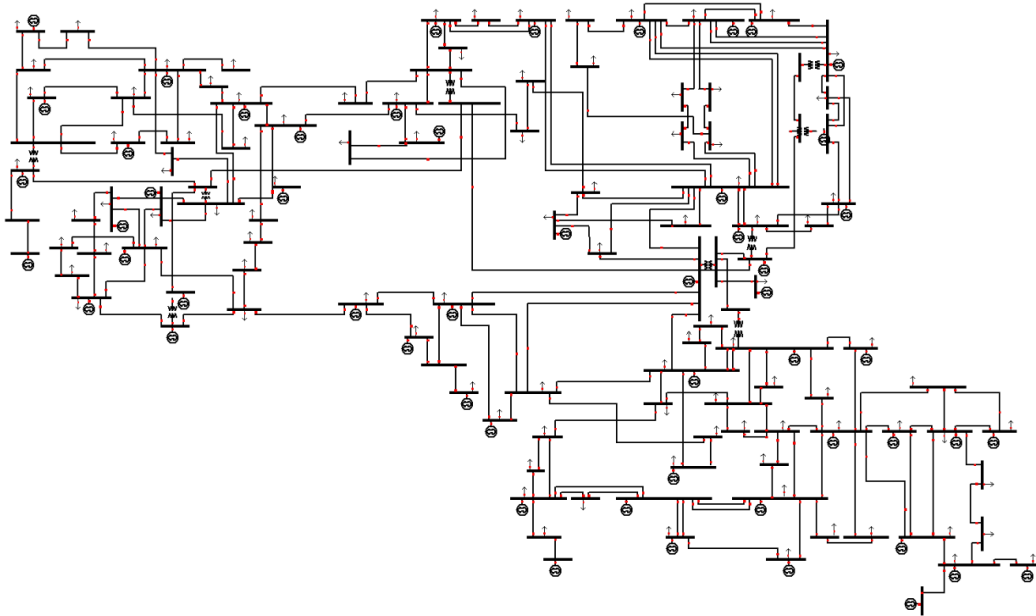


Fig. 2-3 IEEE 118-bus system
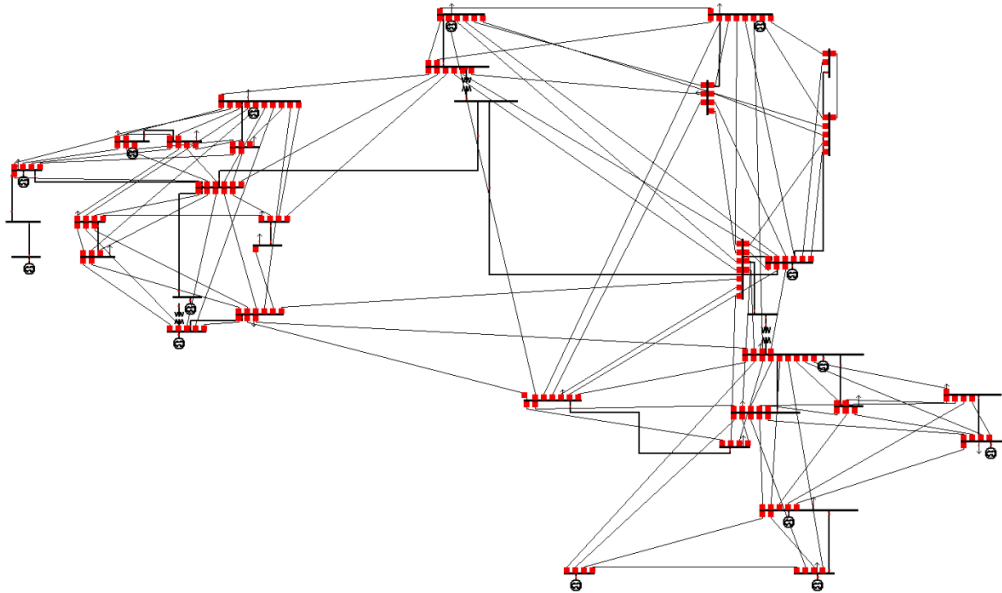


Fig. 2-4 Reduced model of IEEE 118-bus system (35 bus)

The system was divided into three zones shown in Fig. 2-5. The statistical data of the zones is shown in Table 2-1. The motivation for dividing the system was to provide more selective scaling of the loads so that different operating conditions which result in congestion may be easily created.
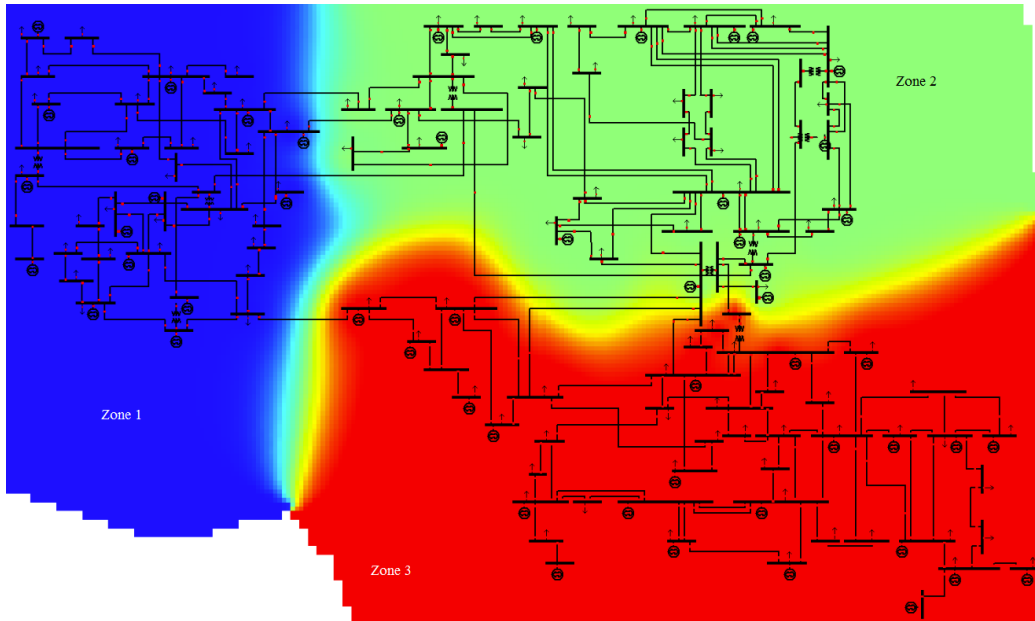


Fig. 2-5 Zone division in IEEE-118 bus system

Table 2-1 Statistics of Zones in IEEE 118 Bus System

| | # of buses | Total load (MW) | Total load (%) | # of generators | Total capacity (MW) | Total capacity (%) |
|---|---|---|---|---|---|---|
| Zone 1 | 35 | 963 | 22.7 | 15 | 2576 | 25.8 |
| Zone 2 | 38 | 1670 | 39.4 | 16 | 3674.2 | 36.9 |
| Zone 3 | 45 | 1609 | 37.9 | 23 | 3716 | 37.3 |

The original IEEE 118-bus system model does not include line limits. It is known that with no line congestion, the bus LMP's will be identical across entire network. In that case,

comparing the average energy cost error is meaningless. Thus it is necessary to add limits to all the transmission lines.

In this work, three different congestion levels are created by adding three different sets of line limits. The congestion levels are set as low (4%), medium (10%) and high (14%). The percentage in the parentheses is the percentage of congested branches out of all branches.

The line limits are generated in three steps. First, the dc OPF is run on the system with no line limits. Second, using the dc OPF results, the limits on the $N_{jr}$ branches with the limits are set at 90% of the line-flow value obtained from the dc OPF solution. Here $N_{jr}$ is the number of congested branches. Other branch limits are set to be 120% of their line flow value obtained from the dc OPF solution. Third, the dc OPF is rerun on the system with the added line limits and the number of congested lines is checked. The total number of lines in the IEEE 118 bus system is 186. Table 2-2 shows the congestion profile data of the three congestion levels.

Table 2-2 Three Congested Level Systems

| $N_{jr}$ | Number of Congested Lines | Percentage of Congested Lines | Congestion Level |
|---|---|---|---|
| 10 | 7 | 4% | Low |
| 20 | 19 | 10% | Medium |
| 30 | 26 | 14% | High |

The tests are performed for four different scenarios for every congestion level. The four different scenarios are generated based on different load scaling metrics.

Table 2-3 Test Scenarios

| Scenario | Load scaled area |
|----------|------------------|
| 1 | Zone 1 |
| 2 | Zone 2 |
| 3 | Zone 3 |
| 4 | Entire system |

As shown in Table 2-3, Scenarios 1 to 3 only scale loads over a range of values in one zone and Scenario 4 scales the load in the entire system. Since load is redistributed by running an inverse power flow, there is no need to scale the load in the reduced model.

The average LMP error comparison results are shown in the figures below. The horizontal axis is the load scaling factors. The vertical axis is the average LMP error ($/MWh). If one generator placement method yields an infeasible solution under an operating condition, its curve is interrupted for such a condition. For example, in Fig. 2-6, the curve of OGP method has no value under load-scaling level from zero to 0.35 indicating the reduced-model dc OPF is infeasible under such operating conditions.

The average LMP error comparison between the three placement methods in the four scenarios of the low-congestion-level system are shown in Fig. 2-6-Fig. 2-9.
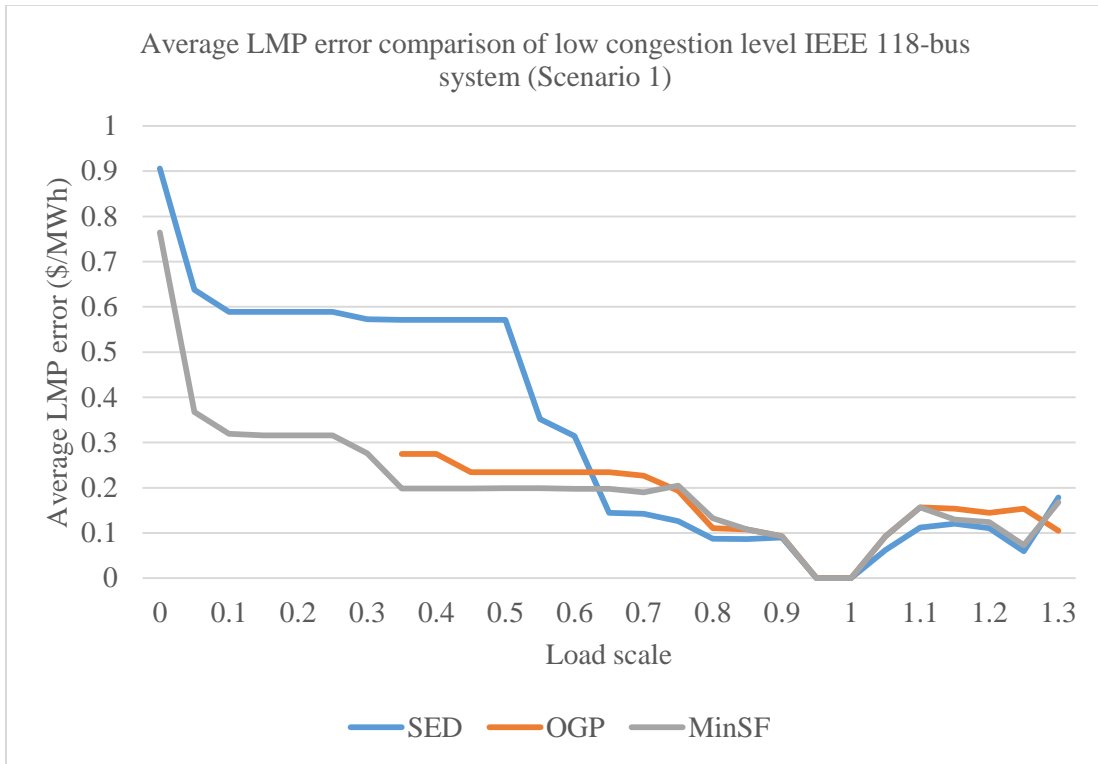
Fig. 2-6 Average LMP error comparison of low congestion level IEEE 118-bus system (Scenario 1)
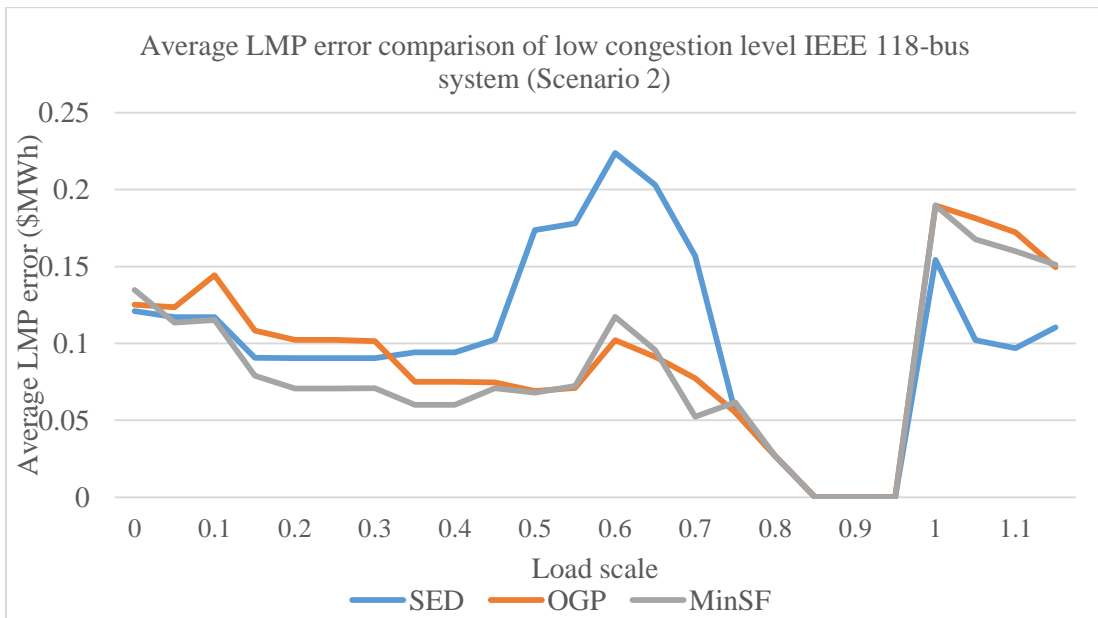


Fig. 2-7 Average LMP error comparison of low congestion level IEEE 118-bus system (Scenario 2)
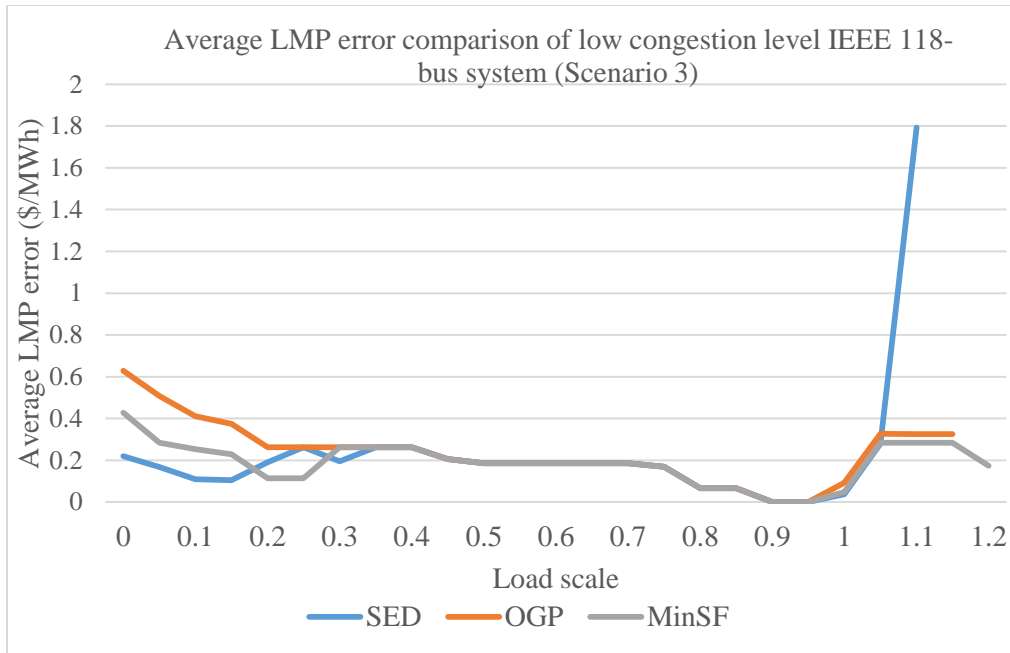
Fig. 2-8 Average LMP error comparison of low congestion level IEEE 118-bus system (Scenario 3)
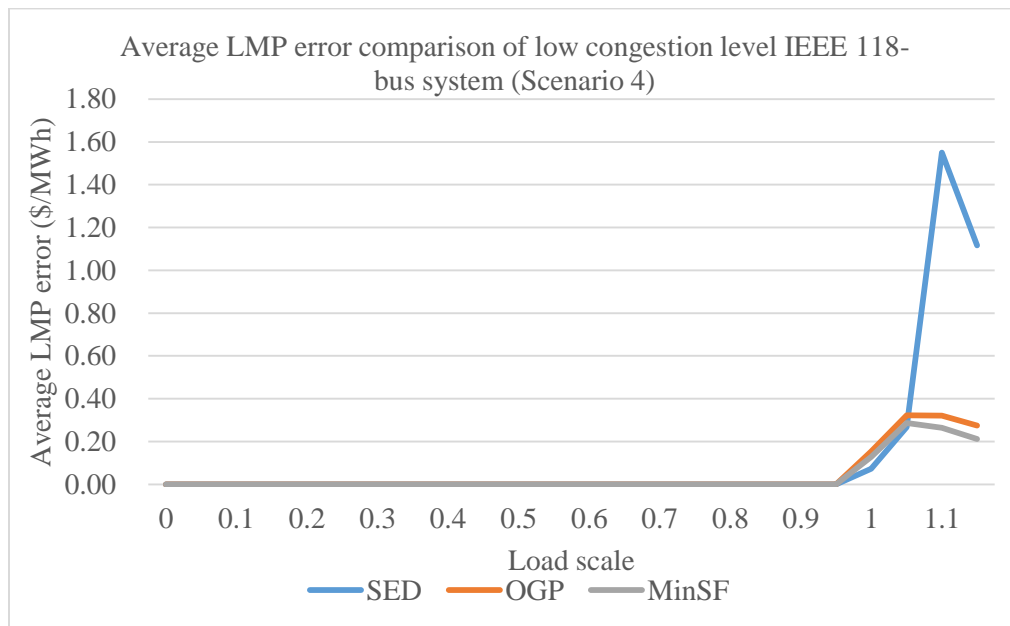


Fig. 2-9 Average LMP error comparison of low congestion level IEEE 118-bus system (Scenario 1)

The average LMP error comparison between the three placement methods in the four scenarios of the medium congestion level system are shown in Fig. 2-10-Fig. 2-13.

25
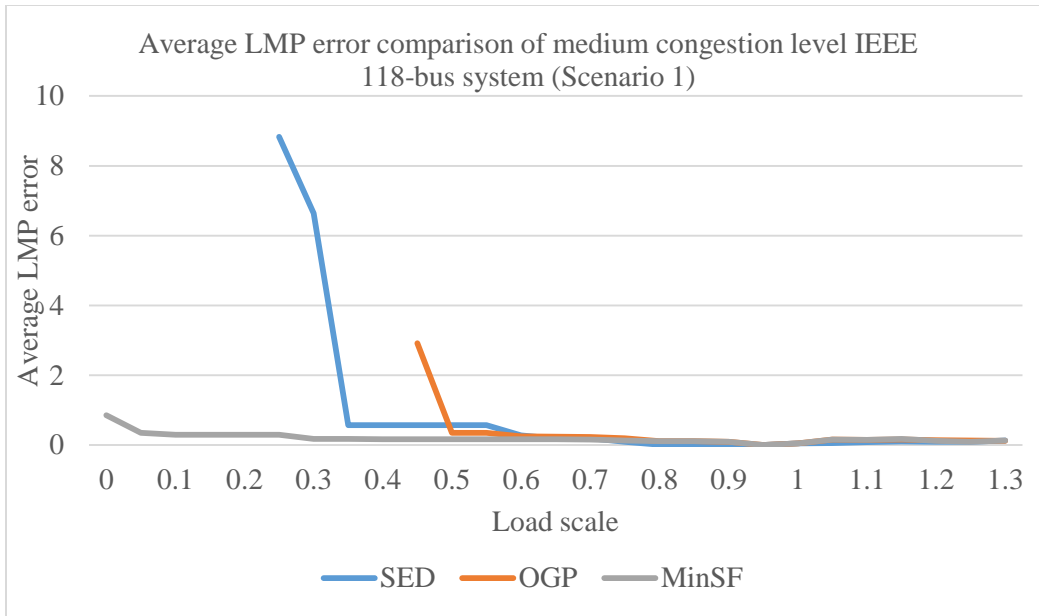
Fig. 2-10 Average LMP error comparison of medium congestion level IEEE 118-bus system (Scenario 1)
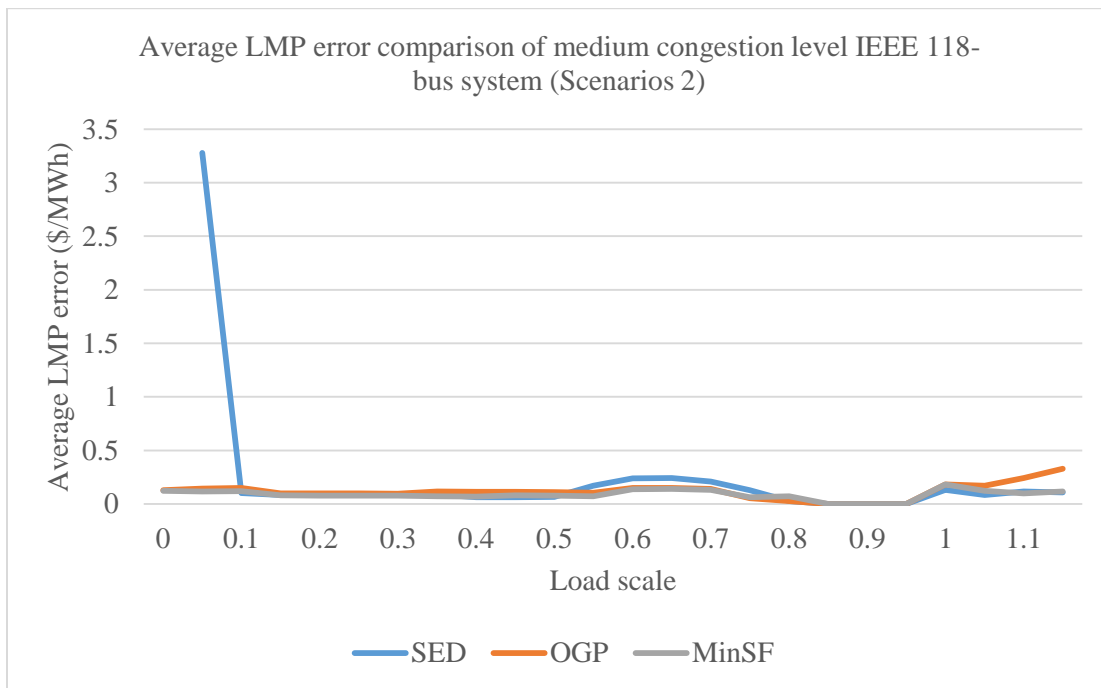


Fig. 2-11 Average LMP error comparison of medium congestion level IEEE 118-bus system (Scenario 2)
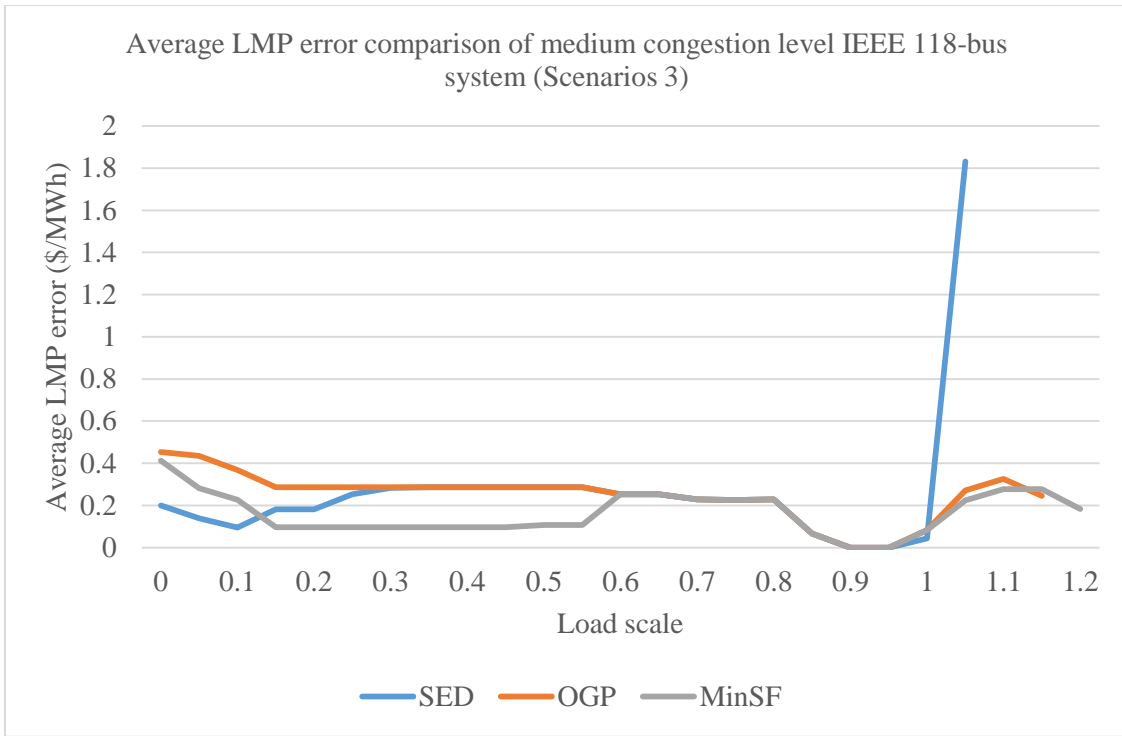
Fig. 2-12 Average LMP error comparison of medium congestion level IEEE 118-bus system (Scenario 3)
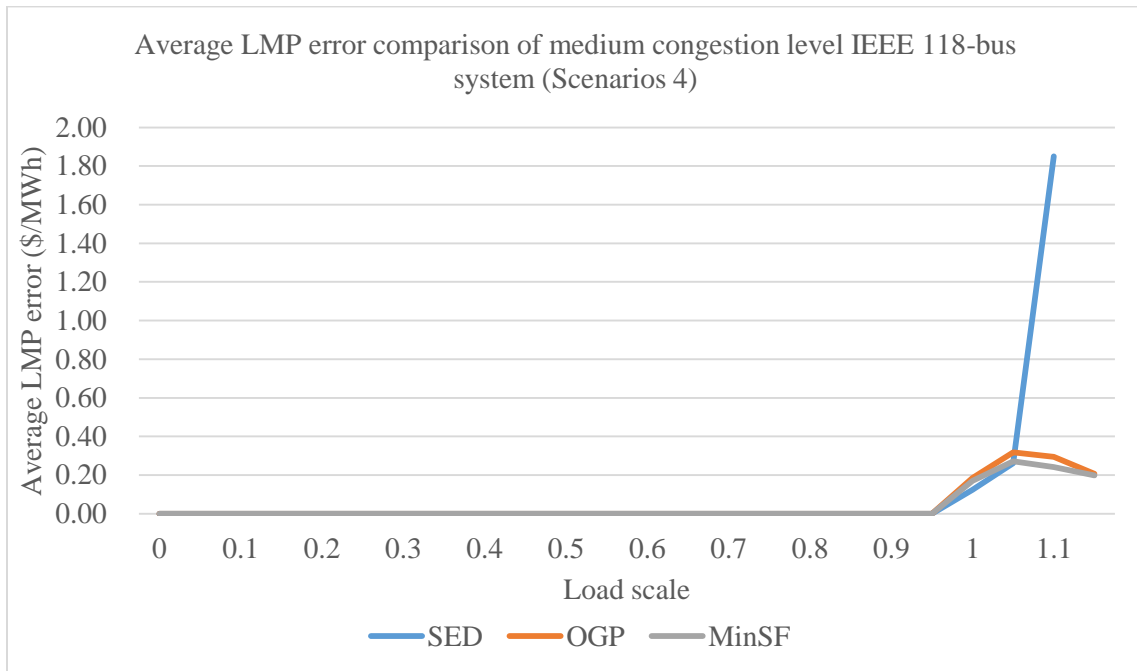


Fig. 2-13 Average LMP error comparison of medium congestion level IEEE 118-bus system (Scenario 4)

The average LMP error comparison between the three placement methods for the four scenarios of the high congestion level system are shown in Fig. 2-14-Fig. 2-17.
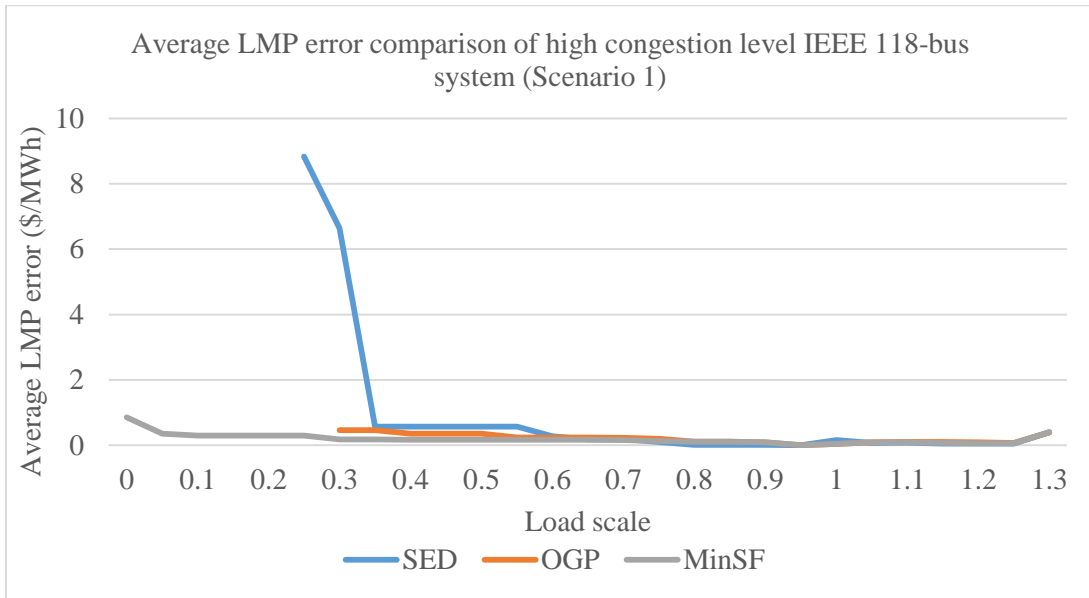


Fig. 2-14 Average LMP error comparison of high congestion level IEEE 118-bus system (Scenario 1)
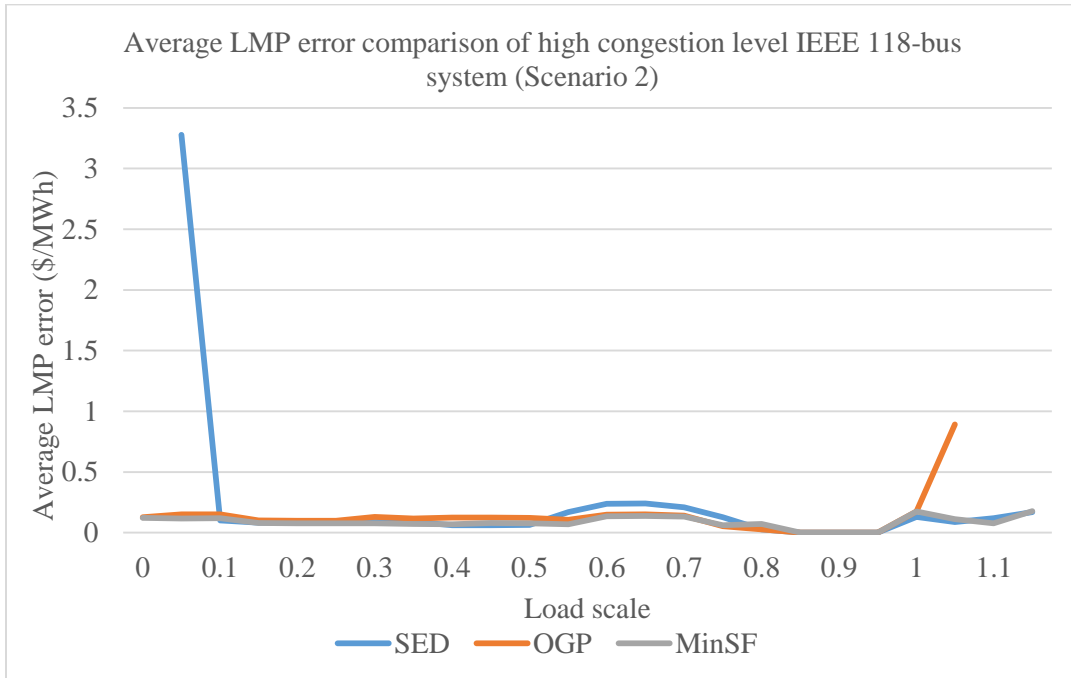


Fig. 2-15 Average LMP error comparison of high congestion level IEEE 118-bus system (Scenario 2)
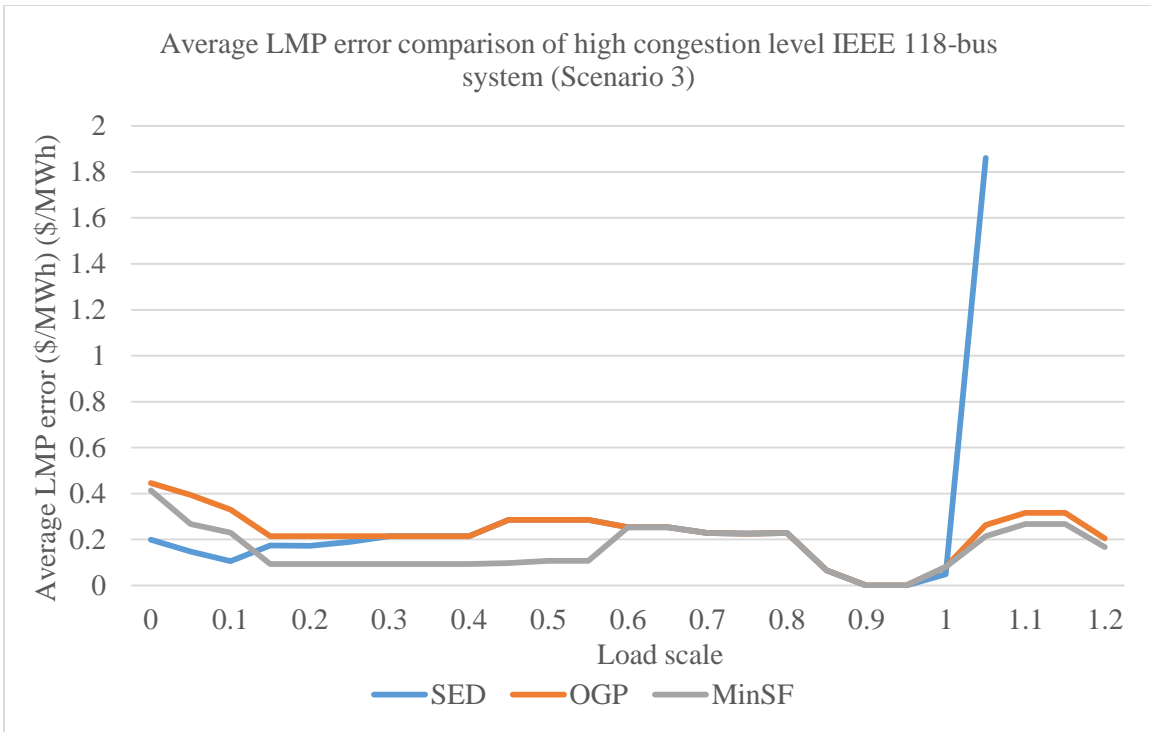
Fig. 2-16 Average LMP error comparison of high congestion level IEEE 118-bus
system (Scenario 3)
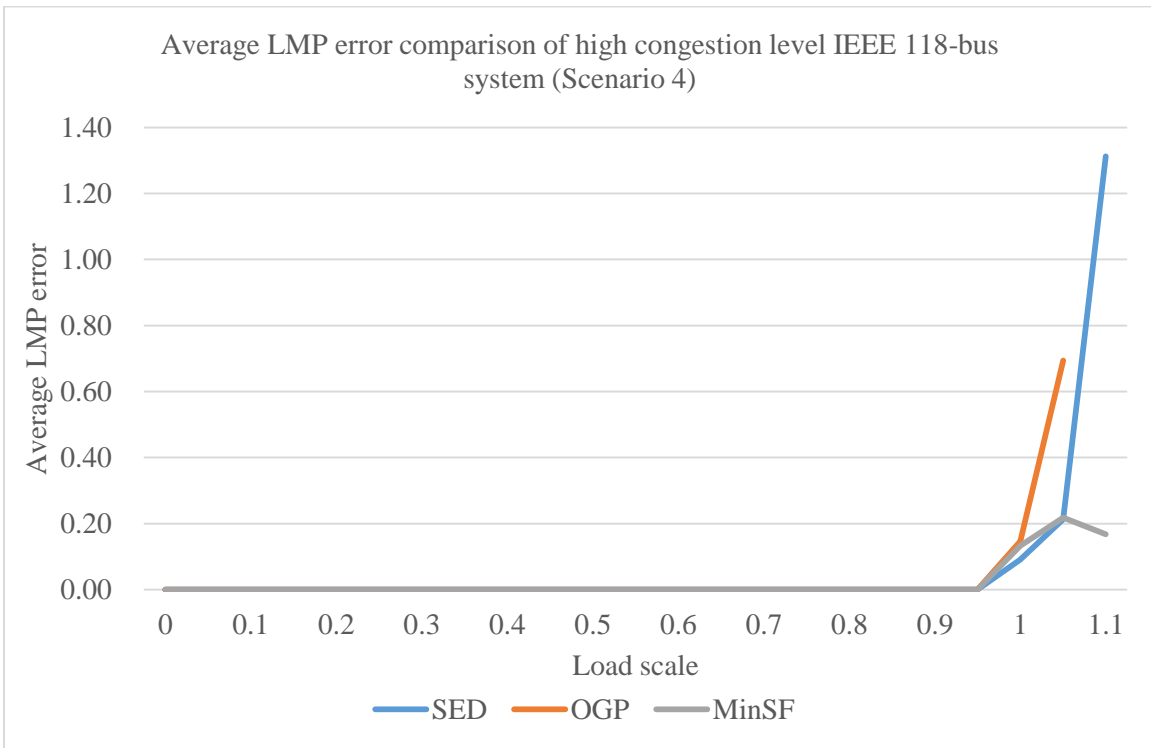


Fig. 2-17 Average LMP error comparison of high congestion level IEEE 118-bus
system (Scenario 4)

The SED method has a high probability of yielding infeasible cases or of yielding very large LMP errors. The OGP method, yielded more infeasible cases then the other two methods. The Min-SF methods was (on average) more accurate than the other two methods, taking account of all operating conditions.

Fig. 2-18-Fig. 2-20 show the AEC error comparisons for all congestion levels where all generator placement methods yielded OPF solutions which were feasible.
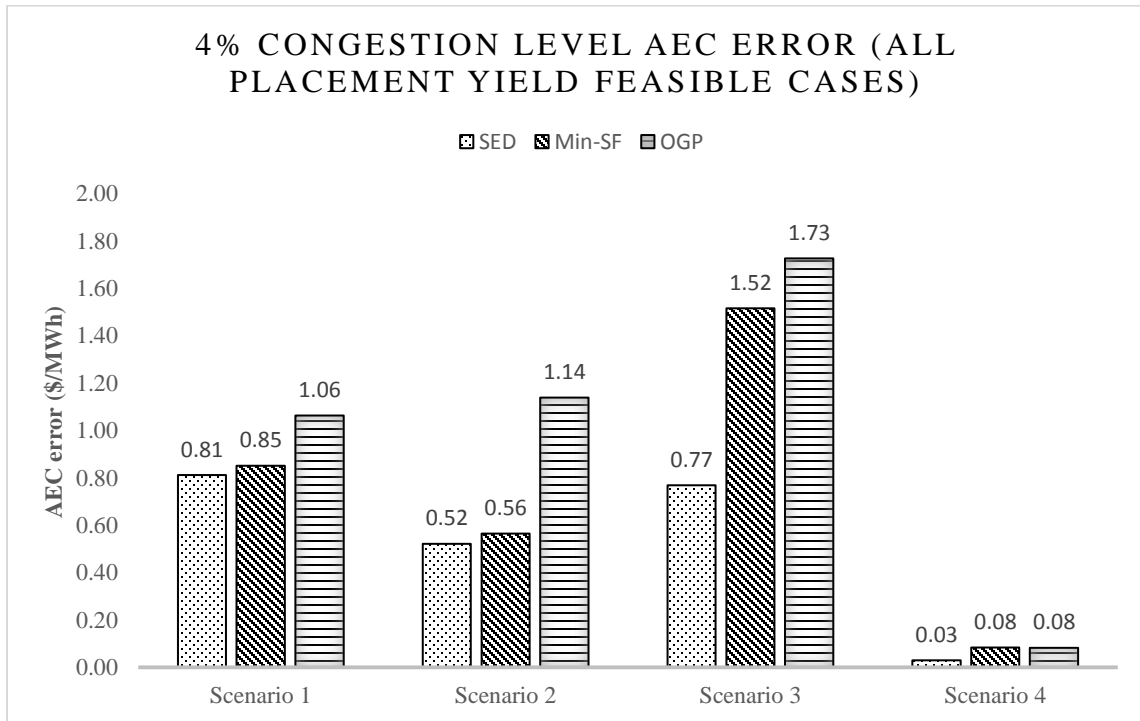


Fig. 2-18 4% Congestion Level AEC error with all placement yield feasible cases
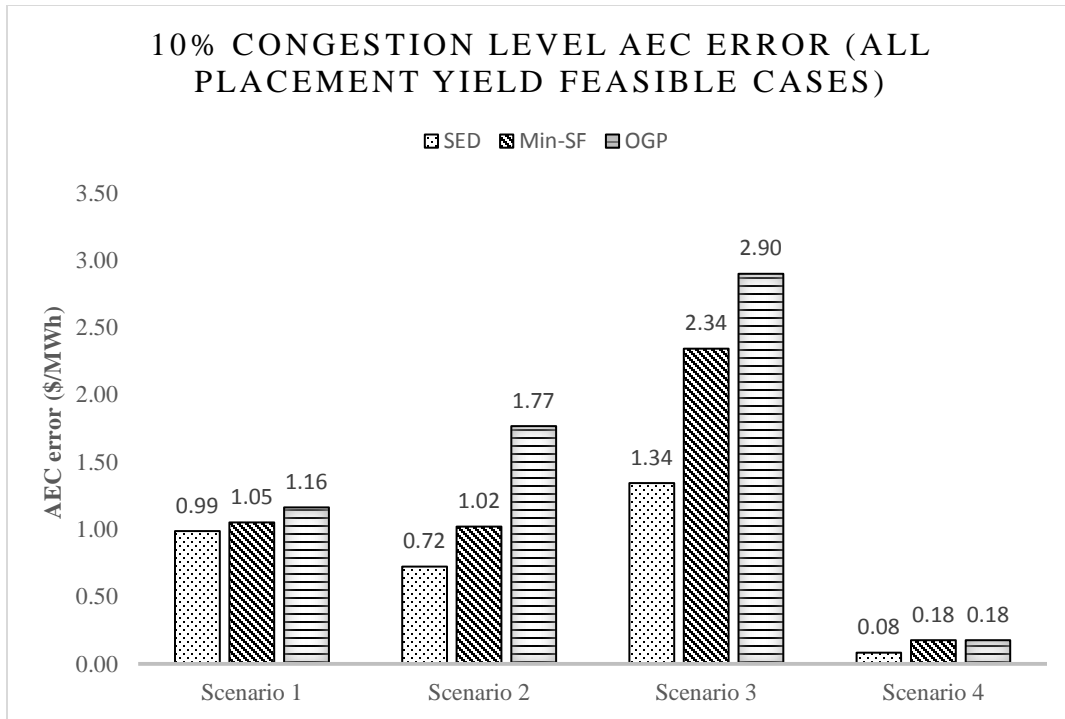
Fig. 2-19 10% Congestion Level AEC error with all placement yield feasible cases
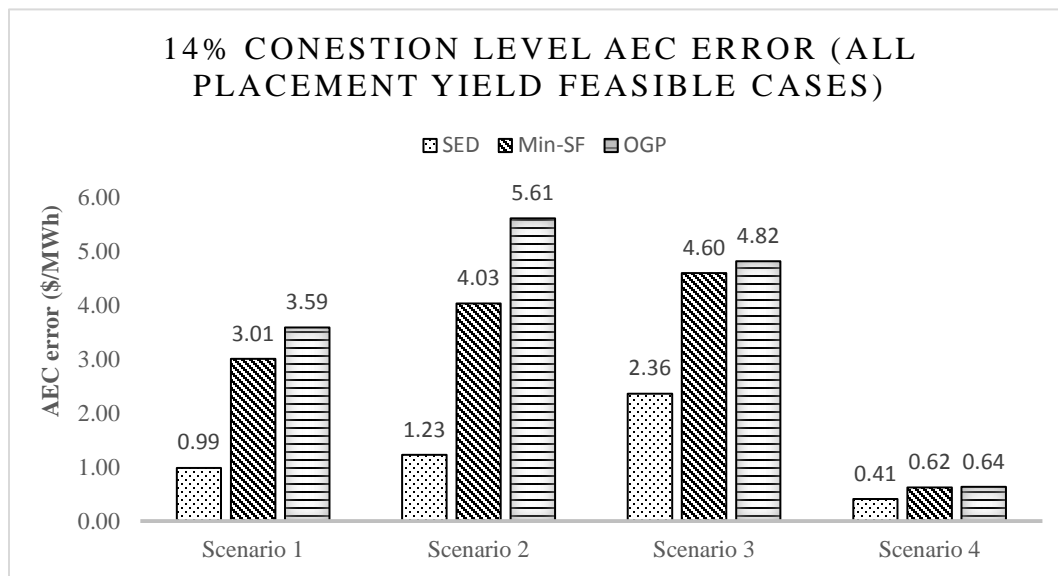


Fig. 2-20 10% Congestion Level AEC error with all placement yield feasible cases

A comparison of the AEC errors for the three different congestion levels over all scenarios shows that the SED method performed better than the OGP and Min-SF methods.

Fig. 2-21-Fig. 2-23 show the number of infeasible cases with different congestion levels for all scenarios.
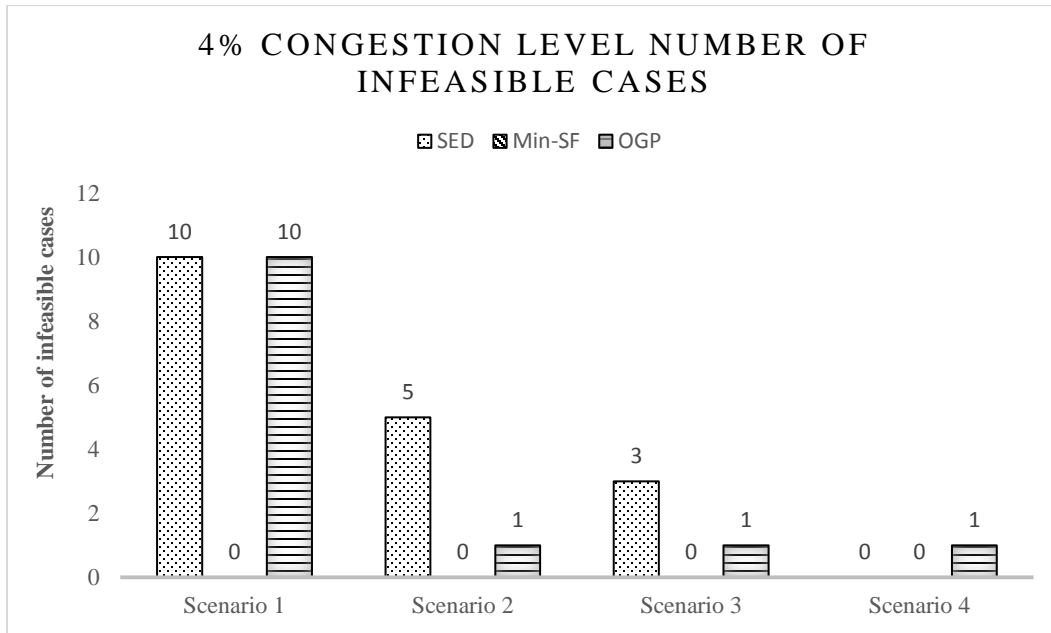


Fig. 2-21 Number of infeasible cases with 4% congestion level system
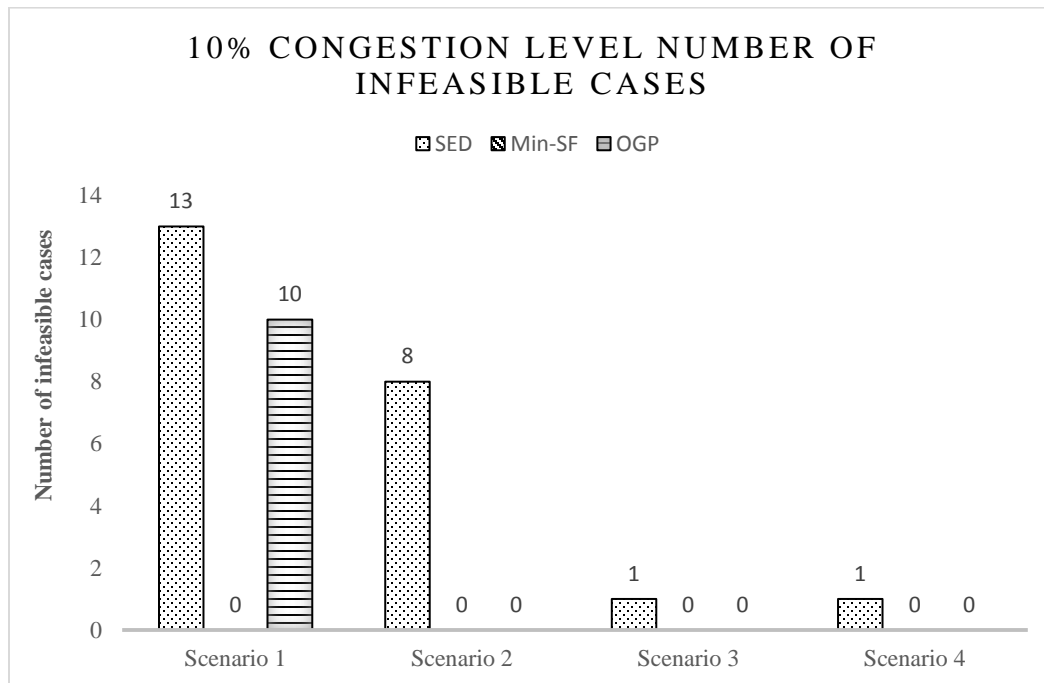


Fig. 2-22 Number of infeasible cases with 10% congestion level system

14% CONGESTION LEVEL NUMBER OF INFEASIBLE CASES
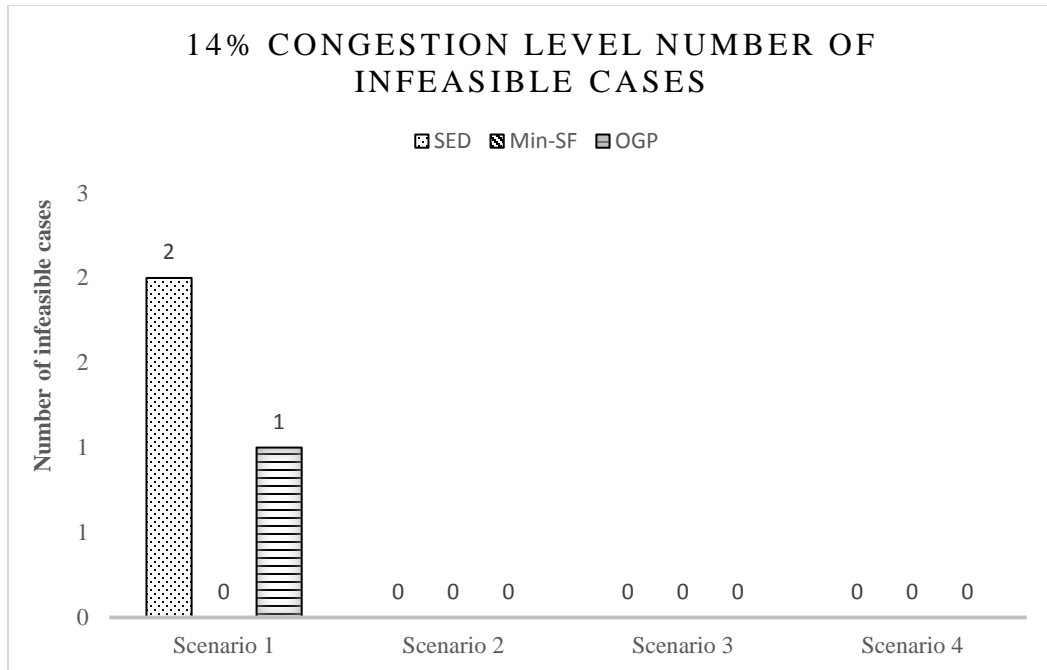
Fig. 2-23 Number of infeasible cases with 14% congestion level system

As shown in Fig. 2-21-Fig. 2-23, (with load redistribution,) all methods yielded feasible cases under the base-case operating point, however, feasibility is not guaranteed when the operating point shifts. The Min-SF method is the most robust method since this method had the highest percentage of cases (tested here) with feasible solutions. The OGP method is less robust than the Min-SF method however it is more robust than the SED method.

The tests on the IEEE 118-bus system showed that the OGP method is less robust and less accurate than the Min-SF method. Compared to the SED method, the OGP method did not show advantages in terms of both accuracy and robustness. Moreover, for large systems the memory requirement is high. As a result, the OGP method was not tested on the ERCOT and the WECC systems in the numerical results that follow.

2.6.3    ERCOT system

The original full ERCOT system is a 5633 bus model. The detailed statistics of the full model are shown in Table 2-4.

Table 2-4 Statistics of the ERCOT Full model

| Number of buses | 5633 |
|---|---|
| Number of branches | 7053 |
| Number of generators | 687 |
| Total load (MW) | 72824.36 |

The statistics of the reduced model of the ERCOT system are shown in Table 2-5.

Table 2-5 Statistics of the ERCOT Reduced Model

| Number of buses | 389 |
|---|---|
| Number of branches | 1658 |
| Number of generators | 687 |
| Total load (MW) | 72824.36 |

The tests on ERCOT were performed using operating conditions obtained by uniform load scaling across the entire system. The cases, in which the full-model dc OPF is infeasible, were eliminated from the test set. The full-model dc OPF had feasible solutions when the load was uniformly scaled between 50% and 110% of base-case load. The average LMP error is shown in Table 2-6.

Table 2-6 ERCOT Test Results of Average LMP Error

| Load Scale (%) | Average LMP Error ($/MWh) | |
| --- | --- | --- |
| | SED | Min-SF |
| 50 | <0.01 | <0.01 |
| 60 | 0.41 | 0.41 |
| 70 | 0.41 | 0.41 |
| 80 | 0.39 | 0.39 |
| 90 | 2.49 | 1.90 |
| 100 | 2.30 | 2.28 |
| 110 | 9.78 | 9.77 |

The AEC error is shown in Table 2-7.

Table 2-7 ERCOT Test Results of AEC Error

| Load Scale (%) | AEC Error ($/MWh) | |
| --- | --- | --- |
| | SED | Min-SF |
| 50 | 3.19E-15 | 1.60E-14 |
| 60 | 0.03 | 0.01 |
| 70 | 0.04 | 0.04 |
| 80 | 0.06 | 0.07 |
| 90 | 0.13 | 0.15 |
| 100 | 0.26 | 0.31 |
| 110 | 0.47 | 0.54 |

As shown in Table 2-6 and Table 2-7 the Min-SF method yielded better accuracy in terms of bus LMP than the SED method. The SED method yielded better AEC accuracy for some operating conditions. The advantage of the Min-SF method over the SED method was small. One reason is that, on most of the branches, the power flows were significantly lower than the branch-flow limits. For example, in the base case only 12 out of 7053 branches are congested.

The reduced-model dc OPF with the SED and the Min-SF methods were feasible under all operating conditions. The robustness of the two methods in these tests was identical because the line flows were far from the branch-flow limits. To further test the robustness performance, another set of tests were performed with reduced line limits. The line ratings were set to 85.6% of the original ratings. For this series of six test scenarios, the dc OPF of the reduced model with the SED method was infeasible in every scenario while for the Min-SF method, all scenarios were feasible. This indicates that the Min-SF method is more robust at times than the SED method, which is the same conclusion reached from the test results from the IEEE-118 bus system.

2.6.4   WECC system

The WECC system statistics are shown in Table 2-8. The reduced-model statistics are shown in Table 2-9.

Table 2-8 Statistics of the WECC Full Model

| Number of buses | 16796 |
|---|---|
| Number of branches | 20280 |
| Number of generators | 3281 |
| Total load (MW) | 1.74E+5 |

Table 2-9 Statistics of the WECC Reduced Model

| Number of buses | 2273 |
|---|---|
| Number of branches | 4433 |
| Number of generators | 3281 |
| Total load (MW) | 1.74E+5 |

The test on the WECC system were performed and the same metrics (as applied on the ERCOT tests) were used to assess performance. On the WECC system, the full model dc OPF was feasible when load was uniformly scaled between 25% and 100% of base-case load. The average LMP error and the AEC error results are shown in Table 2-10 and Table 2-11, respectively.

Table 2-10 Average LMP Error Results of WECC

| Load Scale (%) | Average LMP Error ($/MWh) | |
| | SED | Min-SF |
| --- | --- | --- |
| 30 | 1.39E-14 | 3.33E-14 |
| 40 | 2.23E-8 | 2.43E-9 |
| 50 | 1.22 | 1.22 |
| 60 | 1.06 | 1.05 |
| 70 | 1.99 | 1.98 |
| 80 | 2.53 | 2.52 |
| 90 | 4.51 | 3.77 |
| 100 | 3.51 | 3.32 |

Table 2-11 AEC Error Results of WECC

| Load Scale (%) | AEC Error ($/MWh) | |
| | SED | Min-SF |
| --- | --- | --- |
| 30 | 1.25E-14 | 2.33E-14 |
| 40 | 4.37E-14 | 1.33E-13 |
| 50 | 0.01 | 0.01 |
| 60 | 0.04 | 0.04 |
| 70 | 0.05 | 0.05 |
| 80 | 0.06 | 0.06 |
| 90 | 0.12 | 0.12 |
| 100 | 0.15 | 0.15 |

In terms of the average LMP error, the Min-SF method performed better than the SED method though the advantage is very small. The AEC error yielded by the two methods were almost the same.

2.7    Conclusions

On the lightly congested systems tested here, the performance of the Min-SF method and the SED method were very close. On a tightly constrained system, the Min-SF method is superior to the SED method in terms of the robustness.

# 3 THE OP-WARD REDUCTION

## 3.1 Taxonomy of Network Reduction Methods

For large scale system problems, it is sometimes hard or even impossible to perform analysis or simulations on the full-system model. A reduced "equivalent" model of the original full model is often used. However, the reduced equivalent used is rarely exactly equivalent: a reduced model may be accurate for one study purpose but inaccurate for others. Thus, it is crucial for a researcher to decide which reduction method is required based on the study purposes.
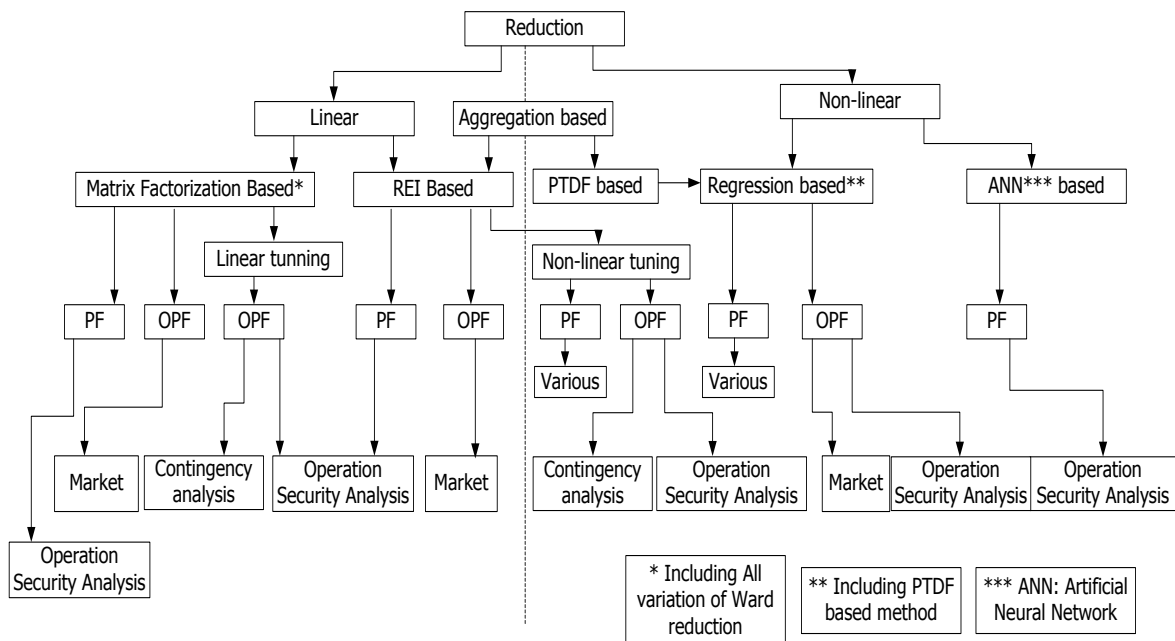
Fig. 3-1 Taxonomy of network reduction

There have been many reduction methods developed. Fig. 3-1 shows a taxonomy of network reduction methods. An inevitable question for researchers is how to determine the best method for their purpose, taking into account the accuracy and complexity of

calculation. An attractive idea is to generate a unified method or framework that can combine all major methods and allow the user to then tailor the reduction method to their needs.

## 3.2    Optimization Based Ward Reduction (OP-Ward) Method

Historically, a Ward equivalent model is generated by matrix factorization [2] which provides the topology, fictitious branch reactance and generator injections at each boundary bus. Rather than using matrix factorization, a different approach is to structure the Ward reduction as an optimization problem. If this optimization approach is successful in duplicating Ward reduction, the next step would be to determine if such an optimization based approach could be generalized to include different variants of the Ward method and variants of the bus aggregation based methods [14]-[25]. The most significant advantage of an optimization-based Ward reduction method is that it is flexible, allowing users to modify the objective function and constraints according to their needs. One implementation is to use the OP-Ward to improve the accuracy and sparsity pattern of the Ward reduction while eliminating high-impedance branches created by the Ward reduction.

Ward reduction performs two operations seamlessly. It performs the network reduction/equivalencing calculation at the same time it parcels generation to guarantee that the reduced network's boundary conditions match those of the full network should it be "cut" at the boundary buses. Modified Ward reduction handles boundary condition matching in various ways [6], [13] and [26]. The idea of the OP-Ward method is to handle the network reduction and boundary condition matching separately. The first step is to duplicate the reduced network (equivalent to that of Ward reduction) but using an

41

optimization-based method. The second step is to perform boundary matching, including generator placement.

Two factors need to be determined to generate the reduced network. One is to determine the topology and the other one is to calculate the network parameters or the equivalent-branch reactance values.

### 3.2.1   Topology of the reduced network

The topology of the reduced network can be determined without performing any numerical calculations. Only symbolic calculations are needed. It is well known that in Ward reduction if one bus is eliminated, equivalent lines will be created to interconnect buses adjacent to the bus that was removed. In other words, during Ward reduction, once an external bus is eliminated, an equivalent branch will be created interconnecting all of its neighboring buses. Fig. 3-2 shows the common "wye-delta" conversion, which can be regarded as a reduction process that eliminates the "star" point bus in the wye connection. The dashed lines in Fig. 3-2 are the equivalent lines created in the reduction process which together with the retained buses construct a complete graph. Calculating the topology of a reduced network may be handled using a simple symbolic calculation that is well known.
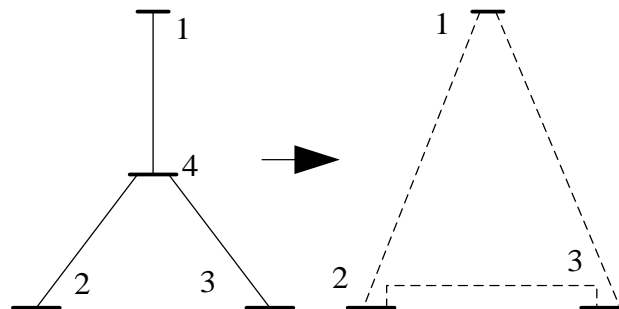


Fig. 3-2 Wye-Delta conversion

With the pre-defined topology of the reduced network obtained from symbolic calculations, we can create the node-branch incidence matrix, $C_r$, of the reduced model in which an element in row $j$ and column $i$ ($C_{r(j,i)}$) is 1 or -1 if and only if branch $j$ connects bus $i$, otherwise the element is 0. The sign depends on the assumed flow direction. The bus admittance matrix, $B_{bus}$, and branch admittance matrix, $B_{branch}$, with variables representing the equivalent lines admittance values can be derived:

$$B_{bus} = C_r^T diag(Y)C_r \tag{3-1}$$

$$B_{branch} = diag(Y)C_r \tag{3-2}$$

where the vector $Y$ includes variables of admittances of the equivalent lines ($y_{i_m i_n}, i_m, i_n \in K_B, (i_m, i_n) \in J_{reduced}$, $K_B$ is the set of boundary buses, $J_{reduced}$ is the set of branches in the reduced model) and values of the admittances of retained lines and the matrix $diag(Y)$ is a diagonal matrix whose diagonal elements are the variables of the equivalent branch reactances and the values of the admittances of the retained branches.

3.2.2   Calculate the reactance value of the equivalent lines

It is well known from Ward reduction that the branch-admittance values of the branches spanning the internal buses or spanning an internal and a boundary bus (internal branches) remain unscathed by the reduction process. Hence the rows corresponding to the internal branches in the branch-admittance matrices of the full model and the reduced model are the same. In this work, superscript $r$ indicates the sub-matrix that only includes data pertaining to the retained branches and retained buses. A schematic of a PTDF matrix is shown in Fig. 3-3:

43

$$\Phi_{full} = \begin{bmatrix} \square & \square & \square & \square & \square \\ \square & \square & \square & \square & \square \\ \square & \square & \square & \square & \square \\ \square & \square & \square & \square & \square \\ \square & \square & \square & \square & \square \end{bmatrix} \left.\vphantom{\begin{bmatrix} \square \\ \square \\ \square \end{bmatrix}}\right\} \text{Retained branches}$$

$\underbrace{\phantom{xxxxxxxx}}$ Retained buses
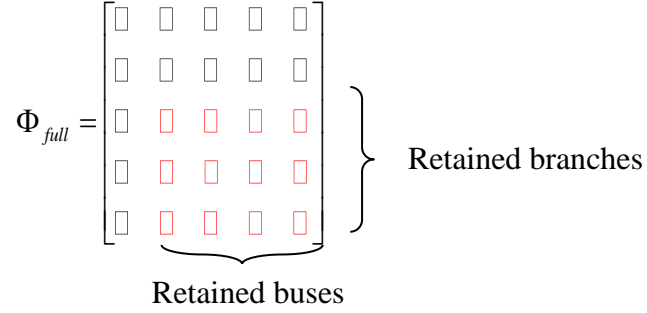
Fig. 3-3 Sub-matrix $\Phi^r$ in the full branch admittance matrix $\Phi_{full}$

In fact, in the PTDF matrix, $\Phi_{full}$, the submatrix corresponding to the retained lines and retained buses ($\Phi^r$, shown as red blocks in Fig. 3-3) remains unchanged after Ward reduction. Based on the two aforementioned properties, we can derive the objective function of the optimization problem:

$$\min \left\| \Phi^r_{full} - \Phi^r_{reduced} \right\|_p \tag{3-3}$$

Using traditional dc-modeling assumptions, the real-power injection at every bus can be calculated as:

$$P_{inj} = B_{bus}\theta \tag{3-4}$$

where $P_{inj}$ is a vector which includes the real-power injections at all buses, $B_{bus}$ is the bus-admittance matrix and $\theta$ is the vector of bus-voltage angles.

Branch flow in the network can be calculated as:

$$P_f = B_{branch}\theta \tag{3-5}$$

where $P_f$ is a vector which includes the real-power flows on all branches.

The PTDF matrix ($\Phi$) describes the relationship between bus-power injection and branch power flow:

$$P_f = \Phi P_{inj} \tag{3-6}$$

Thus combining equations (3-4)-(3-6) we can calculate the PTDF matrix as:

$$\Phi = B_{branch} \cdot B_{bus}^{-1} \tag{3-7}$$

With variables representing the equivalent branch admittances, the symbolic form can be written as:

$$\Phi_{reduced}^r = B_{branch}^r \cdot \left(B_{bus}^r\right)^{-1} \tag{3-8}$$

Both (3-3) and (3-8) involve a symbolic inverse of the bus-admittance matrix in which the reactance of each equivalent line is a variable. As the system size grows, the problem quickly becomes unwieldy. Based on (3-8), the symbolic expression of the branch-admittance matrix can be written as:

$$B_{branch}^r = \Phi_{full}^r \cdot B_{bus}^r \tag{3-9}$$

Based on (3-9) the objective function can be rewritten as:

$$\min \sum_{j \in J^r} \sum_{i \in K_I} \left\| \Delta B_{branch,i,j}^{r,i_{ref}} \right\|_p \tag{3-10}$$

where $i$ is the column index corresponding to bus $i$, $i_{ref}$ is the index of the reference bus, $j$ is the row index corresponding to branch $j$, $J^r$ is the set of indices of the retained branches, and $K_I$ is the set of indices of retained buses.

$$\Delta Branch = \left\| B_{branch,full}^r - \Phi_{full}^r \cdot B_{bus}^r \right\|_p \tag{3-11}$$

Observe that this is an unconstrained minimization problem which is easy to solve. Note that in (3-11) the subscript $p$ indicates the type of norm used in the problem. If $p=1$, the objective is minimizing the sum of absolute value of the mismatches between the elements in the submatrix (denoted with superscript $r$) of the unreduced and reduced

models. With $p=1$, this problem can be reformulated as a linear-programming problem. If $p=2$, the problem is minimizing the sum of square values of the errors. The problem becomes a least-squares problem.

Equation (3-11) can be rewritten as shown in (3-12) from which one can understand the structure of the formulation more clearly,

$$\min_{y_i}\|Ay - b\| \tag{3-12}$$

where

$$A = \begin{bmatrix} PTDF_r \cdot C^T diag(c_1) \\ PTDF_r \cdot C^T diag(c_2) \\ \vdots \\ PTDF_r \cdot C^T diag(c_{N-1}) \end{bmatrix} \tag{3-13}$$

$$b = \begin{bmatrix} b_1 \\ b_2 \\ \vdots \\ b_{N-1} \end{bmatrix} \tag{3-14}$$

and where $C$ is the branch-node incidence matrix of the reduced model; $N$ is the number of buses in the reduced model; $y$ is the vector of the equivalent line susceptances; $y_i$ is the $i$th element in the $y$ vector; $b_i$ is the $i$th column in the partial branch susceptance matrix corresponding to the retained buses and branches.; The dimension of $A$ is $(N-1) \times L_{retained}$ by $L_{eq}$ where $L_{retained}$ and $L_{eq}$ are the number of retained and equivalent branches, respectively.

## 3.3 Rank Deficiency Problem

The aforementioned formulation was tested on various systems and reduction cases. In some pathological cases, the calculated equivalent branch reactance values differed from the equivalent line reactance values calculated from partial LU factorization. It was found that the $\Lambda$ matrix was rank deficient in such cases.

### 3.3.1 Pattern of the pathological cases

#### 3.3.1.1 Star-mesh conversion

The origin of the rank deficiency problem is illustrated by the following example. The star-mesh conversion eliminates the "star point" bus and creates a full graph among the adjacent buses. In Ward reduction, which eliminates buses consecutively, the elimination of one bus is conducted by doing a star-mesh conversion. In other words, the star-mesh conversion is a fundamental and quantum step of the Ward reduction.

A five-bus star-mesh conversion is shown in Fig. 3-4 (the wye-delta conversion shown in Fig. 3-2 is also a star-mesh conversion.)
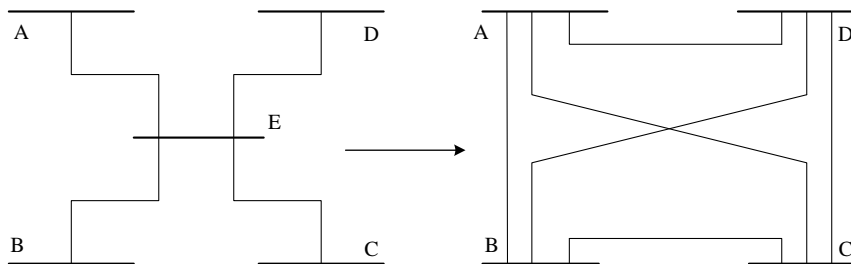


Fig. 3-4 Five-bus star-mesh conversion

Consider the Ward reduction case of eliminating bus E in Fig. 3-4. No physical branches are retained in the reduced model; all branches are fictitious. While there is no

problem applying partial LU factorization to generate the reduced network, the OP-Ward is based on an optimization formulation, rather than partial matrix manipulation. Note that in this case, the matrix $PTDF_r$ is a null matrix in the OP-Ward formulation and the $\Lambda$ matrix in (3-13) is consequently also a null matrix.

### 3.3.1.2 *Conditions of pathological cases*

The star-mesh conversion in the small system reported above is a special pathological case. In fact, it is very rare in an implementation that no branch is retained. However, even if some physical branches are retained, the rank deficiency problem still can and does occur. A general description of the patterns of the pathological cases are discussed as follows. Note these patterns include the star-mesh conversion.

To make the introduction clearer, consider the modified IEEE 14-bus system as an example. The topology of the 14-bus system is shown in Fig. 3-5. Define a radial loop as part of the network which is connected to the rest of the network via one bus referred to as a "semi-radial" bus. For example, each part of the network in the red circle is a radial "loop". Bus 4, 9 and 7 are the semi-radial buses of Loop 1, Loop 2 and Loop 3. Note that the semi-radial loop is same as the cut-node introduced in [14].
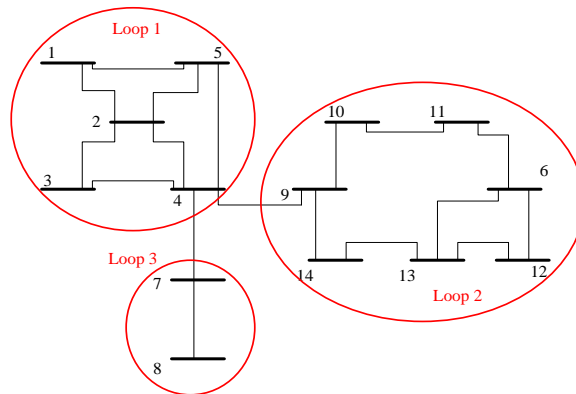


Fig. 3-5 Topology of the modified IEEE 14-bus system

In general, two topology conditions lead to the rank-deficiency problem:

Topology condition 1: There are radially connected buses or radial loops in the original network.

Topology condition 2: If, during a traditional Ward reduction, an equivalent branch is generated which interconnects two different radial loops/radially connected buses.

To illustrate these conditions, consider two reduction cases:

Case 1: Eliminate bus 2.

Case 2: Eliminate bus 9.

Eliminating bus 2 using Ward reduction will create equivalent branches interconnecting buses within Loop 1 thus, Condition 2 is not satisfied and $\Lambda$ is of full rank. For Case 2, eliminating bus 9 will create three equivalent branches which interconnect buses 4, 10 and 14 (in delta form.) Two of these branches are interconnecting radial Loop 1 and radial Loop 2. By Condition 2, this case will (and does) produce the rank deficiency problem.

## 3.3.2  Remedy to the problem

The star-mesh conversion problem reveals that some reduction cases retain no branches therefore, the OP-Ward is not usable. A method to solve this problem is to add pseudo branches in the original network [30].

Fig. 3-6 shows the same star-mesh conversion as shown in Fig. 3-4 but with added pseudo branches shown as green lines. As one can see, the reduction case which eliminates bus E now retains two pseudo branches and the OP-Ward reduction can be formulated based on these two retained branches.
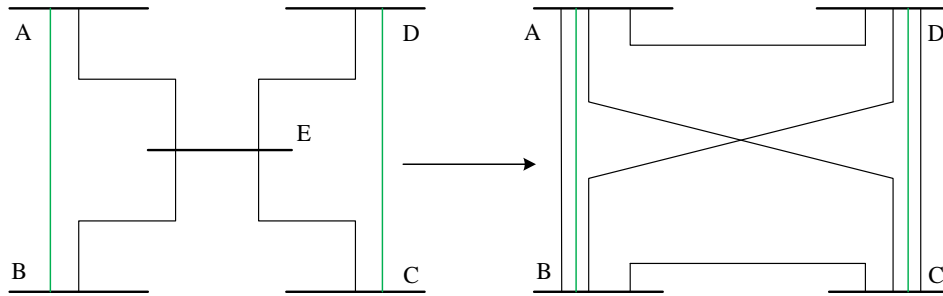
Fig. 3-6 Five bus star-mesh conversion with pseudo branches

### 3.3.2.1 Brute-Force Approach

Two heuristic guidelines were used for constructing a brute-force approach for adding pseudo branches to obtain a $\Lambda$ matrix of full rank.

1). The added pseudo branches must not change the *reduced* network topology or change the reactance value of the equivalent branch from what it would be without the pseudo branches .

2). The added pseudo branches must solve the rank deficiency problem.

To satisfy the first guideline, the pseudo branch must interconnect only the boundary buses.

To satisfy the second guideline, the number of pseudo branches must be sufficient in number to eliminate the rank deficiency problem. A brute-force approach (BFA) based on this heuristic is to add one pseudo branch parallel to every equivalent branch.

While this strategy is guarantee to solve the problem, it will significantly increase the complexity of the calculation by increasing the dimension of the $\Lambda$ matrix. It is desirable to find a minimum set of pseudo branches needed to minimize the complexity. Next, an improved strategy is introduced for finding what is hoped is a near minimum set of pseudo branches.

*3.3.2.2   Minimum Set Selection Strategy (MSSS)*

The MSSS is based on QR factorization [33], [34]. This strategy is an iterative method used to identify the location of pseudo-branches needed to maintain the full rank of the $\Lambda$ matrix. In this approach, rank-revealing QR factorization is used to identify the subset of the most linearly independent columns of the $\Lambda$ matrix. The remaining, linearly dependent columns, each of which corresponds to a fictitious/equivalent branch, identify the location where pseudo-branches need to be added. Consider an *m*-by-*n* $\Lambda$ matrix (*m*>*n*) and rank($\Lambda$) = *k* < *n*. The use of QR factorization with column pivoting can find the *k* linearly-independent columns and also the (*n-k*) linearly-dependent columns. Since each column in the $\Lambda$ matrix corresponds to an equivalent branch, there will be (*n-k*) equivalent branches which are linearly dependent. In parallel with one of the (*n-k*) equivalent branch we add a pseudo branch in the original network and recalculate the $\Lambda$ matrix. If the new $\Lambda$ is rank deficient, we repeat the above steps by performing QR factorization with column pivoting and then add another pseudo branch to the original network. We repeat these steps until the $\Lambda$ matrix is of full rank. Since the number of rows is usually significantly greater than the number of columns in the $\Lambda$ matrix, it is more efficient to perform QR factorization on the ($\Lambda^T\Lambda$) matrix than on the $\Lambda$ matrix.

The MSSS is tested and the test results are introduced in section 3.6.

3.4   Improve Ward Reduction

Clearly, using the OP-Ward approach is more computationally complex than using traditional Ward reduction however it conveys certain advantages. For example, this process can be used to improve Ward reductions that are used in practice as follows.

Typically, a Ward reduction creates a dense reduced model. One way to improve the sparsity pattern of the reduced model is to eliminate the high-reactance equivalent branches. Setting the high-reactance threshold value of the high-reactance equivalent branches to be eliminated is a tradeoff between accuracy and sparsity. If the threshold is too large, then eliminating the high reactance branches cannot effectively improve the sparsity pattern. If the threshold is too small, the reduced model will not match the original model accurately.

With the OP-Ward method, one can eliminate the equivalent branches by constraining their susceptances to be equal to zero in the optimization formulation. In this case, the OP-Ward problem is formulated as (3-15) and (3-16),

$$\min \| \Lambda y - b \| \tag{3-15}$$

s.t.

$$y_{w,i} = 0, i \in \Psi \tag{3-16}$$

where $\Psi$ is the set of all equivalent branches to be eliminated from the reduced model. The reduction is then a two-step process. First, traditional Ward could be used to identify all high reactance equivalent branches and assign them to the set $\Psi$. The second step is to solve (3-15) and (3-16) with the pre-defined $\Psi$, yielding the optimal susceptance values of all retained equivalent branches. Compared to the conventional method which directly eliminates the high reactance equivalent branches, the OP-Ward is more accurate in terms of matching the branch flows over a range of operating conditions, as will be shown later.

Solving (3-15) and (3-16) does not require using a constrained optimization solver. One can simply eliminate the columns in the $\Lambda$ matrix which corresponding to the variables in $\Psi$. Denote the updated $\Lambda$ matrix as $\Lambda_0$. The solution is calculated as (3-17).

$$y = \left( \Lambda_0^T \Lambda_0 \right)^{-1} \Lambda_0^T b \tag{3-17}$$

## 3.5 A Unified Framework of dc Network Reduction

### 3.5.1 Inter-zonal reduction

In references [14]-[16], the inter-zonal reduction was introduced. The inter-zonal reduction aggregates all buses into the respective zones. The topology of the reduced network is pre-defined based on the original model topology. The equivalent branch reactances are calculated by solving an optimization problem formulated (3-18),

$$\min_{y_{\text{int}}^{eq}} \left\| PTDF_r C_r^T diag\left( y_{\text{int}}^{eq} \right) C_r - diag\left( y_{\text{int}}^{eq} \right) C_r \right\| \tag{3-18}$$

where $y_{\text{int}}^{eq}$ is the vector of the equivalent branches susceptances.

The derivation of the reduced-model PTDF matrix $PTDF_r$ is based on (3-19) and (3-20),

$$PTDF_r \Gamma_{inj} P_{inj} = \Gamma_{flow} PTDF \cdot P_{inj} \tag{3-19}$$

$$PTDF_r = \Gamma_{flow} PTDF \cdot \Gamma_{inj}^T \left( \Gamma_{inj} \Gamma_{inj}^T \right)^{-1} \tag{3-20}$$

where $\Gamma_{inj}$ is the matrix which sums the power injections of buses into different zones; $\Gamma_{flow}$ is the matrix which sums the branch flows in the original network into the inter-zonal branch flows. In (3-19), both sides calculate the inter-zonal branch flows. In (3-20), the $PTDF_r$ matrix is calculated. The dimension the matrix $\Gamma_{inj}$ is $N_{zones} \times N_b$ where $N_{zones}$ is the number of zones in the network is. Since $\Gamma_{inj}$ is not a square matrix, calculation of $\Psi^r$ is an over-determined problem.

To find the non-trivial solution one needs to add constraints, shown in (3-21),

$$\left| y_{\text{int}}^{eq} \right| \geq M \tag{3-21}$$

where *M* is a very small number.

The inter-zonal reduction is formulated with the objective (3-18) and subject to the constraint (3-21). The solution of the problem can be obtained based on the eigenvalue decomposition [15].

3.5.2   The framework

Under the dc assumption, the target of the Ward reduction and the inter-zonal reduction is to preserve the relationship between the power injections of retained buses/zones and the flows between them. This property makes them share the same objective: preserve the known part of the reduced-model PTDF matrix.

For the inter-zonal reduction, the buses are aggregated to the respective zones. Thus, in (3-19) and (3-20), the elements in $\Gamma_{inj}$ are equal to either one or zero indicating if the bus is in the respective zone. For the OP-Ward reduction, the external power injections are split and distributed to the boundary buses. One cannot obtain the $\Gamma_{inj}$ matrix for the OP-Ward reduction in the same way. Therefore, the inter-zonal reduction preserves the calculated reduced-model PTDF while the OP-Ward preserves the same fraction of the full-model PTDF as Ward-reduction preserved, that is, the portion corresponding to the retained buses and branches.

Because the inter-zonal reduction preserve no branches in the reduction, the inter-zonal reduction process must solve an *Ax*=0-type problem. Thus, one needs to add additional constraints, (3-21), to avoid the trivial solution that all variables equal to zero. The OP-Ward framework proposed here, devolves to the inter-zonal approach if none of the original

system is preserved. But more importantly, it shows that if at least one real branch is preserved in the system, the solution process becomes much simpler. The solution is then obtained by solving an overdetermined *Ax=b* problem.

The unified objective of the two reduction methods allows us to use one framework to do both reductions shown in (3-22),

$$\min_{y^{eq}} \left\| PTDF_r \cdot C_r^T diag\left(y^{eq}\right)C_r - diag\left(y^{eq}\right)C_r \right\| \tag{3-22}$$

where $y^{eq}$ is the vector of equivalent branch susceptance.

## 3.6    Numerical Tests

The tests in this section focus on two objectives. One is to verify whether the OP-Ward can replicate the Ward reduction results. The other one is to verify whether the OP-Ward can yield more accurate results in cases where high-reactance equivalent branches are eliminated.

## 3.6.1    Replicating Ward reduction

### 3.6.1.1    Test cases and metrics

The OP-Ward method and the two proposed remedies to the rank deficiency problem were tested on systems including the IEEE 118-bus system, the IEEE 300-bus system and an ERCOT 557 bus system. The objective of the tests is twofold. One is to verify whether the OP-Ward can precisely calculate the equivalent line reactances of a reduced model giving the same values (with reasonable precision) as the Ward method. The other one is to evaluate the efficiency of the MSSS.

The metric to evaluate the accuracy of calculation of equivalent line reactance is the branch-reactance error:

$$X_{Error} = \max_{\forall l \in L} |x_l - \hat{x}_l| \qquad (3\text{-}23)$$

where $X_{Error}$ is the calculated error of equivalent line reactance, $x_l$ and $\hat{x}_l$ are the values of the $l$th equivalent line reactance calculated by partial LU factorization and the OP-Ward reduction, respectively, and $L$ is the set of all equivalent branches.

The efficiency of MSSS is measured by two metrics. Denote the number of pseudo branches added to the network by the MSSS and the BFA by $N_{branch}^{MSSS}$ and $N_{branch}^{BFA}$, respectively. The first comparison is between the $N_{branch}^{MSSS}$ and $N_{branch}^{BFA}$. As mentioned, the added pseudo branches affect the size of the $\Lambda$ matrix. Denote the $\Lambda$ matrix of the networks with pseudo branches added by MSSS and BFA respectively by $\Lambda_{MSSS}$ and $\Lambda_{BFA}$. The second comparison is between the number of rows in the $\Lambda_{MSSS}$ and $\Lambda_{BFA}$. The two metrics together show how effective the MSSS can be in terms of reducing the number of pseudo branches and the size of the $\Lambda$ matrix.

The statistics of the three test cases are shown in Table 3-1. The fourth column in the table shows the number of equivalent branches that generated by the Ward method which is also the number of the variables in the optimization problem.

Table 3-1 Statistics of Test Cases

|  | System | Number of external buses | Number of equivalent branches |
|---|---|---|---|
| 1 | IEEE 118-bus | 83 | 338 |
| 2 | IEEE 300-bus | 200 | 384 |
| 3 | ERCOT 557-bus | 200 | 4122 |

The diagram of the IEEE 118-bus system and its 35-bus reduced model are shown in Fig. 2-3 and Fig. 2-4 respectively. The IEEE 300-bus and its 100-bus reduced model are shown in Fig. 3-7 and Fig. 3-8 respectively.
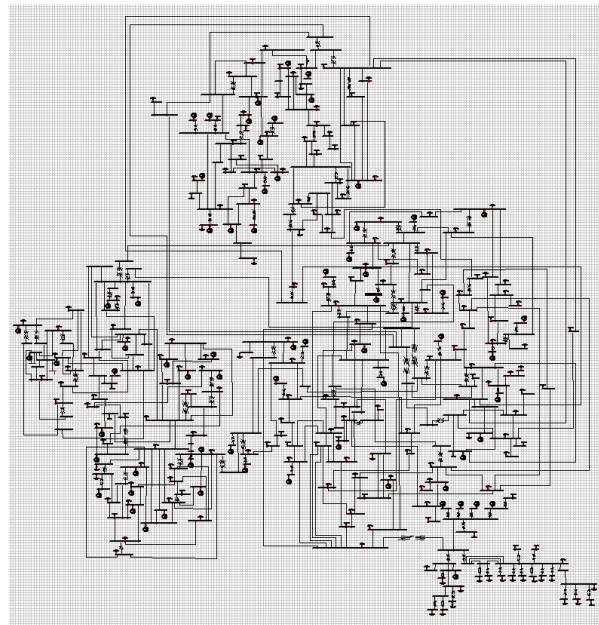


Fig. 3-7 IEEE 300-bus system
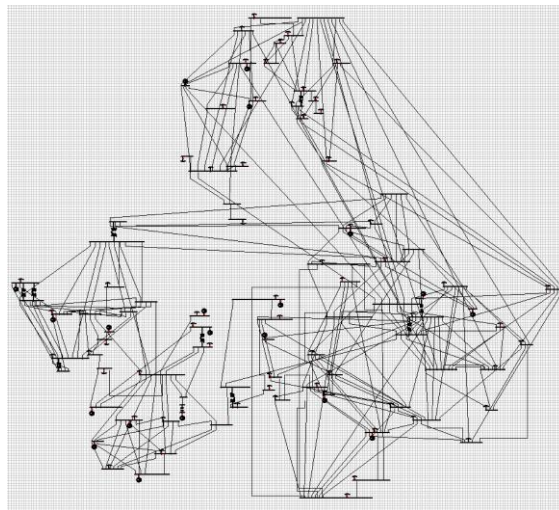


Fig. 3-8 Reduced IEEE 300-bus system (100 bus)

The diagrams of the ERCOT 557 bus and ERCOT 357 bus systems are shown in Fig. 3-9 and Fig. 3-10 respectively.
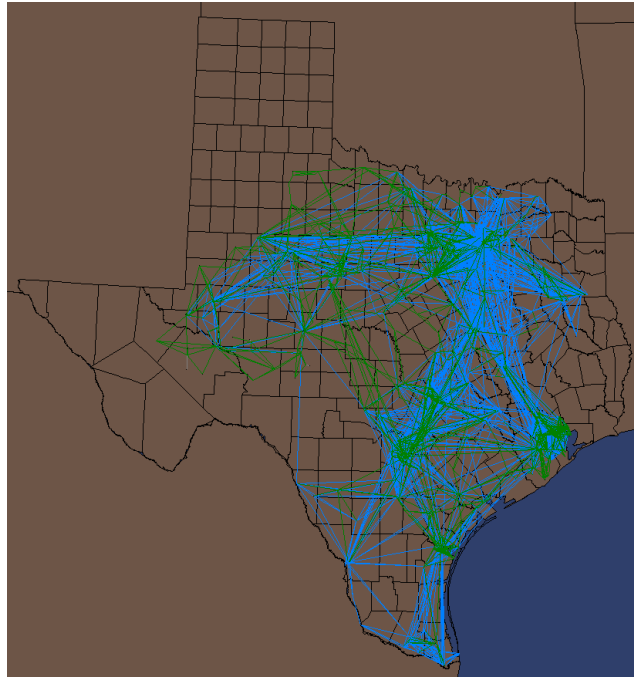


Fig. 3-9 ERCOT 557 bus system
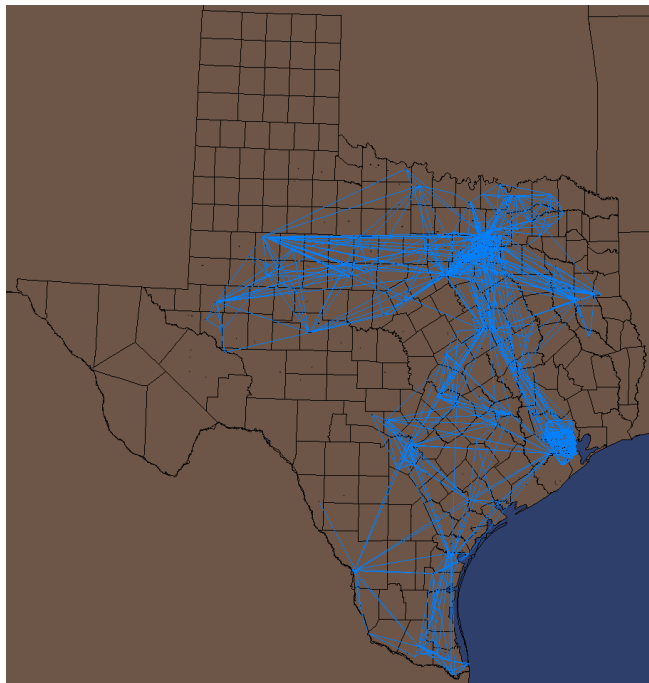


Fig. 3-10 Reduced ERCOT 557 bus system (357 buses)

*3.6.1.2   Results*

The results of the three test cases are shown in Table 3-2. In Table 3-2, the second

column is the degree of rank deficiency without adding any pseudo branches. Parameters

$N_{row}^{BFA}$ and $N_{row}^{MSSS}$ are the number of rows of the $\Lambda_{BFA}$ and $\Lambda_{MSSS}$ matrices. In the table, $X_{Error}$

is the value of the reactance calculation error metric, (link equation in here), with the

pseudo branches added by the MSSS method.

Table 3-2 Test Results of OP-Ward Reduction

| System | Degree of rank deficiency | $N_{branch}^{BFA}$ | $N_{branch}^{MSSS}$ | $N_{row}^{BFA}$ | $N_{row}^{MSSS}$ | $X_{Error}$ |
|--------|---------------------------|--------------------|---------------------|-----------------|------------------|-------------|
| IEEE-118 | 22 | 338 | 9 | 12,705 | 1,190 | 1.4E-11 |
| IEEE-300 | 80 | 384 | 34 | 43,600 | 8,600 | 2.7E-12 |
| ERCOT 557 | 176 | 4122 | 81 | 67,292 | 10,981 | 1.6E-13 |

The $X_{Error}$ value is very small (on the order of expected round off error) which

indicates the OP-Ward reduction yielded results of accuracy consistent with that of the

conventional Ward reduction. The BFA method yielded an $X_{Error}$ value which was on the

same order of magnitude as that produced by the MSSS. The MSSS can significantly

reduce the number of pseudo branches as compared to the BFA, and which consequently

can reduce the dimension of the $\Lambda$ matrix by 80% for cases tested here. Thus the OP-Ward

and MSSS are shown to be accurate and computationally practical for the cases tested here.

3.6.2   Improved Ward reduction

As introduced, Ward reduction creates high-reactance equivalent branches within the

reduced model. Such high reactance branches are typically eliminated using a reactance

threshold. By doing this, sparsity of the reduced model is increased. In the IEEE 118-bus system, the typical branch reactance value is approximately 0.05 pu. To test the accuracy of OP-Ward versus traditional Ward, a range of reactance threshold values for eliminating equivalent branches was chosen from 0.5 pu. to 10 pu. The flows on the retained branches in the reduced model were compared to those in the full model.

The metric used to quantify branch-flow errors in percent is shown in (3-24),

$$Error_{flow} = \max_i \left| \frac{P_{flow,i}^{OP-Ward} - P_{flow,i}^{Ward}}{Lim_i} \right| \times 100, i \in K_{Lre}^{W} \tag{3-24}$$

where $P_{flow,i}^{OP-Ward}$ and $P_{flow,i}^{Ward}$ are the flow on the $i$th retained branch in the base case of OP-Ward reduction and Ward reduction, respectively; $Lim_i$ is the line rating the $i$th retained branch; $K_{Lre}^{W}$ is the set of all retained branches. The error metric quantifies the magnitude of the largest branch-flow error as a percentage of the line-flow limit.

### 3.6.2.1  IEEE 118-bus system

A modified IEEE 118 bus system was used which includes line ratings for all branches in the system [35].
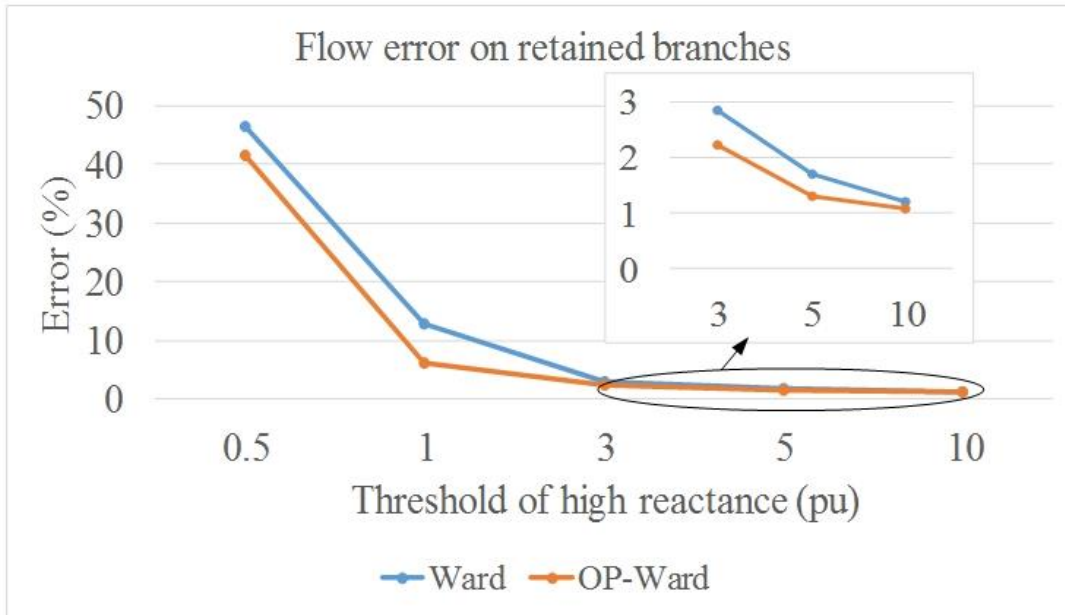
Fig. 3-11 Maximum branch flow error on retained branches in IEEE 118-bus system tests (high reactance equivalent branches eliminated)

The curves in Fig. 3-11 show the results of the maximum branch flow error on retained branches versus threshold values for elimination of high-reactance lines. In general, OP-Ward improves the line-flow accuracy on the retained branches. When the threshold is high, the errors of both methods are low.

Table 3-3 shows the number of equivalent branches created in the reduction process as a function of different threshold settings. Choosing a low threshold improves the sparsity pattern because more equivalent branches are eliminated. However, as expected, the accuracy worsens as more branches are eliminated. In the tests reported here, when the threshold was set as 1.0 pu, the Ward and the OP-Ward methods yielded 13% and 6% maximum branch-flow errors, respectively. In addition, choosing 1.0 pu as the threshold significantly reduced the number of fictitious branches.

Table 3-3 Number of the Equivalent Branches and the Threshold of High Reactance

| Threshold (pu) | Number of equivalent branches |
| --- | --- |
| None | 213 |
| 10 | 94 |
| 5 | 88 |
| 3 | 77 |
| 1 | 46 |
| 0.5 | 29 |

The tests showed that, for this case, the OP-Ward is numerically stable and can be used to increase sparsity of the reduced model while maintaining more acceptable branch-flow errors.

### 3.6.2.2  *ERCOT 6073-bus system*

The diagram of the ERCOT 6073-bus system is shown in Fig. 3-12. The statistics of the system are shown Table 3-4.

A 6073- to 277-bus reduction was generated for the ERCOT system which preserved the high voltage buses (voltages greater than or equal to 230 kV). The diagram of the reduced model is shown in Fig. 3-13. (The equivalent branches are not shown in the figure). In total, there are 6009 equivalent branches generated in the reduction.
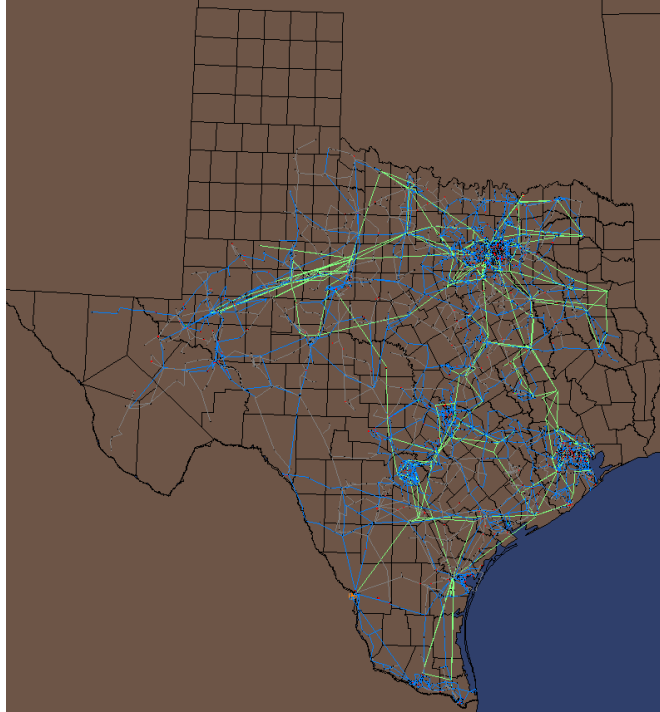
Fig. 3-12 ERCOT 6073 bus system
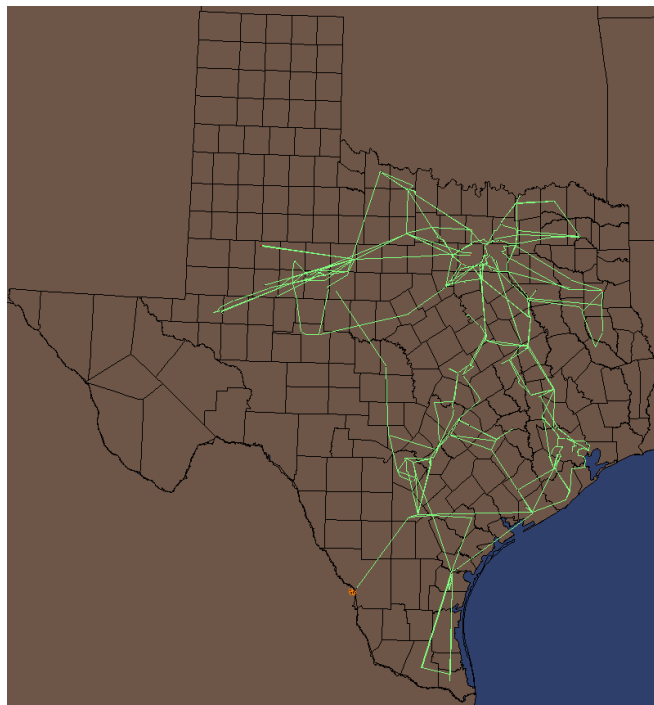


Fig. 3-13 277 bus reduced ERCOT model

Table 3-4 Statistics of the ERCOT System

| | |
|---|---|
| Number of buses | 6073 |
| Number of branches | 7504 |
| Number of generators | 687 |
| Total loads (MW) | 7.28E4 |
| Total generation capacity (mw) | 1.02E5 |

The reduction of the system is very aggressive. (About 95% of buses were eliminated.) This resulted in a large number of high-reactance branches in the reduced model. A histogram of the branch reactances in the reduced model, shown in Fig. 3-14, shows that about 68% branches are high reactance branches whose reactance values are greater or equal to 50 pu.
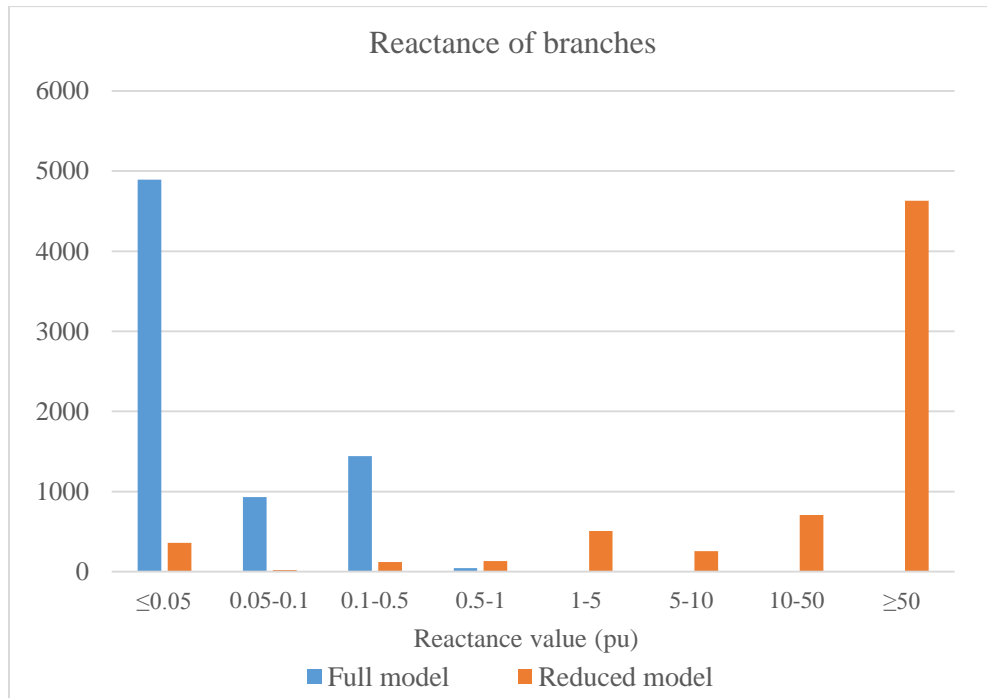


Fig. 3-14 Histogram of branch reactance values in the full and reduced models

The error of the power flow on the retained branches was calculated using (3-24) and plotted versus threshold values as shown in Fig. 3-15 using a logarithmic scale. As can be seen from Fig. 3-15, for both the Ward and the OP-Ward reduction, if the threshold was chosen less than or equal to 20 pu the error was prohibitively large, greater than 50%. When the threshold was chosen as 30 pu, the error of the Ward and the OP-Ward were 61.5% and 20.4% respectively. When the threshold was chosen as 60 pu, the error of the Ward and the OP-Ward were 30.3% and 5.6% respectively. The number of equivalent branches in the reduced model with different threshold values for high reactance fictitious branches is shown in Table 3-5.

Table 3-5 Number of Equivalent Branches in the Reduced Model with Different Threshold of High Reactance

| Threshold | Number of equivalent branches |
|---|---|
| 20 | 1485 |
| 30 | 1669 |
| 60 | 2307 |

Another test was performed to validate the reduced-model performance under different operating conditions. Perturbations (in percentage of base loading) were added to all power injections in the full and the reduced models at the retained buses. For every bus, the perturbation was a random number in a fixed range, 0-5%, 5-10%, etc. For every perturbation range, the 100 sets of such random numbers were generated, and the line flows calculated on the full and reduced models were compared. The maximum error was calculated.

Results shown in Fig. 3-16 indicate that the OP-Ward can approximate the flows on the retained branches over a range of operating condition better than the Ward method when the high-impedance branches were eliminated. An error duration curve shown in Fig. 3-17 reveals the error distribution among all retained branches in the 100 runs under the 10-15% load perturbations. The results shown in Fig. 3-17 indicates that the OP-Ward is significantly more accurate than the Ward reduction and more than 92% of errors were lower than 10%.
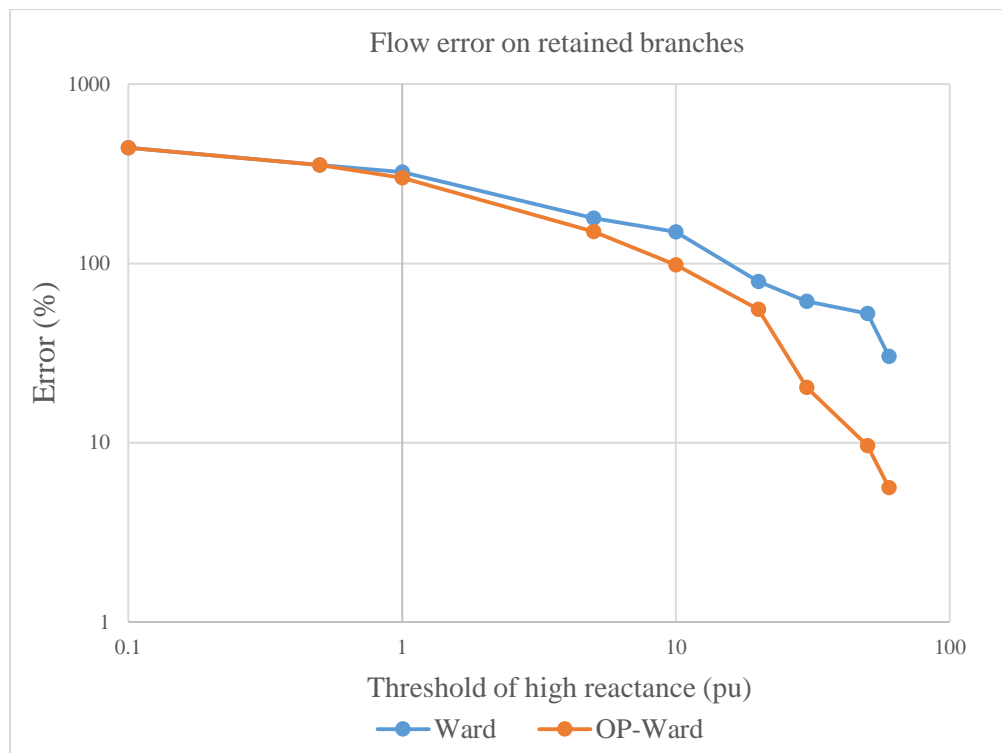


Fig. 3-15 Flow error on the retained branches
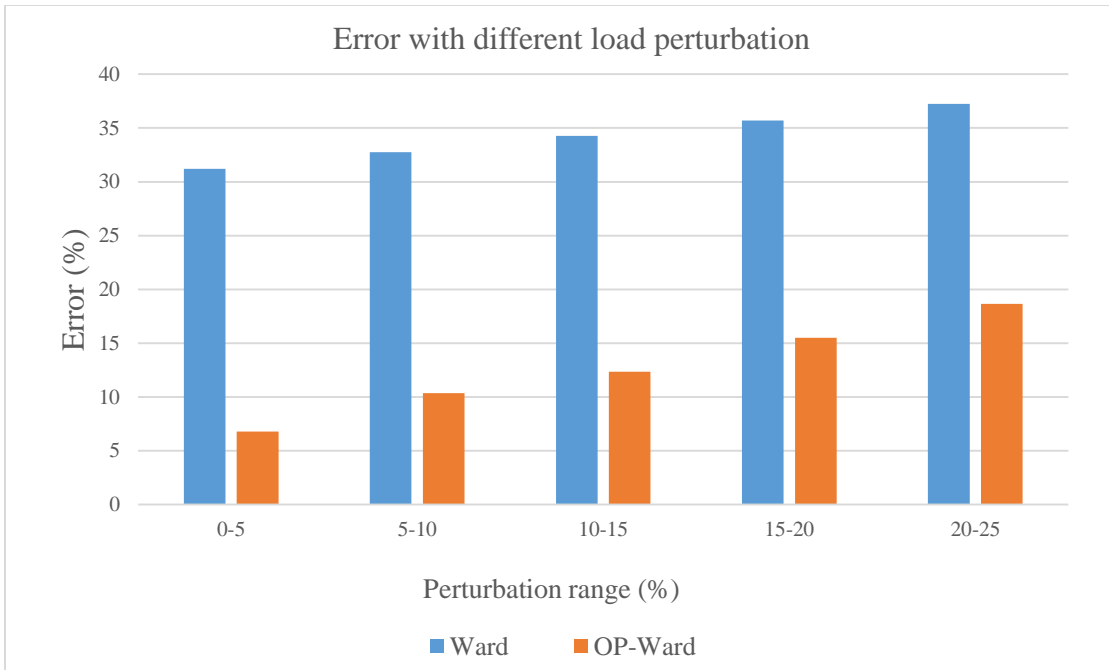
Fig. 3-16 Flow error under different operating conditions
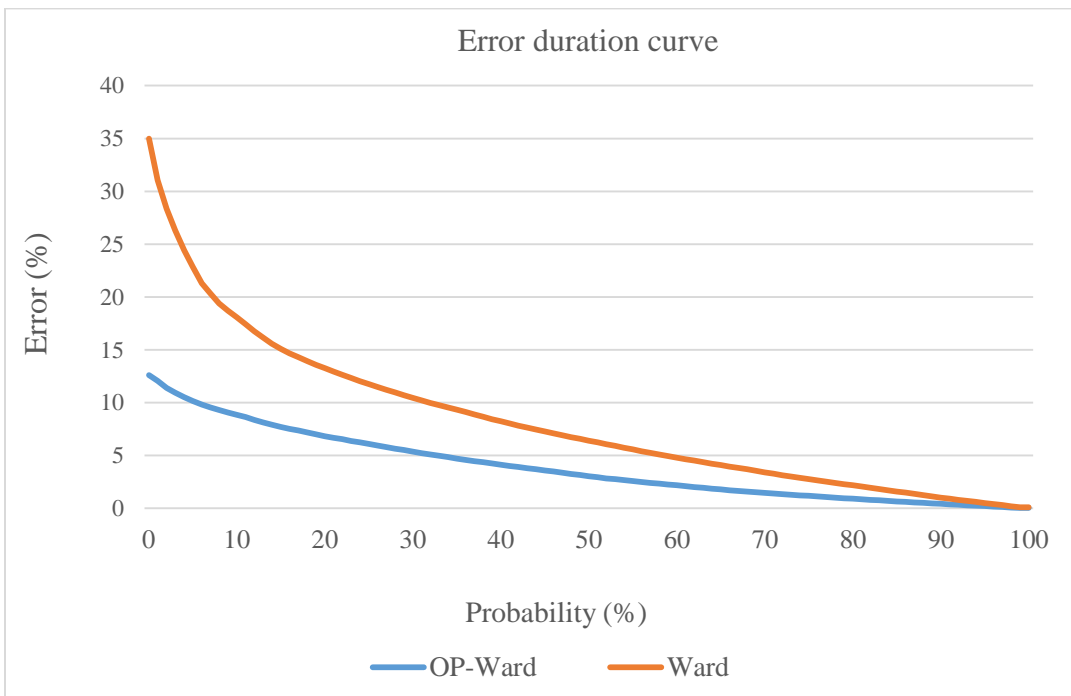


Fig. 3-17 Error duration curve under 10-15% load perturbation

3.7    Conclusions

A new approach for generating the Ward reduction is introduced which casts the Ward reduction as an optimization problem. The objective of the OP-Ward is to preserve the PTDF submatrix which corresponds to the retained buses and branches in the original model. We show that the OP-Ward framework encompasses the inter-zonal (bus aggragation) reduction and has numerical advantages over the strict inter-zonal approach if at least one branch in the original network can be retained.

The proposed OP-Ward reduction method can be used to improve upon the Ward reduction when eliminating high-reactance branches is desired, a strategy often employed to improve sparsity of the reduced model. While there is an expected tradeoff between the accuracy and the sparsity we show that the OP-Ward provides superior performance over traditional Ward as measured by branch-flow accuracy.

# 4 HOLOMORPHIC EMBEDDING NETWORK REDUCTION METHOD

## 4.1 Background Introduction

The conventional network reduction methods like Ward or REI methods, can match the original system solution with high accuracy at the base case. However, when the operating condition deviates, the accuracy deteriorates. The reason is that these methods treat the power injections at the boundary buses from the external network (external injections) and the losses of the external network as fixed values. However, when the operating condition changes, the external injection and the external system losses also change. The conventional reduction methods are unable to approximate the changes of power injection at the boundary buses and external system losses, especially the change of the reactive power generation of external generators. Some methods, like the extended Ward, were proposed to deal with this problem but still lack accuracy. Some methods, like S-REI [7] and X-REI [9] require online calibration which may increase the computational burden. In this chapter, a novel HE-based network-reduction method is introduced, which takes the advantage of the HE-based power-flow method and can perform nonlinear approximation to the external power injections. Test results show that the HE reduction method is superior to the conventional methods.

### 4.1.1 The ac power-flow problem

The ac power flow problem is formulated in order to determine the value of the following four quantities at every bus:

- Voltage magnitude $|V|$

- Voltage magnitude $\theta$

- Net real power injection $P$

- Net reactive power injection $Q$

Each bus in the network has two quantities specified and two variables to be determined. The assignment of the specified variables of every bus depends on the type of the bus. Typically, the buses are categorized into three types:

- Slack bus: provides voltage reference of the network.

- PQ bus: also called the load bus at which the net-real and net-reactive power injections are specified.

- PV bus: also called a generator bus at which the bus voltage magnitude and the net-real-power injection are specified.

Table 4-1 shows the specified and unknown variables of each type of buses.

Table 4-1 Variables of Different Bus Types

| Bus type | Specified | Unknown |
|---|---|---|
| slack bus | $|V|, \theta$ | $P, Q$ |
| PQ bus | $P, Q$ | $|V|, \theta$ |
| PV bus | $P, |V|$ | $Q, \theta$ |

Based on the specified bus variables and the network parameters (including the branch admittances and shunt admittances), the ac power-flow solution is calculated by solving the power-balance equations (PBEs) (in current-balance form for the purposes here) described in (4-1). Noted that in the PBE, the bus voltage is complex ($V=V_{re}+jV_{im}$)where $V_{re}$ and $V_{im}$ are the real and imaginary parts respectively. The net real- and reactive-power

70

injections (P and Q) are the difference between the generation and load: $P = P^g - P^l$ $Q = Q^g - Q^l$.

$$\sum_{k \in K} Y_{ik} V_k = \left( \frac{P_i^g + jQ_i^g - P_i^l - jQ_i^l}{V_i} \right)^* , \quad i \in K \tag{4-1}$$

In (4-1), $Y_{ik}$ is the $(i, k)$ element in the bus admittance matrix; $V_i$ and $V_k$ are the complex bus voltages of bus $i$ and bus $k$, respectively; $P_i^l$ and $Q_i^l$ are the real and reactive loads, respectively, at bus $i$; $P_i^g$ and $Q_i^g$ are the real and reactive generation values, respectively, at bus $i$ (equal to zero for a PQ buses).

### 4.1.2   Conventional methods

The most widely used conventional methods are iterative methods. Such methods include the Newton-Raphson method, Gauss-Seidel method, and fast-decoupled methods [36]-[39]. These methods are usually able to solve the problem efficiently if the operating condition is not close to a saddle-node bifurcation point (SNBP). However, if the operating condition is close to the SNBP the Jacobian matrix calculated at every iteration is close to singular or, at minimum, ill-conditioned and the iteration process can diverge. If the process is divergent or non-convergence (oscillates), the power flow program may terminate for a number of reasons, e.g., division by zero, but often ends after reaching a programmed limit on the maximum number of iterations. In this case, it is impossible, using the program's output, for the user to judge whether:

1)  A solution exists, but the algorithm did not converge.

2)  A solution does not exist.

The continuation power flow (CPF) [40] is an improved iterative method. Compared to the full Newton-Raphson method, this method adds a new load parameter in the problem formulation and uses a predictor-corrector scheme to find the solution on the trajectory. With the new parameter, the Jacobian matrix calculated at each iteration is non-singular even when the operating condition is close to the bifurcation point. Thus, the CPF is widely used to estimate the voltage collapse point [41]. However, as an iterative method, the convergence of CPF depends on proper selection of the initial solution and the step size between consecutive iterations. In other word, the CPF cannot guarantee convergence [42]. In subsequent sections the holomorphic-embedding-based method is applied to the power flow problem.

## 4.2 HE Based Power Flow Formulation

Both sides of the PBEs are formulated to balance the current injection at every bus as shown in (4-1). With the HE technique, the solution of the unknown voltage variables will be holomorphic in the variable $\alpha$ and therefore must have a Maclaurin series [44]; hence, the bus voltage of bus $i$ may be approximated as the truncated series:

$$V_i(\alpha) = V_i[0] + V_i[2]\alpha^{2\cdots} + V_i[n]\alpha^n \tag{4-2}$$

where $V_i(\alpha)$ is the Maclaurin series of complex voltage solution of bus $i$; $V_i[n]$ is the complex-valued coefficient of the $n$th term in the power series.

The aforementioned three different types of buses must be modelled in the power-flow problem. The holomorphic embedding approach has many formulations [43]. To be useful for the network reduction application envisioned here, the reduced model must be valid over a range of different operating conditions. Hence the ac power-flow problem is

72

represented by a scalable HE formulation. The following subsection gives the HE equations in scalable form.

## 4.2.1 Scalable form of HE

- Slack bus

For the slack bus, the voltage magnitude and voltage angle are specified. The power injection of the slack bus provides power which balances the network power injections and losses. The model of the slack bus can be simply written as,

$$V_0(\alpha) = V_{slack} \tag{4-3}$$

where $V_{slack}$ is the specified complex bus voltage of the slack bus; in this work, a single slack bus is assumed whose index is assumed to be 0.

- PQ bus

For a PQ bus, the relationship between the complex voltage and the load (real and reactive) is described as shown in (4-4),

$$\sum_{k \in K} Y_{ik} V_k(\alpha) = \alpha \left( -P_i^l - jQ_i^l \right)^* W_i^*(\alpha^*), \quad i \in K_{pq} \tag{4-4}$$

where, $K_{pq}$ is the set of all PQ buses $W_i(\alpha)$ is the reciprocal of the voltage power series $V_i(\alpha)$ satisfying (4-5)

$$V_i(\alpha) W_i(\alpha) = 1, \quad i \in K \tag{4-5}$$

where $K$ is the set of all buses ( $K = K_{pq} \cup K_{pv}$ , $K_{pv}$ is the set of PV buses).

- PV bus

For a PV bus (e.g., bus $i$), the bus voltage angle and reactive generation, $Q_i^s(\alpha)$ must be consistent with the voltage magnitude constraint (4-6) and the PBE in (4-7), in which

73

the following are assumed to be known: the specified voltage magnitude $\left|V_i^{sp}\right|$ and the real

power generation $P_i^g$ .

$$V_i(\alpha) = \left|V_i^{sp}\right|^2 W_i^*(\alpha^*), \quad i \in K_{pv} \tag{4-6}$$

$$\sum_{k \in K} Y_{ik} V_k(\alpha) = \alpha\left(- P_i^l + P_i^g - jQ_i^l\right)^* W_i^*(\alpha^*) + \left(- jQ_i^g(\alpha)\right) W_i^*(\alpha^*), \quad i \in K_{pv} \tag{4-7}$$

Combining equations (4-3)-(4-7), the scalable form of the HE representation of the ac

power-flow problem is given as shown in the equation set (4-8).

$$V_0(\alpha) = V_{slack}$$

$$\sum_{k \in K} Y_{ik} V_k(\alpha) = \alpha\left(- P_i^l - jQ_i^l\right)^* W_i^*(\alpha^*), \quad i \in K_{pq} \tag{4-8}$$

$$V_i(\alpha) = \left|V_i^{sp}\right|^2 W_i^*(\alpha^*), \quad i \in K_{pv}$$

$$\sum_{k \in K} Y_{ik} V_k(\alpha) = \alpha\left(- P_i^l + P_i^g - jQ_i^l\right)^* W_i^*(\alpha^*) - jQ_i^g(\alpha) W_i^*(\alpha^*), \quad i \in K_{pv}$$

$$V_i(\alpha) W_i(\alpha) = 1, \quad i \in K$$

4.2.2   The germ solution

Solving the HE power flow problem results in obtaining a truncated power series of all

variables. To calculate the coefficients of all terms of the power series of the unknowns,

one starts the series form of the solution using a solution to a known operating point. The

formulation introduced in this work requires using the no-load condition solution as that

operating point, which is known as the germ. Observing (4-8), we find that the scaling

parameter, $\alpha$, is effectively scaling the loads and real power generation across the system. The no-load condition power-flow solution is equivalent to the solution obtained when $\alpha=0$.

Observing (4-8), when $\alpha=0$, the equation set is rewritten as (4-9).

$$V_0[0]=V_{slack}, \ i \in K_{slack}$$

$$\sum_{k \in K}Y_{ik}V_k[0]=0, \quad i \in K_{pq}$$

$$V_i[0]=\left|V_i^{sp}\right|^2 W_i^*[0], \quad i \in K_{pv}$$

$$\sum_{k \in K}Y_{ik}V_k[0]=-jQ_i^g[0]W_i^*[0], \quad i \in K_{pv}$$

$$V_i[0]W_i[0]=1, \quad i \in K$$

(4-9)

Note that the last two equations are nonlinear. Obtaining a closed-form solution for a multi-bus system is nontrivial. Solving this nonlinear problem numerically may be handled in a number of ways. One approach is to use a non-scalable form of the HE method, treating (4-9) as a nonlinear power flow problem, which is described in the next section. The non-scalable form has following properties:

a.  The calculation based on this formulation only involves solving linear equations.

b.  The non-scalable form is constructed to solve (4-9) so that its germ can be found by inspection.

c.  The result is only meaningful when $\alpha=1$.

The non-scalable form is only used to obtain the numerical value of the germ solution of the scalable form. Once the germ solution is found for the scalable form, we can calculate the higher-order-term coefficients of the scalable form.

### 4.2.3 Non-scalable form

In order to distinguish the solutions between the scalable (original power-flow problem formulation) and the non-scalable form (power-flow-like problem for finding the germ of the series solution to the original power-flow problem, i.e., (4-9) ), the letters $E$ and $F$, are used for voltages and reciprocal of voltages in the non-scalable form which satisfy (4-10). In the non-scalable form, $\beta$ is used as the scaling parameter.

$$E_i(\beta)F_i(\beta)=1, \quad i \in K \tag{4-10}$$

In the non-scalable form, the slack bus PBE is formulated as (4-11).

$$E_0(\beta)=1+\beta(E_{slack}-1) \tag{4-11}$$

The PQ bus PBE is formulated as (4-12).

$$\sum_{k \in K} Y_{ik}^{trans} E_k(\beta)=-\beta Y_i^{sh} E_i(\beta), \quad i \in K_{pq} \tag{4-12}$$

Since the germ problem is the no-load condition, the only current injection at the PQ bus is the current through the bus shunt. In (4-12), $Y_i^{sh}$ is the shunt admittances (including the bus shunt admittance, branch charging admittance and the equivalent shunt branch from the pi model of any transformers with off-nominal voltage-magnitude taps incident on the bus) at bus $i$. The parameter $Y_{ik}^{trans}$ which is defined by (4-13) is the $(i, k)$ element in a modified bus admittance matrix $Y^{trans}$.

$$Y_{ik}^{trans} = \begin{cases} Y_{ik}, i \neq k \\ Y_{ii} - Y_i^{sh}, i = k \end{cases} \tag{4-13}$$

The PV bus is formulated as (4-14) and (4-15).

$$E_i(\beta) = \left(1 + \beta\left(\left|V_i^{sp}\right|^2 - 1\right)\right)F_i^*(\beta^*), \quad i \in K_{pv} \tag{4-14}$$

$$\sum_{k \in K} Y_{ik}^{trans} E_k(\beta) = \left(-jQ_i^g(\beta)\right)F_i^*(\beta^*) - \alpha Y_i^{sh} E_i(\beta), \quad i \in K_{pv} \tag{4-15}$$

Equation (4-14) is used to constrain the voltage magnitude and (4-15) is the PBE of the PV bus. In the no-load condition, the current injected at a PV bus includes the current through the bus shunt and the reactive power generation from the generators.

The non-scalable form is defined by (4-10)-(4-15).

Since the non-scalable form is used to calculate the germ for the series solution of the original power-flow problem, which is the solution of the no-load condition of the scalable form, all loads and real power generation must be zero and are forced to zero when $\beta=0$, which of course is consistent with (4-9).

The identical steps are used for solving the scalable and non-scalable forms: we first must obtain the germ of the $E$ series, which is the solution of case $\beta=0$. When $\beta=0$, the equations (4-10)-(4-12) and (4-14)-(4-15) are written as:

$$E_0[0] = 1 \tag{4-16}$$

$$\sum_{k \in K} Y_{ik}^{trans} E_k[0] = 0, \quad i \in K_{pq} \tag{4-17}$$

$$E_i[0] = F_i^*[0], \quad i \in K_{pv} \tag{4-18}$$

$$\sum_{k \in K} Y_{ik}^{trans} E_k[0] = \left(-jQ_i^g[0]\right)F_i^*[0], \quad i \in K_{pv} \tag{4-19}$$

$$E_i[0]F_i[0] = 1, \quad i \in K \tag{4-20}$$

Note that in (4-12) and (4-15), $Y_i^{sh}$ is moved to the RHS. Since $Y_i^{sh}$ is multiplied by $\beta$ in this formulation, no shunt elements exist at $\beta=0$; therefore, if no phase shifters are

present, there is no place for current to flow from the slack bus and therefore there are no branch voltage drops and all voltages must be 1.0 pu. Hence, the constant term of the voltage power series ($E(0)$) must be $1\angle 0$ and therefore the constant term of $F(\beta)$ and $Q_i^g(\beta)$ are $1\angle 0$ and zero respectively.

Given the germ of the $E$ series defined by the flat voltage profile, the coefficients of the non-constant terms in the power series are then calculated (illustrated in section 4.2.4.1).

## 4.2.4 Calculating the power series

### 4.2.4.1 Solve the germ and voltage solution of the no-load case

As mentioned earlier, the germ solution of the non-scalable form for the no-load case power-flow problem (4-10)-(4-15) is trivial to find, ($E=1$, $F=1$, $Q^g=0$). Given the flat voltage profile as the constant term (germ solution of the no-load case), calculating the $n$th ($n\geqslant 1$) term coefficients are performed using the following recursion relationships.

$$E_i[n]= \delta_0 + \delta_1\left(E_{slack} -1\right) \tag{4-21}$$

$$\sum_{k\in K}Y_{ik}^{trans} E_k[n]=- Y_i^{sh} E_i[n-1], \quad i \in K_{pq} \tag{4-22}$$

$$E_i[n]= F_i^*[n]+\left(\left|V_i^{sp}\right|^2 -1\right)F_i^*[n-1], \quad i \in K_{pv} \tag{4-23}$$

$$\sum_{k\in K}Y_{ik}^{trans} E_k[n]=\sum_{t=0}^{n}\left(- jQ_i^g[n-t]\right)F_i^*[t]- Y_i^{sh} E_i[n], \quad i \in K_{pv} \tag{4-24}$$

$$\sum_{t=0}^{n}\left(E_i[n-t]\right)F_i[t]= 0, \quad i \in K \tag{4-25}$$

The parameter $\delta_i$ satisfies following relationship:

$$\delta_i = \begin{cases} 1, \text{ if } n = i \\ 0, \text{otherwise} \end{cases}$$

Solving the linear equations (4-21)-(4-25) recursively yields the $n$th term coefficients, which yields the power series for all unknowns. The respective Padé approximant of every power series is then calculated as introduced in section 4.3. Evaluating the power series with $\beta$=1 will yield the germ solution of the scalable form; however, the power series may suffer from the non-convergence problem. This problem and its solution is discussed in 4.3.

### *4.2.4.2   Solve the scalable form for the base case*

Given the germ solution ($n$=0) for the base case, the calculation of the $n$th ($n \geq 1$) term coefficients are performed by solving equation (4-26)-(4-30).

$$V_0[n] = 0 \tag{4-26}$$

$$\sum_{k \in K} Y_{ik} V_k[n] = \left(P_i^l + jQ_i^l\right)^* W_i^*[n-1], \quad i \in K_{pq} \tag{4-27}$$

$$V_i[n] - \left|V_i^{sp}\right|^2 W_i^*[n] = 0, \quad i \in K_{pv} \tag{4-28}$$

$$\sum_{k \in K} Y_{ik} V_k[n] + jQ_i^g[0] W_i^*[n] + jQ_i^g[n] W_i^*[0] =$$
$$\left(-P_i^l + P_i^g + jQ_i^l\right) W_i^*[n-1] - \sum_{t=1}^{n-1} jQ_i^g[t] W_i^*[n-t], \quad i \in K_{pv} \tag{4-29}$$

$$V[0]W[n] + V[n]W[0] = -\sum_{t=1}^{n-1} V[t]W[n-t], \quad i \in K \tag{4-30}$$

The coefficients of all terms are calculated recursively from $n$=1 to $n$=2$L$+1.

## 4.3   Padé Approximants

Solving the aforementioned formulations yields a truncated power series with solved values for all of the Maclaurin-series coefficients. No power series converges for every

value of the series parameter. The radius of convergence (ROC) is defined as the region where the power series converges. More precisely, the ROC is the radius of the largest disk, within which the power series converges to a unique solution.

For the voltage function power series, $V(\alpha)$, the ROC is often smaller than 1.0 [44], which indicates the solution cannot be calculated directly from the power series. Though the power series diverges outside of the ROC, the power series carries enough information to calculate the solution anywhere else on one branch of the multivalued problem, if it can converge at one point on the branch [44][1]. Analytic continuation is a technique to extend the domain of an analytic function. The diagonal and the near-diagonal Padé approximants have been proven to be an effective tool of analytic continuation. If the function obeys the conditions of Stahl's theorem [45], [46], the Padé approximant is the maximal analytic continuation of the function. In this work, the diagonal Padé is exploited.

## 4.4 Calculating the Padé Approximants

With the coefficients of all series evaluated, the Padé approximants of the corresponding variables are then obtained as described in this section.

The Padé approximant is a rational fraction [47], which can be written as:

$$[L/M] = \frac{a_0 + a_1\alpha + a_2\alpha^2 + \cdots + a_L\alpha^L}{b_0 + b_1\alpha + b_2\alpha^2 + \cdots + b_M\alpha^M}$$

(4-31)

where, $L$ is the degree of the numerator polynomial and $M$ is the degree of the denominator polynomial. In this work, since the diagonal Padé is used, we have $L=M$. Given a power

---

[1] This assumes that the entire domain of the function is contiguous and uninterrupted by singularities.

series, calculating its Padé approximant is synonymous with calculating the coefficients in its Padé approximant.

Define the Taylor expansion centered at zero (Maclaurin series) of an analytic function $f(\alpha)$ as:

$$f(\alpha) = \sum_{i=0}^{\infty} c_i \alpha^i \tag{4-32}$$

where $c_i$ is the coefficient of the $i$th degree term.

The coefficients of the Padé approximant are obtained by solving (4-33).

$$\left(c_0 + c_1\alpha + \cdots\right)\left(b_0 + b_1\alpha + b_2\alpha^2 + \cdots + a_M\alpha^M\right) - \left(a_0 + a_1\alpha + a_2\alpha^2 + \cdots + a_L\alpha^L\right)$$
$$= O\left(\alpha^{L+M+1}\right) \tag{4-33}$$

Equating both sides of the equation (4-33), two sets of linear equations are derived. The first set of equations (4-34) equates the coefficients for terms whose degree are less or equal to $L$.

$$c_0 b_0 = a_0$$

$$c_0 b_1 + c_1 b_0 = a_1$$

$$\vdots \tag{4-34}$$

$$c_0 b_L + c_1 b_{L-1} + \cdots c_L b_0 = a_L$$

The second set of equations (4-35) equals the coefficients for terms whose degree are greater than $L$.

$$c_{L+1} b_0 + c_L b_1 + \cdots + c_{L-M+1} b_M = 0$$

$$c_{L+2} b_0 + c_{L+1} b_1 + \cdots + c_{L-M+2} b_M = 0 \tag{4-35}$$

$$\vdots$$

81

$$c_{L+M}b_0 + c_{L+M-1}b_1 + \cdots + c_L b_M = 0$$

The homogeneous system (4-34) always has a trivial solution with all variables equal to zero. Since there are M equations and M+1 unknowns, thus one of its variable can be chosen freely [48] which effectively scales the coefficients in the denominator and numerator. In this work, $b_0$ is set to 1.0. Rewriting (4-35) in the matrix form and moving the column of $b_0$ to the RHS yields:

$$\begin{bmatrix} c_L & c_{L-1} & c_{L-2} & & c_{L-M+1} \\ c_{L+1} & c_L & c_{L-1} & \cdots & c_{L-M+2} \\ c_{L+2} & c_{L+1} & c_L & & c_{L-M+3} \\ & \vdots & & \ddots & \vdots \\ c_{L+M-1} & c_{L+M-2} & & \cdots & c_L \end{bmatrix} \begin{bmatrix} b_1 \\ b_2 \\ b_3 \\ \vdots \\ b_M \end{bmatrix} = - \begin{bmatrix} c_{L+1} \\ c_{L+2} \\ c_{L+3} \\ \vdots \\ c_{L+M} \end{bmatrix} \qquad (4\text{-}36)$$

The numerator coefficients are then calculated based on:

$$\begin{bmatrix} c_0 & & & & \\ c_1 & c_0 & & & \\ c_2 & c_1 & c_0 & & \\ \vdots & & & \ddots & \\ c_L & c_{L-1} & & \cdots & c_0 \end{bmatrix} \begin{bmatrix} 1 \\ b_1 \\ b_2 \\ \vdots \\ b_L \end{bmatrix} = \begin{bmatrix} a_0 \\ a_1 \\ a_2 \\ \vdots \\ a_L \end{bmatrix} \qquad (4\text{-}37)$$

In general, the equations (4-21)-(4-25) and (4-26)-(4-30) are applied to obtain the power series of all unknowns. The equations (4-36) and (4-37) are applied to obtain the Padé approximants of all variables.

## 4.5    Solve the HE Power Flow Problem

Solving the ac power-flow problem involves calculation of the unknown Maclaurin series coefficients for every bus as illustrated in Table 4-1. Unlike the conventional power-flow methods which yield the numerical value of the unknown voltages as complex-valued scalars, the HE method uses Padé approximants of the (possibly divergent) Maclaurin

series to obtain a converged solution that represents the behavior of the PV curve for any scaling of the load, VAr limits ignored for the moment. The scalable form of HE formulation of the power flow problem is solved in six steps:

1) Calculate the germ of no-load problem

2) Calculate the voltage series for the no-load problem.

3) Calculate the Pade approximant of the no-load problem

4) Evaluate the Pade approximant at $\beta=1$ to obtain the germ of the base-case problem.

5) Calculate the voltage series for the base-case problem, $V(\alpha)$.

6) Calculate the Pade approximant of the base-case problem.

## 4.6    Convergence of Power Flow Solution

The result of the power flow solution is validated by checking its convergence based on the convergence criterions. The convergence check is done in the base case. Evaluating the Padé approximant with $\alpha=1$ yields the base case power flow solution.

The convergence criteria are set as follows:

a. The tolerance of the largest power mismatch among all buses is 0.1 MW or 0.1 MVar.

b. The difference between consecutive Padé approximant values for the bus-voltage magnitude and angle are calculated. The tolerance of the largest voltage magnitude difference is selected as 1E-4 p.u. The tolerance of the largest voltage-angle difference is selected as 1.0 degree.

4.7     Calculating the Saddle Node Bifurcation Point (SNBP)

The SNBP indicates the voltage stability margin of the static system defined by the system model parameters and injections, i.e., the power-flow equations. In this work, the SNBP is calculated as the smallest load scaling factor which pushes the system to voltage collapse. Hence the power flow solution, defined by the Padé approximants of the bus voltages, is valid in the load scaling range between zero and the SNBP.

As mentioned earlier, the Padé approximant is the maximal analytic continuation of a power series given that the defining function meets Stahl's theorem requirements [45], [46]. Theoretically if there are a sufficient number of terms in the Maclaurin series, the Padé approximant can find the solution on the branch on which the germ resides for any loading level provided the $\alpha$ scaling factor is limited between zero and the SNBP, with a caveat of numerical precision limitations and Stahl's theorem conditions.

To guarantee the number of terms of the Padé approximant is sufficient, the algorithm checks the convergence once the solution is obtained. If the convergence criteria are not satisfied, then the HEM power flow is recalculated with two more terms added to the power series and consequently the denominator and numerator power series of the Padé approximant will have one more term. The convergence check and term increment are repeated until the criteria are met. In this work, the power series are started with 60 terms and the corresponding Padé approximant is started with 30 terms in the numerator/denominator polynomials.

Since convergence must be check at the SNBP, which is unknown *a priori*, the SNBP must be calculate. The SNBP can be calculated by following steps:

1. Solve the power flow using a scalable form of the HEM and obtain Padé approximants for all unknowns.

2. Start with $\alpha=0$.

3. Evaluate the approximant using the present estimate of the SNBP load-scaling factor, $\alpha$, and check the convergence criteria.

If the convergence criteria are satisfied in step 2 then increment $\alpha$ by 0.01 and go back to step 3. If the convergence criteria are not satisfied and the maximum number of terms in the power series is not reached, then increment the number of terms in the power series by two and go back to step 3. If the convergence criteria are not satisfied and the maximum number of terms in the power series is reached, then the current $\alpha$ value exceeds the SNBP and the SNBP should be set to $\alpha$-0.01. In this study, the maximum number of terms in the power series is chosen as 121. The HEM power flow is formulated and solved as introduced in the previous subsections. The HEM reduction is based on the HEM power flow solution which is also referred as the "full-model solution" in the reduction process. In the following subsections the HEM reduction is introduced.

## 4.8 Generating an Improved Reduced Network Using the HEM

When constructing a reduced network, the buses in the full model are divided into three groups: the external buses, the boundary buses and the internal buses. Based on this division, we can group and order the PBEs into PBEs of external buses, boundary buses and internal buses, respectively. Correspondingly, the bus admittance matrix ($Y_{bus}$) is written as shown in (4-38).

$$Y_{bus} = \begin{bmatrix} Y_{EE} & Y_{EB} & \\ Y_{BE} & Y_{BB} & Y_{BI} \\ & Y_{IB} & Y_{II} \end{bmatrix} \qquad (4\text{-}38)$$

In (4-38), the block $Y_{EE}$ includes all the branches spanning only the external buses and includes the bus shunts of all external buses. The block $Y_{BE}$ (transpose of $Y_{EB}$) includes all branches spanning one external and one boundary bus. The block $Y_{BB}$ includes all branches spanning only boundary buses and includes the shunt admittances of boundary buses. The block $Y_{BI}$ (transpose of $Y_{IB}$) includes all branches spanning one boundary and one internal bus. The block $Y_{II}$ includes all branches spanning two internal buses and includes the bus shunts of the internal buses.

Given the HEM power-flow-formulation notation and the notation of (4-38), the power-flow equations can be written schematically as shown in (4-39).

$$\begin{bmatrix} Y_{EE} & Y_{EB} & \\ Y_{BE} & Y_{BB} & Y_{BI} \\ & Y_{IB} & Y_{II} \end{bmatrix} \begin{bmatrix} V_E(\alpha) \\ V_B(\alpha) \\ V_I(\alpha) \end{bmatrix} = \begin{bmatrix} S_E^*(\alpha^*)W_E^*(\alpha^*) \\ S_B^*(\alpha^*)W_B^*(\alpha^*) \\ S_I^*(\alpha^*)W_I^*(\alpha^*) \end{bmatrix} \qquad (4\text{-}39)$$

In (4-39), $V_E(\alpha)$, $V_B(\alpha)$ and $V_I(\alpha)$ are vectors of voltages of the external, boundary and internal buses respectively. $S_E(\alpha)$, $S_B(\alpha)$ and $S_I(\alpha)$ are vectors representing the shunt complex power injections at the external, boundary and internal buses, respectively.

The HEM reduction generates the reduced-model network in the same way as Ward, which is by doing partial LU factorization upon the full-model bus admittance matrix shown in (4-40). In this process, all the external components are factorized.

$$Y_{bus} = L_r Y_{bus}^{reduced} U_r \qquad (4\text{-}40)$$

In (4-40), $L_r$ and $U_r$ are the partially factored lower and upper triangular matrices respectively; $Y_{bus}^{reduced}$ is the reduced-model bus-admittance matrix. The reduced-model

network topology and network parameters (branch impedances, bus shunt admittances) are obtained from $Y_{bus}^{reduced}$. This process is explained in more detail later.

## 4.9 Distribute the External Current Injection

After generating the reduced-model network, the external current is distributed to the boundary buses so that the system power injection can be balanced. To distribute the external current, we need to revisit the partial LU factorization process.

### 4.9.1 Distribution factor

The partial LU factorization shown in (4-40) can be explicitly written as (4-41).

$$Y_{bus} = \begin{bmatrix} L_{EE} & & \\ L_{BE} & I & \\ & & I \end{bmatrix} \begin{bmatrix} I & & \\ & Y_{BB} - Y_{BE}Y_{EE}^{-1}Y_{EB} & Y_{BI} \\ & Y_{IB} & Y_{II} \end{bmatrix} \begin{bmatrix} U_{EE} & U_{EB} \\ & I & \\ & & I \end{bmatrix} \tag{4-41}$$

Combining (4-39) and (4-41), the power-flow equations are rewritten as (4-42).

$$\begin{bmatrix} L_{EE} & & \\ L_{BE} & I & \\ & & I \end{bmatrix} \begin{bmatrix} I & & \\ & Y_{BB} - Y_{BE}Y_{EE}^{-1}Y_{EB} & Y_{BI} \\ & Y_{IB} & Y_{II} \end{bmatrix} \begin{bmatrix} U_{EE} & U_{EB} \\ & I & \\ & & I \end{bmatrix} \begin{bmatrix} V_E(\alpha) \\ V_B(\alpha) \\ V_I(\alpha) \end{bmatrix} = \begin{bmatrix} S_E^*(\alpha^*)W_E^*(\alpha^*) \\ S_B^*(\alpha^*)W_B^*(\alpha^*) \\ S_I^*(\alpha^*)W_I^*(\alpha^*) \end{bmatrix} \tag{4-42}$$

Multiply both sides of (4-42) by the inverse of the lower triangular matrix ($L_r^{-1}$), the equation is then rewritten as (4-43).

$$\begin{bmatrix} I & & \\ & Y_{BB} - Y_{BE}Y_{EE}^{-1}Y_{EB} & Y_{BI} \\ & Y_{IB} & Y_{II} \end{bmatrix} \begin{bmatrix} U_{EE} & U_{EB} \\ & I & \\ & & I \end{bmatrix} \begin{bmatrix} V_E(\alpha) \\ V_B(\alpha) \\ V_I(\alpha) \end{bmatrix} = \begin{bmatrix} L_{EE} & & \\ L_{BE} & I & \\ & & I \end{bmatrix}^{-1} \begin{bmatrix} S_E^*(\alpha^*)W_E^*(\alpha^*) \\ S_B^*(\alpha^*)W_B^*(\alpha^*) \\ S_I^*(\alpha^*)W_I^*(\alpha^*) \end{bmatrix} \tag{4-43}$$

Define $L_r^{-1}$ as:

$$L_r^{-1} = \begin{bmatrix} \hat{L}_r^{ee} & & \\ \hat{L}_r^{be} & I_1 & \\ & & I_2 \end{bmatrix}_{N_b^{full} \times N_b^{full}} \tag{4-44}$$

where

$\hat{L}_r^{ee}$: a $N^e \times N^e$ submatrix. $N^e$ is the number of external buses.

$\hat{L}_r^{be}$: a $N^b \times N^e$ submatrix. $N^b$ is the number of boundary buses.

$I_1$: a $N^b \times N^b$ identity matrix.

$I_2$: a $N^i \times N^i$ identity matrix. $N^i$ is the number of internal buses.

The omitted part of the matrix are all zeros.

Equation (4-43) is written as (4-45). Observing (4-45), we can find the voltages of the reduced model at the boundary buses and at the internal buses remain unchanged from those of the full model. The current injections at the internal buses also remain unscathed. For the boundary buses, the added current injection terms in (4-45) are nonlinear injections accounting for injections from the external buses and external system losses. The matrix $\hat{L}_r^{be}$ effectively provides the distribution factors based on which the external current is split and added to the boundary buses. The external current injection ( $S_E^*(\alpha^*)W_E^*(\alpha^*)$ ) is distributed to the boundary buses based on the distribution factors

$$\begin{bmatrix} I & & \\ Y_{BB} - Y_{BE}Y_{EE}^{-1}Y_{EB} & Y_{BI} \\ Y_{IB} & Y_{II} \end{bmatrix} \begin{bmatrix} U_{EE}V_E(\alpha) + U_{EB}V_B(\alpha) \\ V_B(\alpha) \\ V_I(\alpha) \end{bmatrix} = \begin{bmatrix} \hat{L}_r^{ee} S_E^*(\alpha^*)W_E^*(\alpha^*) \\ \hat{L}_r^{be} S_E^*(\alpha)W_E^*(\alpha^*) + S_B^*(\alpha)W_B^*(\alpha^*) \\ S_I^*(\alpha^*)W_I^*(\alpha^*) \end{bmatrix} \tag{4-45}$$

In $\hat{L}_r^{be}$, the element $\hat{l}_{ij}$ which is on the $i$th row and $j$th column of the matrix defines the proportion of injected power of external bus $j$ split to the boundary bus $i$, where, typically $0 \le \left|\hat{l}_{ij}\right| \le 1$.

4.9.2    Distribute the external power with HE based power flow solution

*4.9.2.1    Methodology*

Distributing the external power to the boundary buses involves four steps: 1) solve the HEM power flow and obtain $V(\alpha)$, 2) convert the external power injections to nonlinear current injections; 3) split the external nonlinear current injections to the boundary buses based on the distribution factors; 4) calculate the nonlinear power injections (in series form) from the external network at every boundary buses, if power injections (rather than nonlinear current injections) are desired.

An example of splitting the power injection of the external bus $e$ and distributing the respective proportion to the boundary bus $a$ is shown as follows:

Step 1: Given a solved power flow problem using HEM, the current injected as a nonlinear power series in $\alpha$ at bus $e$ is calculated by evaluating (multiplying out) (4-46). Note that (4-46) represents the general case of a PV bus injection. If the bus is a PQ bus, then $P_e^g$ and $Q_e^g(\alpha)$ should be zero.

$$I_e(\alpha) = \left[ \alpha\left(P_e^g - P_e^l - jQ_e^l\right)^* - jQ_e^g(\alpha^*) \right] W_e^*(\alpha^*) \qquad (4\text{-}46)$$

Step 2: The current distribution from the external bus $e$ to the boundary bus $a$ is $I_e^a(\alpha)$ calculated by performing the multiplication indicated by (4-47). Note that the distribution factor may be a complex number.

$$I_e^a(\alpha) = \hat{l}_{ae} I_e(\alpha) \tag{4-47}$$

If there are multiple buses contributing power/current to bus $a$, the power series of total external current injections $I_a^{ex}(\alpha)$ at bus $e$ is:

$$I_a^{ex}(\alpha) = \sum_{e \in K_{ex}^a} I_e^a(\alpha) \tag{4-48}$$

where $K_{ex}^a$ is the set of the external buses which contribute power/current to bus $a$.

Step 3: Calculate the complex power injection from the external network to the bus $a$ if such is needed. The preference between using a power-injection-model power series and a current-injection-model power series may depend on the purpose of the study to be conducted, which is beyond the scope of this work.

The power injected at bus $a$ from the external network is:

$$S_a^{ex}(\alpha) = \left[ I_a^{ex}(\alpha^*) \right]^* V_a(\alpha) \tag{4-49}$$

Two notes should be made. First the current injection term in (4-49) may originate from two different types of complex power injection models: PQ or PV bus models, which are modeled as either constant (fixed) values (load and real power generation) or modeled as a function of $\alpha$ (reactive power generation of the PV buses). These two different current injection models are subscripted by "*fixed*" and "*qg*" respectively. The equations of current injection $I_a^{ex}(\alpha)$ and the $S_a^{ex}(\alpha)$ are then written as:

$$I_a^{ex}(\alpha) = \sum_{e \in K_{ex}^a} I_{e,fixed}^a(\alpha) + \sum_{e \in K_{ex}^a} I_{e,qg}^a(\alpha) \tag{4-50}$$

$$S_a^{ex}(\alpha) = S_{a,fixed}^{ex}(\alpha) + S_{a,qg}^{ex}(\alpha) = \left( \sum_{e \in K_{ex}^a} I_{e,fixed}^a(\alpha^*) \right)^* V_a(\alpha) + \left( \sum_{e \in K_{ex}^a} I_{e,qg}^a(\alpha^*) \right)^* V_a(\alpha) \tag{4-51}$$

The second note is that the identity of each external power injection must be preserved as follows. The $(a,e)$ element of $\hat{L}_r^{be}$, denoted as $\hat{l}_{ae}$, distributes the power injection from external bus $e$ to boundary bus $a$. If bus $a$ has equivalent boundary injections from multiple sources, the external power injection into bus $a$ can be written as (4-52),

$$S_a^{ex}(\alpha) = \left[ \sum_{k \in K_{ex}^a} \hat{l}_{ae} \left( P_e^g - P_e^l - jQ_e^l + jQ_e^g(\alpha) \right) W_e(\alpha) \right] V_a(\alpha) \qquad (4\text{-}52a)$$

$$= \left[ \sum_{k \in K_{ex}^a} \hat{l}_{ae} \left( \alpha S_e^{l,p_g} + jQ_e^g(\alpha) \right) W_e(\alpha) \right] V_a(\alpha) \qquad (4\text{-}52b)$$

4.10   Solve the Reduced-Model Power Flow

Solving the reduced-model power flow is very similar to solving the full-model power flow. The difference is that the power injection at the boundary bus includes not only the native power injections but also the external power injections which are represented as series, which may possibly be divergent.

The problem is formulated in a scalable form and the germ of the scalable form is solved based on a non-scalable form. To avoid conflict and confusion of the notation, the scalable form of the reduced-model power flow takes $\gamma$ as the scaling parameter and the non-scalable form takes $\eta$ as the scaling parameter.

4.10.1   Calculate the germ of the reduced model

Either a scalable or non-scalable HE power-flow formulation may be use to solve the power-flow problem associated with the reduced model. To find the germ of the reduced model, the no-load case must be solved. In the no-load case using a scalable form, the only power injection to the system is the reactive-power generation. Therefore, in the reduced

model, the external power injections of the boundary buses are sourced from the reactive-power generation from the external system.

The external current-injection-model power series, $I_e^a(\eta)$, of a boundary bus, $a$, is calculated as (4-46) with $P_e^g$, $P_e^l$ and $Q_e^l$ equal to zero. The external power-injection-model power series ($S_i^{ex}(\eta)$) is calculated based on (4-49).

Denote a variable $\sigma_i$ where

$$\sigma_i = \begin{cases} 1, \text{if bus } i \text{ is a boundary bus} \\ 0, \text{otherwise} \end{cases}, \quad i \in K$$

The reduced-model power-flow germ (germ$_r$) problem is formulated as shown in (4-53)-(4-57).

$$E_{0,r}(\eta) = 1 + \eta(E_{slack} - 1) \tag{4-53}$$

$$\sum_{k \in K, i \neq k} Y_{ik} E_{k,r}(\eta) = -\eta Y_i^{sh} E_{i,r}(\eta) + \sigma_i \left( S_i^{*ex}(\eta^*) F_{i,r}(\eta^*) \right)^*, \quad i \in K_{pq} \tag{4-54}$$

$$E_{i,r}(\eta) = \left( 1 + \eta \left( \left| V_i^{sp} \right|^2 - 1 \right) \right) F_{i,r}^*(\eta^*), \quad i \in K_{pv} \tag{4-55}$$

$$\sum_{k \in K} Y_{ik} E_{k,r}(\eta) = \left( -jQ_{i,r}^g(\eta) \right) F_{i,r}^*(\eta^*) - \eta Y_i^{sh} E_{i,r}(\eta)$$
$$+ \sigma_i \left( S_i^{*ex}(\eta^*) F_{i,r}(\eta^*) \right)^*, \quad i \in K_{pv} \tag{4-56}$$

$$E_{i,r}(\eta) F_{i,r}(\eta) = 1, \quad i \in K \tag{4-57}$$

where the subscript "$r$" indicates reduced-model solution/parameter. The term $\left( S_i^{ex}(\eta^*) F_{i,r}(\eta^*) \right)^*$ is the current injection of the boundary bus from the external network.

The problem formulation (4-53)-(4-57) is solved recursively starting from the case of $\eta=0$. At $\eta=0$, the external injections at the boundary buses are zero. For all bus voltage

power series, the constant term $E_{i,r}[0]=1$ and therefore, the constant term of the reciprocal

power series $F_{i,r}[0]=1$. The constant term of the reactive-support series $Q_{i,r}[0]=0$. The $n$th

term of all power series are calculated as:

$$E_{0,r}[n] = \delta_1(V_{slack} - 1) \tag{4-58}$$

$$\sum_{k \in K} Y_{ik} E_{k,r}[n] = -Y_i^{sh} E_{i,r}[n-1] + \sigma_i \sum_{t=0}^{n} S_i^{ex*}[t] F_{i,r}[n-t], \quad i \in K_{pq} \tag{4-59}$$

$$E_{i,r}[n] = \left( \left| V_i^{sp} \right|^2 - 1 \right) F_{i,r}^*[n-1] + F_{i,r}^*[n], \quad i \in K_{pv} \tag{4-60}$$

$$\sum_{k \in K} Y_{ik} E_{k,r}[n] = \sum_{t=0}^{n} -jQ_{i,r}^g[t] F_{i,r}^*[n-t] - Y_i^{sh} E_{i,r}[n-1] + \sigma_i \sum_{t=0}^{n} S_i^{ex*}[t] F_{i,r}^*[n-t], \quad i \in K_{pv} \tag{4-61}$$

$$E_{i,r}[0] F_{i,r}[n] + E_{i,r}[n] F_{i,r}[0] = -\sum_{t=1}^{n-1} E_{i,r}[t] F_{i,r}[n-t], \quad i \in K \tag{4-62}$$

The power series of the germ$_r$ is obtained by solving (4-58)-(4-62) based on which, the

corresponding Padé approximants are obtained by solving (4-36) and (4-37). Evaluating

the Padé approximants at $\eta=1$, the value of germ$_r$ for the reduced model is obtained.

4.10.2 Calculate coefficients of the high power order terms of the reduced model

With the external power-injection power series at the boundary buses, the reduced-

model power-flow problem is formulated as shown in (4-63)-(4-67).

$$V_{0,r}(\gamma) = V_{slack} \tag{4-63}$$

$$\sum_{k \in K} Y_{ik} V_{k,r}(\gamma) = \gamma \left( -P_i^l - jQ_i^l \right)^* W_i^*(\gamma^*) + \sigma_i \left( \gamma S_{i,fixed}^{*ex}(\gamma^*) + S_{i,qg}^{*ex}(\gamma^*) \right) W_{i,r}^*(\gamma^*), \quad i \in K_{pq} \tag{4-64}$$

$$V_{i,r}(\gamma) = \left| V_i^{sp} \right|^2 W_{i,r}^*(\gamma^*), \quad i \in K_{pv} \tag{4-65}$$

$$\sum_{k \in K} Y_{ik} V_{k,r}(\gamma) = \gamma \left( -P_i^l + P_i^g - jQ_i^l \right)^* W_{i,r}^*(\gamma^*) + \left( -jQ_{i,r}^g(\gamma) \right) W_{i,r}^*(\gamma^*) +$$
$$\sigma_i \left( \gamma S_{i,fixed}^{ex}(\gamma^*) + S_{i,qg}^{ex}(\gamma^*) \right)^* W_{i,r}^*(\gamma^*), \quad i \in K_{pv} \tag{4-66}$$

$$V_{i,r}(\gamma) W_{i,r}(\gamma) = 1, \quad i \in K \tag{4-67}$$

Starting from germ$_r$ obtained in 4.10.1, the high-order-term coefficients are calculated recursively based on (4-63)-(4-67). The *n*th (*n*>0) term coefficients of the power series are calculated as (4-68)-(4-72).

$$V_{0,r}[n] = 0 \tag{4-68}$$

$$\sum_{k \in K} Y_{ik} V_{k,r}[n] = \left( -P_i^l - jQ_i^l \right)^* W_i^*[n-1] + \sigma_i \left( \sum_{t=0}^{n-1} \left( S_{i,fixed}^{ex}[t] W_{i,r}[n-t] \right)^* + \sum_{t=0}^{n} \left( S_{i,qg}^{ex}[t] W_{i,r}[n-t] \right)^* \right), \quad i \in K_{pq} \tag{4-69}$$

$$V_{i,r}[n] - \left| V_i^{sp} \right|^2 W_{i,r}^*[n] = 0, \quad i \in K_{pv} \tag{4-70}$$

$$\sum_{k \in K} Y_{ik} V_{k,r}[n] = \left( -P_i^l + P_i^g - jQ_i^l \right)^* W_{i,r}^*[n-1] + \sum_{t=0}^{n} \left( -jQ_{i,r}^g[t] W_{i,r}^*[n-t] \right) +$$
$$\sigma_i \left( \sum_{t=0}^{n-1} S_{i,fixed}^{ex}[t] W_{i,r}[n-t] + \sum_{t=0}^{n} S_{i,qg}^{ex}[t] W_{i,r}[n-t] \right)^*, \quad i \in K_{pv} \tag{4-71}$$

$$V_{i,r}[0] W_{i,r}[n] + V_{i,r}[n] W_{i,r}[0] = -\sum_{t=1}^{n-1} V_{i,r}[t] W_{i,r}[n-t], \quad i \in K \tag{4-72}$$

## 4.11 Implementation

The conventional linearization-based reduction methods, like Ward-type or REI reductions, match the full-model solution exactly only at the base case. However, without online boundary matching, [6], [9], when the system operating condition deviates from the base case the conventional reduction does not approximate the full-model performance accurately. In this dissertation, three types of operating-condition deviations are considered.

4.11.1 Scaling the system injections uniformly—on the $\alpha$ line

In this scenario, where all loads and real-power generation are scaled uniformly, the solution of the full and reduced-model voltages are identical for all values of $\alpha$ between zero and the SNBP. (Recall that, as introduced in Section II, the embedded parameter $\alpha$ functions as a scaling parameter of loads and real power generation.) Hence, once the full-model solution is obtained, the bus voltages of the reduced-model solution, which are a subset of the full model, are calculated by simply evaluating the corresponding full-model Padé approximants at the desired $\alpha$ value. In other words, solving the power-flow problem for the reduced model is not necessary. However, for the purpose of validating the numerical stability of these algorithms, the reduced-model power flow for cases along the $\alpha$ line was solved by modeling the external injections both as fixed values (evaluated at the desire $\alpha$ using (4-52)) and using external injections as the series defined by (4-52), with results essentially identical.

4.11.2 Change the loads on retained buses non-uniformly—off the $\alpha$ line

In practice, the power injections of different buses do not all change uniformly over time and we tested whether we could handle non-uniform load/generation changes theoretically as well as numerically as described below.

Ideally, if parameters are embedded in the PBE's to scale each injection independently in the full model, one can use the scaling parameters to describe all operating conditions. In the next chapter, a bivariate HEM which embeds two parameters in the formulation is introduced and tested. The bivariate HEM yields promising results in terms of accuracy, however, it also reveals that the bivariate (or multi-variate) HEM has some important

drawbacks which motivated us to propose an alternative method (illustrated below) to handle the non-uniformly-varying loads.

Our approach was to determine whether we could derive an equivalent $\alpha$ value that would allow the Padé approximants of the full-model bus voltages (obtained using the univariate HEM) to approximate the reduced-model's response to the non-uniform system injections with sufficient accuracy as to be useful. This, again, allows the bus voltages of the reduced model to be calculated by simply evaluating the Padé approximants of interest that were obtained from the full-model solution. This calculation is computationally less complex than re-solving the power-flow problem, as required when using conventional reduced-order equivalents.

In [50], five different methods for calculating an equivalent $\alpha$ for radial distribution systems were tested. The two best-performing methods, shown in (4-73) and (4-74), were used to calculate the equivalent $\alpha$ values in this work and are given by,

$$\alpha_1 = \frac{\sum_{m \in K_{\text{int}}} \left| P_{m,new}^l + jQ_{m,new}^l \right|}{\sum_{m \in K_{\text{int}}} \left| P_{m,old}^l + jQ_{m,old}^l \right|} \tag{4-73}$$

$$\alpha_2 = \left| \frac{\sum_{m \in K_{\text{int}}} \left( P_{m,new}^l + jQ_{m,new}^l \right)}{\sum_{m \in K_{\text{int}}} \left( P_{m,old}^l + jQ_{m,old}^l \right)} \right| \tag{4-74}$$

where $P_{m,new}^l$ and $Q_{m,new}^l$ are the perturbed real and reactive loads at bus $m$, $P_{m,old}^l$ and $Q_{m,old}^l$ are the real and reactive loads without the perturbation, and $K_{int}$ is the set of all retained buses. Once the equivalent $\alpha$ is calculated, it is used to evaluate Padé approximants, $V^{pade}(\alpha)$, $Q^{g,pade}(\alpha)$, obtained from the full model power flow solution.

As with the "on-the-$\alpha$-line" scenario, there is no need to solve the reduced-model power flow for different operating conditions if the base-case full-model solution is given. One only needs to evaluate the retained bus solutions (Padé approximants) and use the equivalent $\alpha$. In the next section, we show test results quantifying the accuracy of the reduced-model bus-voltage solutions when using these equivalent $\alpha$ values by comparing the results with the full-model power-flow solution.

4.11.3 Scale the system injections uniformly and imposing VAr limits on external PV buses

Different generators will hit their VAr limits at different power scaling levels. When each term in the summation in (4-52) is treated as a separate injection, the identity of the external bus producing that injection will be preserved. With the HE reduction, $\hat{l}_{ae}Q_e^g(\alpha)$ is the part of the equivalent boundary power injection sourced from the partial reactive-power generation of external PV bus $e$ and acts to model bus voltage support.

Assume $\alpha_{\min}^e$ and $\alpha_{\max}^e$ are the loading levels at which the generators at bus $e$ collectively reach their lower and the upper VAr limits, respectively. When $\alpha_{\min}^e < \alpha < \alpha_{\max}^e$, bus $e$ is not on VAr limits and the equivalent boundary injection of bus $e$ is calculated as shown in (4-52). If $\alpha \leq \alpha_{\min}^e$ ($\alpha \geq \alpha_{\max}^e$), the generators modeled at bus $e$ will be on their lower VAr limit (upper VAr limit); the equivalent boundary injection should be calculated as shown in (4-52) in which the term $Q_e^g(\alpha)$ is replaced by $Q_e^{g,\min}$ ($Q_e^{g,\max}$).

Unlike the previous two scenarios, when VAr limits are encountered, the reduced-model power flow must be solved (as opposed to evaluating the existing Padé

approximants). In this case, the equivalent injections must be modeled following the strategy illustrated in the previous paragraph.

## 4.12 Simulations

Simulations were performed to evaluate the HE reduction accuracy under the three loading scenarios mentioned in the previous section. Two systems were used in the tests: the IEEE 118-bus system and an ERCOT-based 6057-bus system. Three different scenarios were simulated in the tests: loads changed uniformly (on the $\alpha$ line); loads changed non-uniformly (off the $\alpha$ line); and imposing VAr limits while loads changed uniformly. The reduced-model performance is compared to the full-model solution.

### 4.12.1 Models

For the tests performed on the IEEE 118-bus system, a 35-bus reduced-order model was produced. In the reduced model, all buses whose nominal voltages were greater than 138 kV and the terminal buses of frequently congested branches were retained. The 118-bus system includes 53 PV buses, 14 of which were preserved in the reduced model.

The ERCOT 6057-bus system was obtained from Energy Visual [51]. The diagram of the full model is shown in Fig. 4-1. The reduced model generated in the test was a backbone reduction which preserved 3721 buses. The reduced model included all buses whose nominal voltage were no lower than 138 kV and the terminals of the frequently congested branches. The full model included 530 PV buses. The reduced model preserved 275 PV buses.
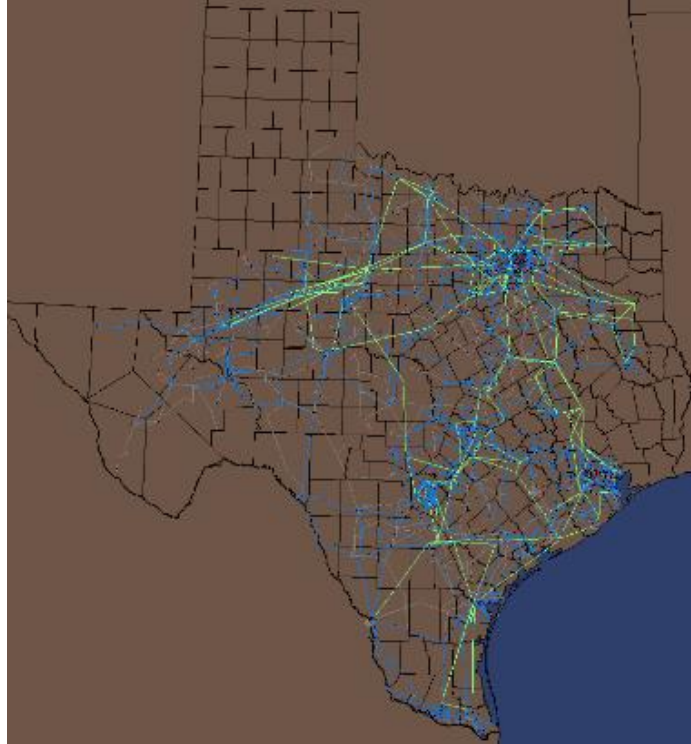
Fig. 4-1 ERCOT 6057-bus system (full model)

### 4.12.2 On the $\alpha$ line

In this scenario, loads and real power generation across the entire system were scaled uniformly using the parameter $\alpha$.

The performance of the HE reductions was compared with the performance of conventional reduction methods: Ward, Extended-Ward and the REI method. Two metrics were chosen for the comparisons. One measured the maximum voltage magnitude error (in pu) and one measured the maximum voltage angle error (in degrees) over all retained buses in the system. The HEM-based power-flow solution of the full system model was taken as the reference.

The voltage-magnitude and angle-error results of the IEEE 118-bus reduction are shown in Fig. 4-2 and Fig. 4-3, respectively. The curves shown in the two figures use a

logarithmic scale. The voltages for the HE reduction were calculated by solving the reduced-model power flow to test the numerical accuracy of the approach, though in practice one need only evaluate $V(\alpha)$ and $Q_g(\alpha)$, which yielded numerically identical results after taking into account the roundoff error and the processor precision limitations. To solve the power-flow problem using the reduced-order models obtained from conventional methods, the traditional Newton-Raphson method was used with a starting voltage profile equal to the base-case voltage solution. The results of equivalent tests on the ERCOT system are shown in Fig. 4-4 and Fig. 4-5.
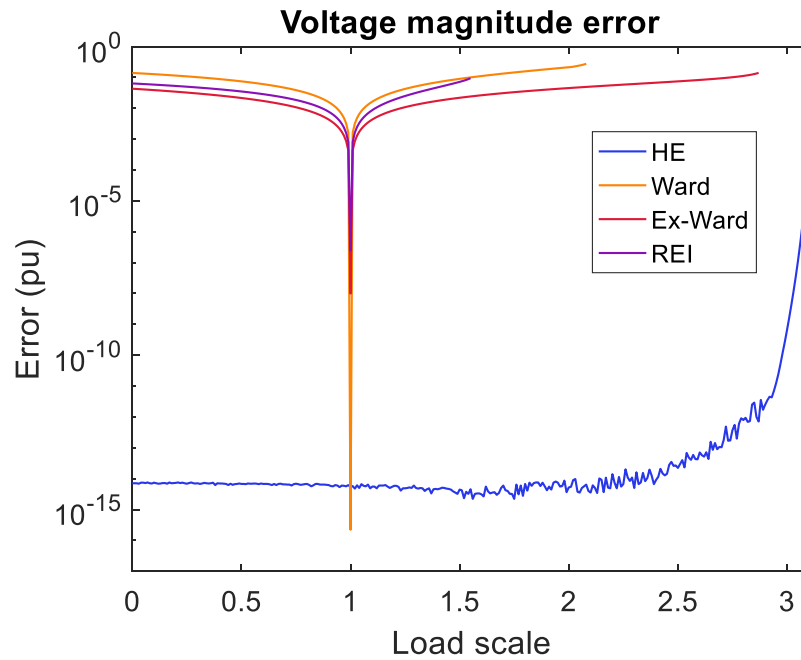


Fig. 4-2 Maximum voltage-magnitude error comparison (on the $\alpha$ line) for IEEE 118-bus system reduction
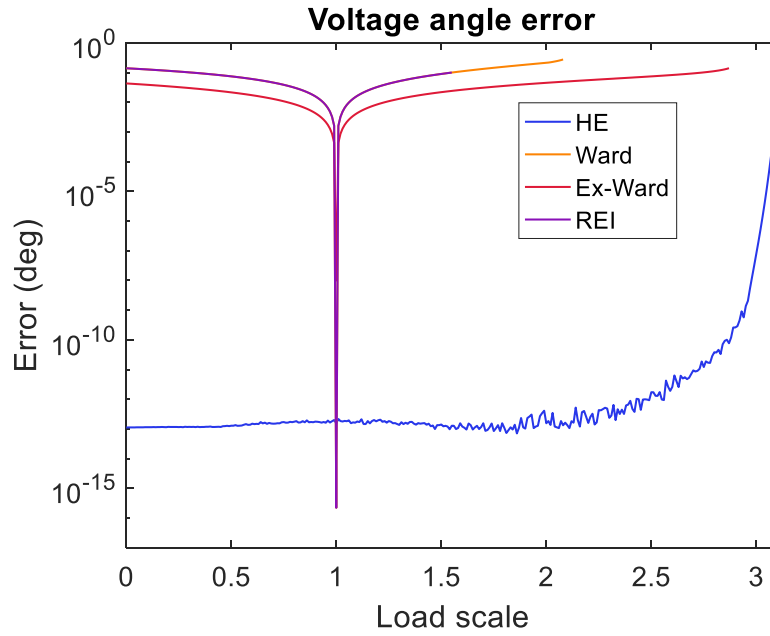
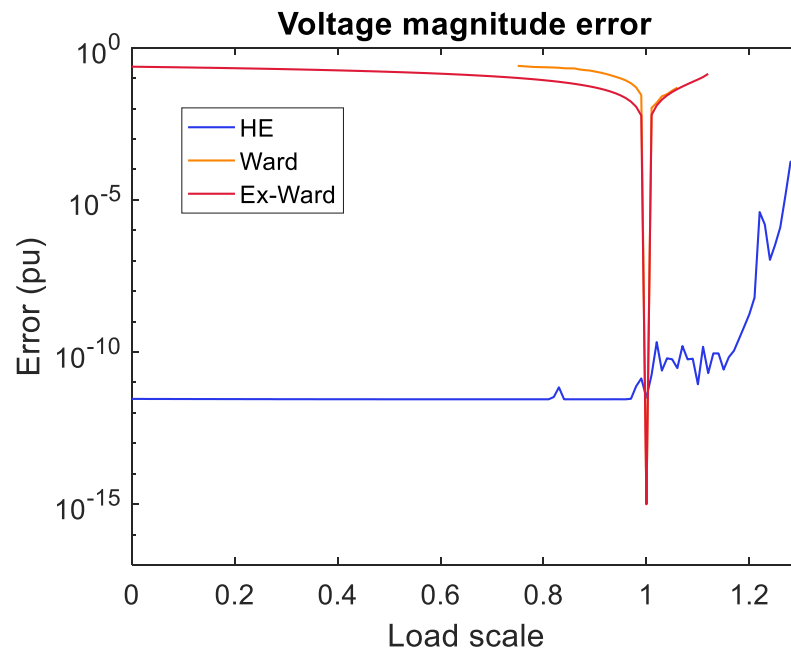Fig. 4-3 Maximum voltage-angle error comparison (on the $\alpha$ line) for IEEE 118-bus

reduction



Fig. 4-4 Voltage-magnitude error comparison (on the $\alpha$ line) in ERCOT system test
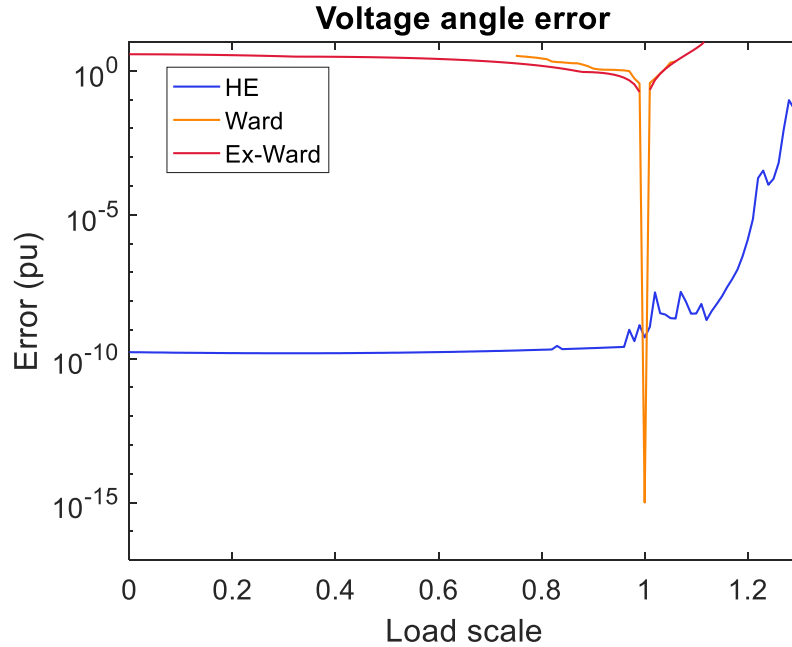
Fig. 4-5 Voltage-angle error comparison (on the $\alpha$ line) in ERCOT system test

The results shown in Fig. 4-2-Fig. 4-5 indicate that the HE reductions match the full-model performance with voltage-magnitude (and angle) errors better than E-10 pu (deg) for much of the loading range. The HE reductions perform better because they can match the external boundary power injections as precisely as desired, given the limitation of precision, roundoff and number of voltage power-series terms calculated. The error performance of the HE reductions decreases as loads approach the SNBP due to the numerical limitations that are more pronounced near the SNBP. As expected, the linearization-based methods have extraordinary accuracy only at the base case, with the errors due to linearization and non-scalability of the generator equivalent reactive power injections growing quickly as one moves away from the base case. Note also, that Newton's method fails to converge when using these conventional reductions much in advance of the SNBP, which is another limitation of the conventional reduced-order models.

### 4.12.3 Getting ofF the $\alpha$ line

In this test scenario, the desire was to model loads that changed non-uniformly. There are of course many ways to vary loads. The approach here was to recognize that loads vary somewhat uniformly during a day or between seasons, but each injection will deviate somewhat, but generally not radically, from uniform scaling. Therefore, the load at each bus was modified by adding a 0-5% random perturbation to the scaled base-case loading to every retained PQ bus, as shown in (4-75).

$$P_{m,new}^{l} + jQ_{m,new}^{l} = P_{m,old}^{l}\left(1 \pm \varepsilon_{m}^{p}/100\right) + Q_{m,old}^{l}\left(1 \pm \varepsilon_{m}^{q}/100\right) \tag{4-75}$$

In (4-75), the $\varepsilon_{m}^{p}$ and $\varepsilon_{m}^{q}$ are the perturbation factors of the real and reactive loads, respectively, of bus $m$ that were drawn from a random sample uniformly distributed between 0-5%. The generation values on the retained PV buses were uniformly scaled by $\mu$ which is calculated by (4-76).

$$\mu = \frac{\displaystyle\sum_{m} P_{m,new}^{l}}{\displaystyle\sum_{m} P_{m,old}^{l}} \tag{4-76}$$

In the plots below, the $\varepsilon_{m}^{p}$ and $\varepsilon_{m}^{q}$ were applied to the loads at all retained buses for base-load scalings of 0%, 5%, 10% etc., up to 25%.

For every base-load scaling, 100 sample vectors of random-load increments were generated and the resultant loads applied to the full and reduced-order models. Two metrics were used in the tests. One was the maximum voltage magnitude error, calculated as shown in (4-77). The other one was the average retained branch flow error calculated as shown in (4-78).

$$V_{Err}^{mag} = \max_{t=\{1,2\cdots100\}} \left( \max_{m \in K_{int}} \left| V_{m,t}^{mag,f} - V_{m,t}^{mag,r} \right| \right) \qquad (4\text{-}77)$$

$$F_{Err} = \max_{t=\{1,2\cdots100\}} \left( \underset{i \in L_{int}}{mean} \left| \frac{S_{i,t}^{flow,f} - S_{i,t}^{flow,r}}{Lim_i} \right| \right) \qquad (4\text{-}78)$$

In (4-77), $V_{m,t}^{mag,f}$ and $V_{m,t}^{mag,r}$ are the voltage magnitudes of bus $m$ in the full- and reduced-model solutions, respectively and $t$ is the index of the random sample. In (4-78), the $S_{i,t}^{flow,f}$ and $S_{i,t}^{flow,r}$ variables are the apparent-power flows on branch $i$ in the full and reduced models, respectively; $Lim_i$ is the rating of branch; $K_{int}$ is the set of all retained buses; $L_{int}$ is the set of all branches spanning the retained buses. As shown in (4-78), the flow error calculated in this work is in percentage of the line rating. For this off-the-$\alpha$-line scenario, the HE reduction performance is compared to the extended-Ward method, which gave the best performance of the conventional reduction methods.

The voltage-magnitude-error and branch-flow-error results for the reduced-order model created from the IEEE 118-bus system are shown in Fig. 4-6 and Fig. 4-7, respectively, using the two equivalent $\alpha$ values calculate by (4-77) and (4-78). Equivalent results for the ERCOT system tests are shown in Fig. 4-8 and Fig. 4-9, respectively.
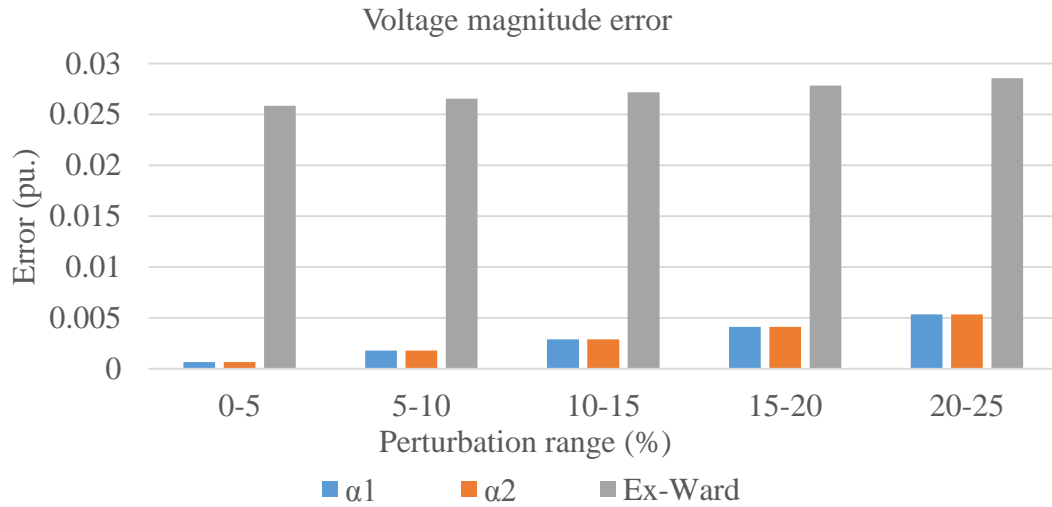
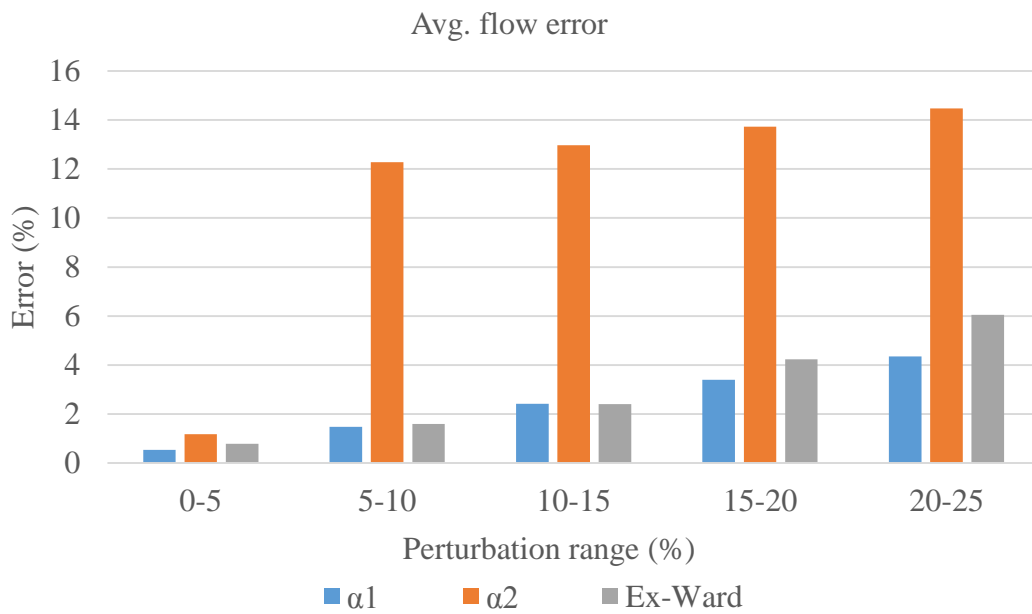Fig. 4-6 Maximum voltage-magnitude error for IEEE 118-bus reduction



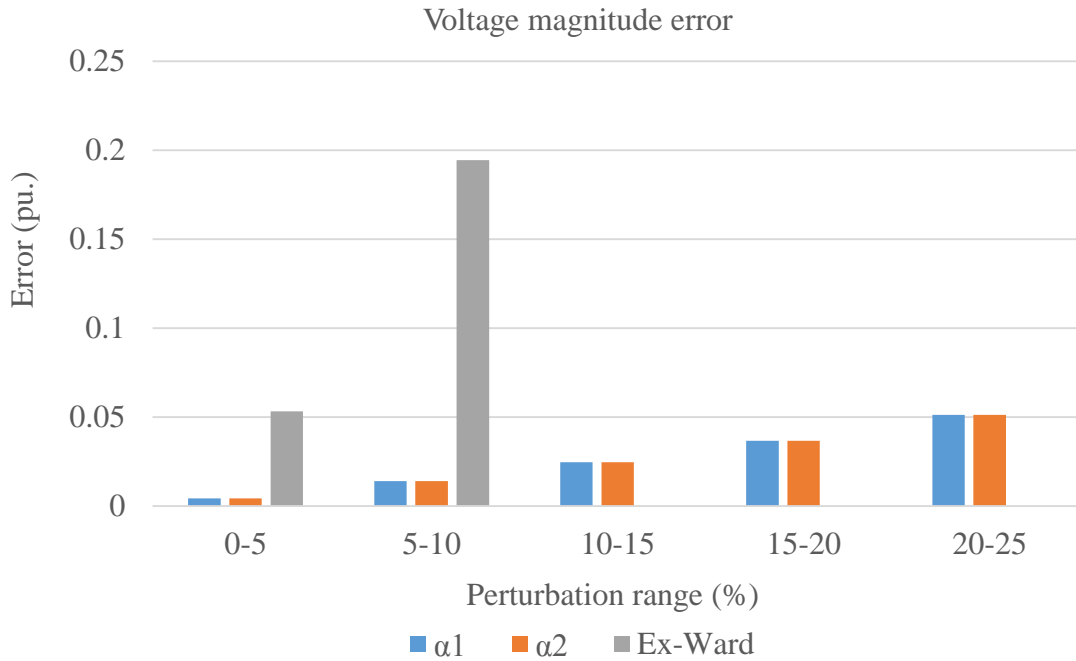Fig. 4-7 Average branch-flow error IEEE 118-bus reduction

Fig. 4-8 Maximum voltage-magnitude error for 3721 bus reduction of ERCOT 6057
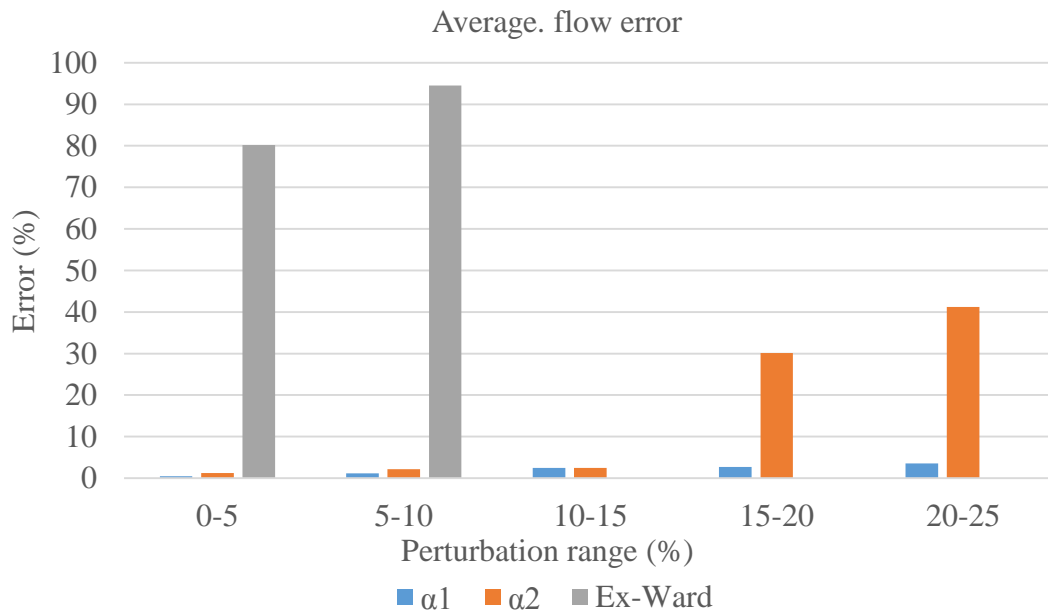
bus system



Fig. 4-9 Average branch-flow error for 3721 bus reduction of ERCOT 6057 bus system

The HE reduced-order model is clearly superior to the extended-Ward approach as the voltage-magnitude and branch flow errors are consistently smaller when using type-one $\alpha$ equivalent, $\alpha_1$. Further, convergence at higher load values is not a problem for the HE approach, while it is problematic for NR applied to the conventional reductions. Note that the voltage magnitude error is less sensitive to selection of equivalent $\alpha$ than branch-flow error. The type-one equivalent, $\alpha_1$, was more accurate than the type-two equivalent, $\alpha_2$, and both were more accurate than the extended-Ward method in the ERCOT test. In the IEEE 118-bus test, the type-two equivalent is less accurate than the extended-Ward in terms of the branch flow. The HE reduction performed better than the extended-Ward method because the external injections at the boundary buses were approximated more accurately. It is believed that $\alpha_1$ is more accurate than the $\alpha_2$ (at least in terms of the branch flow error) because $\alpha_2$ allows reactive power cancellation to occur in estimating the overall system flow levels, while $\alpha_1$ does not. Since one of the advantages of the HE reductions is retention of the nonlinear characteristics of the load and the appropriate calculation of system flow losses, it would not be surprising that allowing reactive power flow cancellation to occur might underestimate losses.

4.12.4  Imposing VAr limits

In this scenario, the loads are scaled uniformly and the VAr limits are imposed on all generators. The conventional methods like the Ward-type methods and the REI methods cannot easily impose VAr limits on the external generators, because the reactive generation of every generator under different loading levels is unknown. With HE reduction, the VAr

107

limits can be imposed on the external generators following the method introduced in section 4.11.3.

The maximum voltage-magnitude and maximum angle errors of the tests conducted on the IEEE 118-bus system are shown in Fig. 4-10 and Fig. 4-11, respectively. Equivalent results for the ERCOT system are shown in Fig. 4-12 and Fig. 4-13 respectively. In the figure legend "HE Lim" and "HE" denote the HE reduction with and without imposing VAr limits, respectively.
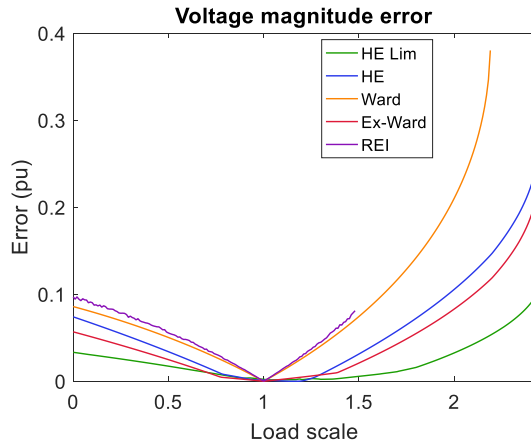


Fig. 4-10 Maximum voltage-magnitude error comparison (on the $\alpha$ line, with VAr limits) in IEEE 118-bus reduction
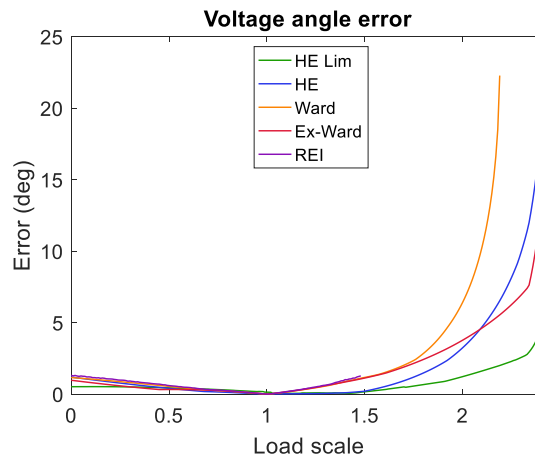


Fig. 4-11 Maximum voltage-angle error comparison (on the $\alpha$ line, with VAr limits) in IEEE 118-bus reduction
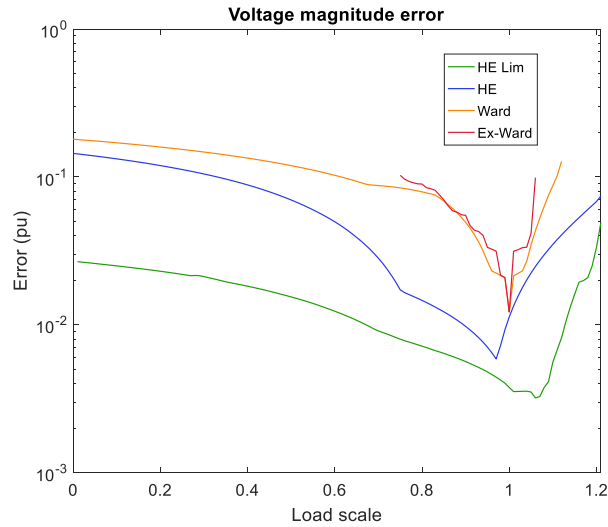
Fig. 4-12 Voltage-magnitude error comparison (on the $\alpha$ line, with VAr limits) in ERCOT system test
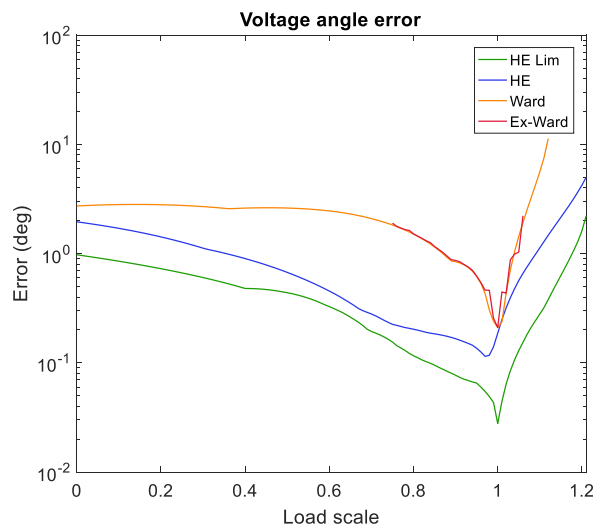


Fig. 4-13 Voltage-angle error comparison (on the $\alpha$ line, with VAr limits) in ERCOT system reduction

The errors shown in Fig. 4-10-Fig. 4-13 indicate that the HE reductions are more accurate over nearly all of the operating points tested and have acceptable accuracy over a broader load range than the conventional reduction methods because of the ability to accurately model nonlinear load/generation injections and to more accurately model VAr limits of external generators in the reduced model.

109

4.12.5  Conclusions

The conventional reduction methods generate reduced-order models by using linearization about the base case somewhere in the process. Therefore, power-flow solutions of these reduced-order models only match the full-model solutions at the base case and the errors grow rapidly as one moves away from the base case. The HE reduction method is a nonlinear-structure-preserving reduction approach that matches the full-model solution numerically exactly when the operating condition changes along the so-called $\alpha$ line. (Exact matching is expected theoretically and supported by numerical results when the limitations of roundoff error, processor precision and number of terms included in the voltage series are accounted for.) Moreover, when one moves off the $\alpha$ line an equivalent $\alpha$ value can be easily calculated that allows the model to retain surprising accuracy. Whether on or off the α line, the solution for the reduced-model bus voltages is obtained by evaluating existing Padé approximants if the VAr limits are not imposed, which is numerically much less complex than re-solving the reduced-model power flow, as required when using conventional reductions. The HE reduction has additional capabilities that conventional methods do not: it allows the enforcement of VAr limits on the external generators in an approximate way that turns out to be quite accurate outright and much more accurate the any of the conventional methods. Also, the method has the potential to be embedded into the more complicated problem of reactive-power planning (RPP) which is of high computational complexity when applied to a large system.

# 5 APPLYING BIVARIATE HOLOMORPHIC EMBEDDING POWER FLOW WITH CHISHOLM APPROXIMANTS

The HEM method introduced in Chapter 4 is univariate. The user is limited to using only one variable to scale the power injections across the entire system. In practice, the power injections of different buses are independent from each other, thus it is desirable to improve the flexibility of the HEM so that the method can yield accurate results when multiple independent scaling parameters are used. In this chapter, the bivariate HEM which involves two scaling parameters is formulated and tested. The bivariate HEM applies a bivariate Padé approximant, known as a Chisholm approximant, to achieve analytic continuation. The assessment of the bivariate HEM gives an estimate of the effectiveness and efficiency of the multi-variate HEM.

## 5.1    Formulation

As the name suggests, the bivariate HEM includes two variables which separately scale different system parameters. A three-bus example is taken here to show the formulation which uses two variables to scale the loads of the two load buses respectively. Note that for a system including more than three buses, one can divide the systems into two zones and use two variables to scale the loads in the two zones.

The diagram of the three-bus system is shown as Fig. 5-1. Bus 1 is the slack bus. Bus 2 and bus 3 are the PQ buses.
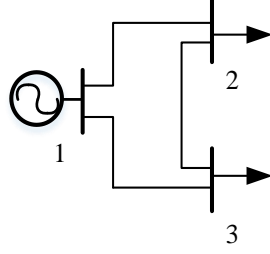
Fig. 5-1 Diagram of the three-bus system

In this three-bus system example, two scaling parameters, $\alpha$ and $\beta$, are embedded as scaling factors of the bus 2 and bus 3 loads, respectively.

The slack-bus voltage is assumed to be independent of the loading level of the system. Therefore, the equation defining the slack bus remains the same as in (5-1). The PBE's of bus 2 and bus 3 are separately formulated as (5-2) and (5-3).

$$V_0(\alpha, \beta) = V_{slack} \tag{5-1}$$

$$\sum_{k \in K} Y_{ik} V_k(\alpha, \beta) = \frac{\alpha S_2^*}{V_2^*(\alpha^*, \beta^*)} \tag{5-2}$$

$$\sum_{k \in K} Y_{ik} V_k(\alpha, \beta) = \frac{\beta S_3^*}{V_3^*(\alpha^*, \beta^*)} \tag{5-3}$$

where the voltage power series $V(\alpha, \beta)$ has the form shown as (5-4),

$$
\begin{aligned}
V(\alpha, \beta) &= V[0,0] + V[1,0]\alpha + V[1,1]\alpha\beta + V[0,1]\beta + \cdots \\
&\quad + \sum_{t=0}^{n-1} V[t,n]\alpha^t \beta^n + \sum_{t=0}^{n-1} V[n,t]\alpha^n \beta^t + V[n,n]\alpha^n \beta^n
\end{aligned}
\tag{5-4}
$$

and where $V[m,n]$ is the coefficient of the term $\alpha^m \beta^n$.

For the bivariate power series, define $D_z$ as the set of the coefficients of the terms whose combined degrees of $\alpha$ and $\beta$ is $z$ ($m+n=z$).

## 5.2    Solve the Bivariate HEM Power Flow

The three-bus system power flow problem is formulated explicitly by (5-1)-(5-3). As with solving the univariate HEM, we assume $W(\alpha,\beta)$ is the reciprocal of $V(\alpha,\beta)$, which must satisfy the relationship (5-5).

$$V(\alpha, \beta)W(\alpha, \beta)=1 \tag{5-5}$$

The coefficients of all bivariate power series are calculated term-by-term based on the following equations,

$$V_0[m,n]= \delta_{00}V_{slack} \tag{5-6}$$

$$\sum_{k \in K}Y_{2k}V_k[m,n]= S_2^*W_2^*[m-1,n] \tag{5-7}$$

$$\sum_{k \in K}Y_{3k}V_k[m,n]= S_3^*W_3^*[m,n-1] \tag{5-8}$$

$$V[0,0]W[m,n]+V[m,n]W[0,0] = -\sum_{k=1}^{n-1}\sum_{t=1}^{m-1}V[t,k]W[m-t,n-k] \tag{5-9}$$

where

$$\delta_{00} = \begin{cases} 1, & m=0,n=0 \\ 0, & o.w. \end{cases} \tag{5-10}$$

As for the univariate HEM, the germ solution for all bus voltages is 1.0 if there are no shunts in the system. If shunts exist in the system, the germ solution is obtained by solving (5-11).

$$\sum_{k \in K}Y_{ik}V_k[0]=0, \ i \in K \tag{5-11}$$

## 5.3    Chisholm Approximants

### 5.3.1    Definition

Given a bivariate voltage power series, $V(\alpha,\beta)$, written as (5-12), its corresponding $[L/L]$ Chisholm approximant is defined by (5-13) which must therefore satisfy (5-14) through substitution,

$$V(\alpha,\beta) = \sum_{m=0}^{\infty}\sum_{n=0}^{\infty} c[m,n]\alpha^m \beta^n \tag{5-12}$$

$$V(\alpha,\beta)_{[L/L]Chisholm} = \frac{\displaystyle\sum_{m=0}^{L}\sum_{n=0}^{L} a[m,n]\alpha^m \beta^n}{\displaystyle\sum_{m=0}^{L}\sum_{n=0}^{L} b[m,n]\alpha^m \beta^n} \tag{5-13}$$

$$\sum_{m=0}^{L}\sum_{n=0}^{L} b[m,n]\alpha^m \beta^n \cdot \sum_{m=0}^{\infty}\sum_{n=0}^{\infty} c[m,n]\alpha^m \beta^n = \sum_{m=0}^{L}\sum_{n=0}^{L} a[m,n]\alpha^m \beta^n + o\left(\sum_{m,n,m+n>2L}\alpha^m \beta^n\right) \tag{5-14}$$

where, $a[m,n]$ and $b[m,n]$ are the coefficients of the $(m,n)$ terms in the numerator and the denominator. The second component on the right-hand-side (RHS) of (5-14) is the error from the truncation of the terms in the sets $\{D_z, z>2L\}$.

### 5.3.2    Calculate the Chisholm approximant

Because the degree of $\alpha$ and $\beta$ vary between zero and $L$, the numerator and denominator power series includes in total $2(L+1)^2$ coefficients. The $[0, 0]$ term satisfies (5-15), which indicates $b[0,0]$ is arbitrary. In this work, $b[0,0]$ is set to 1.0 and $a[0,0]$ is equal to $c[0,0]$. Given $a[0,0]$ and $b[0,0]$ as known coefficients, there are in total $2(L+1)^2-2=2L^2+4L$ coefficients yet to be determined.

$$c[0,0] \cdot b[0,0] = a[0,0] \tag{5-15}$$

Based on the assumptions about the values of the $a[m,n]$ and $b[m,n]$ power series coefficients given in (5-16), we write equations in the form of (5-17) and (5-18) to calculate these coefficients.

$$a[m,n] = b[m,n] = 0, \left(m > L \operatorname{or} n > L\right) \tag{5-16}$$

$$\sum_{m=0}^{t}\sum_{n=0}^{k} b[m,n]c[t-m,k-n] = a[t,k], \ t \leq L, k \leq L \tag{5-17}$$

$$\sum_{m=0}^{t}\sum_{n=0}^{k} b[m,n]c[t-m,k-n] = 0, \ t \geq L+1 \operatorname{or} k \geq L+1, t+k \leq 2L \tag{5-18}$$

Equation (5-17) and (5-18) equate the coefficients of the terms in the set $\{D_z, 1 \leq z \leq 2L\}$ on both sides. Given a specific $z$, based on the combinatorial analysis, the number of elements in a set $D_z$ is $z+1$. The number of the elements in $\{D_z, 1 \leq z \leq 2L\}$ is $2L^2+3L$. Compared to the number of unknown coefficients, $2L^2+4L$, $L$ additional equations are needed to obtain a unique solution. These additional equations are formulated by equating the coefficients of terms whose power order is $2L+1$ derived from (5-14). The additional $L$ equations are written as (5-19).

$$\sum_{m=0}^{t}\sum_{n=0}^{k} \left(b[m,n]c[t-m,k-n] + b[n,m]c[k-n,t-m]\right) = 0, \ t+k = 2L+1, \ 1 \leq t,k \leq L \tag{5-19}$$

Using (5-18) and (5-19), we can calculate the denominator coefficients. Given the denominator coefficients the numerator coefficients are calculated based on (5-17).

## 5.4 Simulation Results

In this work, the focus is on demonstrating the flexibility and accuracy of the bivariate HEM and the accuracy of Chisholm approximants.

### 5.4.1 Tests on three-bus system

#### *5.4.1.1 System parameters*

The system diagram is shown as Fig. 5-1. The loads on bus 2 and 3 are (0.5+j0.2) MVA

and (1.0+j0.4) MVA respectively and the impedance of branches (1, 2), (1, 3) and (2, 3)

are (0.8+j2.0) pu, (0.4+j1.0) pu and (0.2+j1.6) pu, respectively.

#### *5.4.1.2 Test metrics*

Three different metrics were used to assess accuracy in the simulations: bus voltage

magnitude, bus voltage angle and system SNBP.

To compare the voltage magnitudes and angles, the loads of the two buses were scaled

by different combinations of $\alpha$ and $\beta$ which is equivalent to different loading levels of the

system. The benchmark used in comparing voltage calculations was the results obtained

with the NR algorithm whose convergence tolerance was set to 1E-8. In some operating

conditions, the NR algorithm failed to converge. Such operating conditions are labeled as

the non-convergent point (NCP) in this work.

The SNBP for different $\alpha$ to $\beta$ ratios was also used as a metric. These simulation

scenarios are succinctly characterized by the angle $\theta$ in (5-20).

$$\theta = \arctan\left(\frac{\alpha}{\beta}\right) \tag{5-20}$$

With the univariate HEM, the power flow problem needs to be resolved as $\theta$ changes.

The original loads in zone 1 and zone 2 are multiplied by $\sin\theta$ and $\cos\theta$ respectively as the

input to the HEM. As one can see, the solution of the univariate HEM with different $\theta$

values are the solutions of different load profiles.

With the base-case bivariate HEM solution (Chisholm approximants of all bus voltages), the SNBP$_{Chisholm}$ of the system was calculated using the following iterative procedure:

1. Obtain the bus voltages by evaluating the Chisholm approximant with the scaling of ($\alpha$, $\beta$) given for a specific $\theta$ starting from (0, 0).

2. Calculate the PBE mismatch based on the voltages calculated in step 1 under the corresponding load scaling. If the mismatch is less than 0.1 MVA, then increment the scaling factor by 0.01 and repeat step 1. If the mismatch is greater than or equal to 0.1 MVA, the SNBP$_{Chisholm}$ (in terms of ($\alpha$, $\beta$) scaling) is the current scaling level minus 0.01.

The benchmark that the SNBP$_{Chisholm}$ was compared to is the SNBP$_{Padé}$ [49] with the base case loading level ratio set according to the specified $\theta$.

*1) Test results*

The SNBP comparison between SNBP$_{Padé}$ and SNBP$_{Chisholm}$ is shown in Fig. 5-2. The markers in Fig. 5-2 show the SNBP calculated by the Padé and the Chisholm approximants. Since the two different markers almost exactly overlap each other, the SNBP calculated by different methods are almost identical. Fig. 5-2 also indicates that bus 2 is weaker than bus 3 because the SNBP in the cases of $\theta > 45°$ is smaller than the SNBP in the cases of $\theta \leq 45°$. The reason is that the impedances of branch (1, 2) is greater than branch (1, 3).

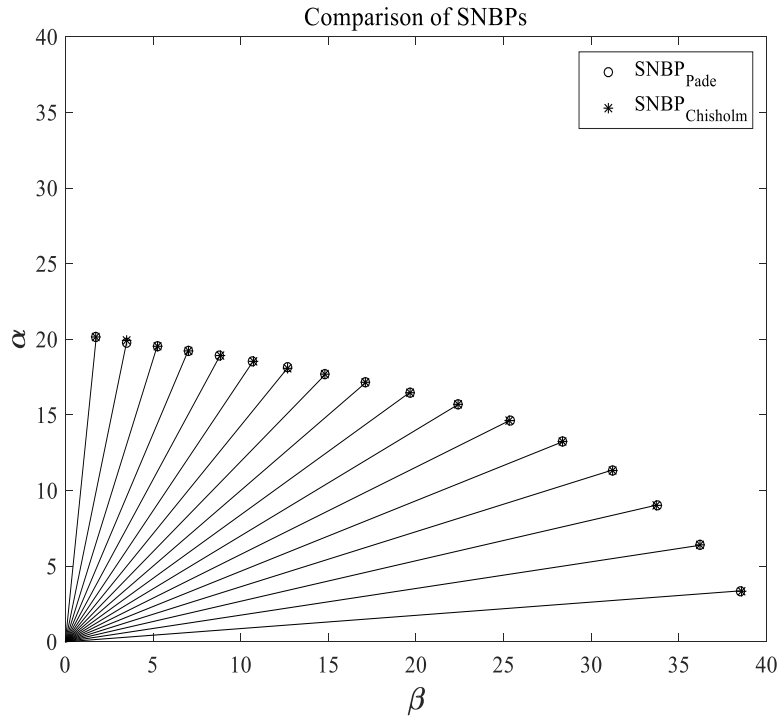Comparison of SNBPs



Fig. 5-2 Comparison of SNBP
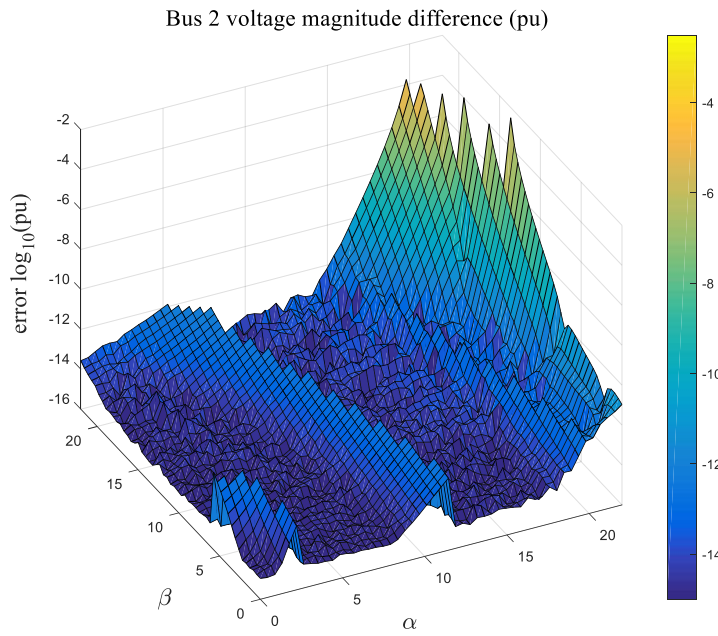
Bus 2 voltage magnitude difference (pu)



Fig. 5-3 Bus 2 voltage-magnitude error

118
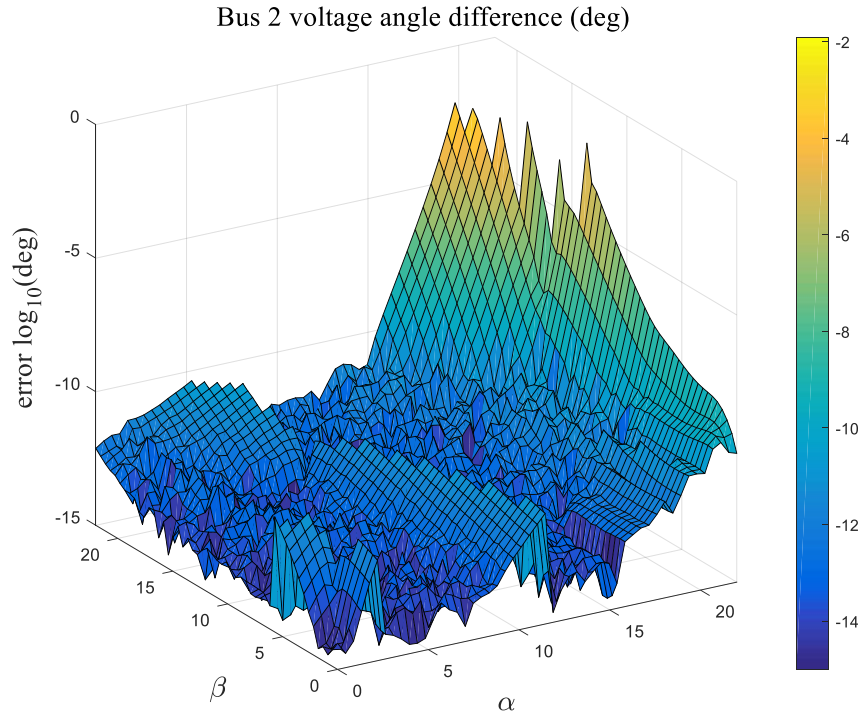
Fig. 5-4 Bus 2 voltage-angle error

The surface plots of the bus 2 voltage-magnitude error and voltage-angle error are shown, respectively, in Fig. 5-3 and Fig. 5-4. In general, the voltage-magnitude error is less than 1E-3 pu and the voltage angle error is less than 1E-2 deg. when the load/generation profile scaling is less than 95% of the SNBP. Increasing the number of terms in the Chisholm approximant will allow it to accurately predict voltages arbitrarily close to the SNBP, numerical precision issues notwithstanding. As mentioned earlier, the univariate HEM requires a constant $\theta$ value equal to that of the base case as we scale the load/generation profile, and with this constant $\theta$ the errors of the univariate HEM are very similar to the bivariate formulation.

5.4.2   Tests on the 14-bus system

The bivariate HEM was also tested on a modified IEEE 14-bus system. In this 14-bus

system, all buses are modified to become PQ buses except bus 1, which is the slack bus.

Compared to the un-modified IEEE 14-bus system, the topology is not changed. The base-

case real and reactive power generation in the original IEEE 14-bus system were treated as

negative constant P/constant Q loads.

In the three-bus system tests, $\alpha$ and $\beta$ scale the loads on the two load buses respectively.

In the 14-bus system test, $\alpha$ and $\beta$ were used to scale all the loads in zone 1 and zone 2

respectively. Zone 1 includes buses 1 to 5 and zone 2 includes the rest. The loading

statistics of the two zones are shown in Table 5-1. The real load in zone 1 is negative. This

is because in the original IEEE 14-bus systems, zone 1 includes more generation than load.

Table 5-1 Statistics of Zones in the 14-Bus System

|                     | Zone 1 | Zone 2 |
|---------------------|--------|--------|
| Real load (MW)      | -112   | 393.9  |
| Reactive load (MVar)| 24.2   | 229.5  |

The SNBP comparison is shown in Fig. 5-5. As can be seen in Fig. 5-5 the SNBP

calculated by the Chisholm approximant is very close to the value calculated with the Padé

approximant.
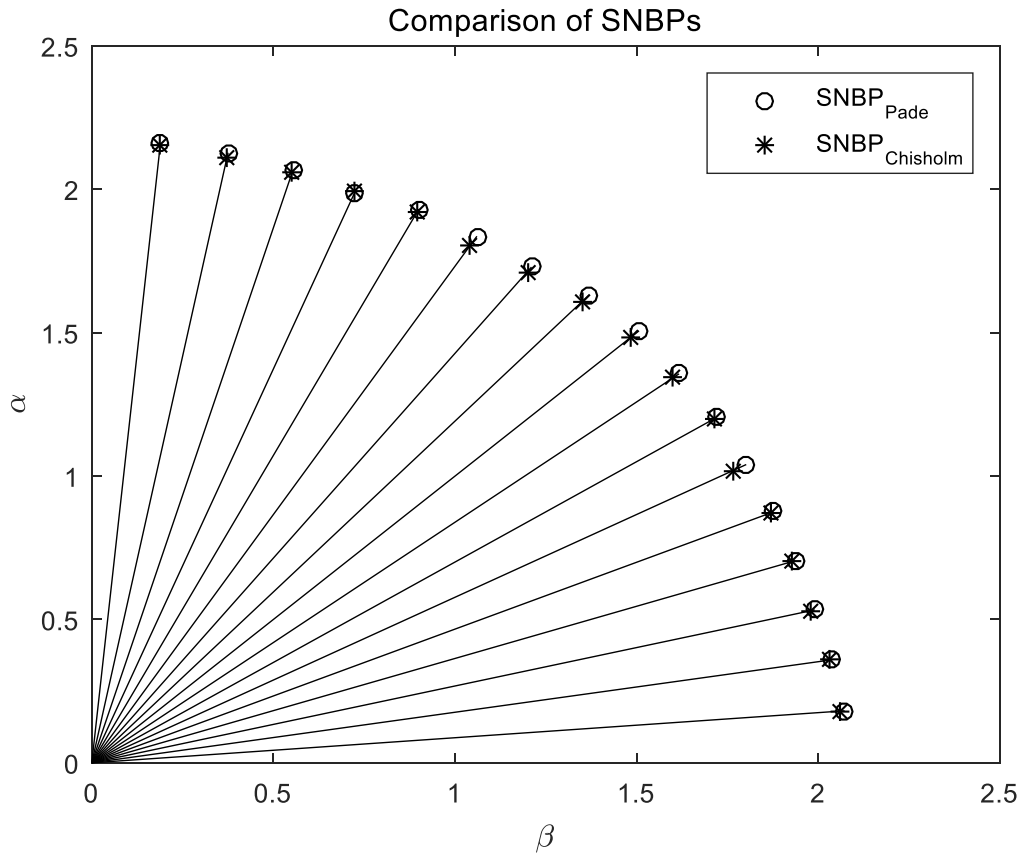
Fig. 5-5 SNBP comparison of the 14-bus system

The surface plots of bus 14 voltage-magnitude and voltage-angle error are shown in Fig. 5-6 and Fig. 5-7, respectively. As shown in these figures, the voltage-magnitude error is less than 1E-3 and voltage angle error is less than 1E-2 when the load scaling is less than 99% of the SNBP. Arbitrary accuracy may be obtained by increasing the number of terms used in the power series, precision issues notwithstanding.

Bus 14 voltage magnitude difference (pu)



Fig. 5-6 Bus 14 voltage-magnitude error

Bus 14 voltage angle difference (deg)



Fig. 5-7 Bus 14 Voltage-angle error

## 5.5    Discussion and Conclusion

### 5.5.1    Discussion on complexity of bivariate HEM
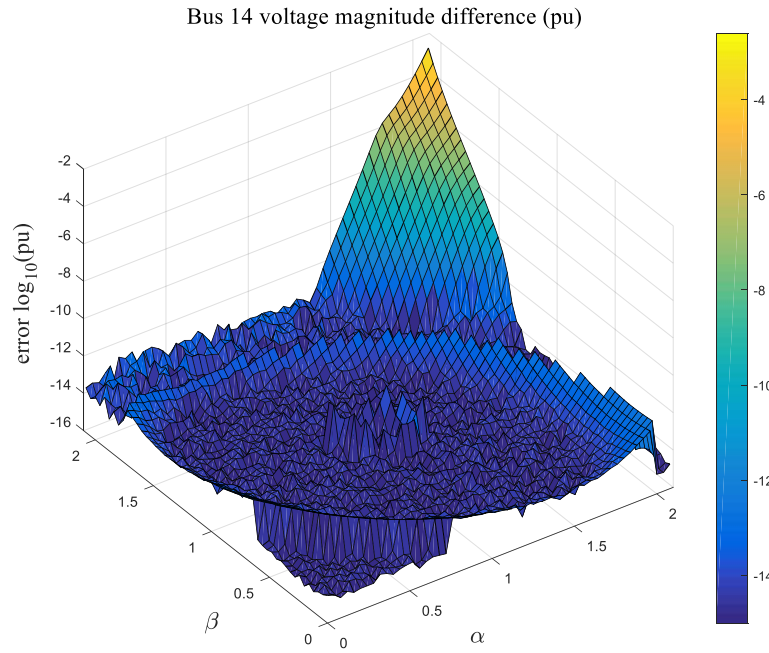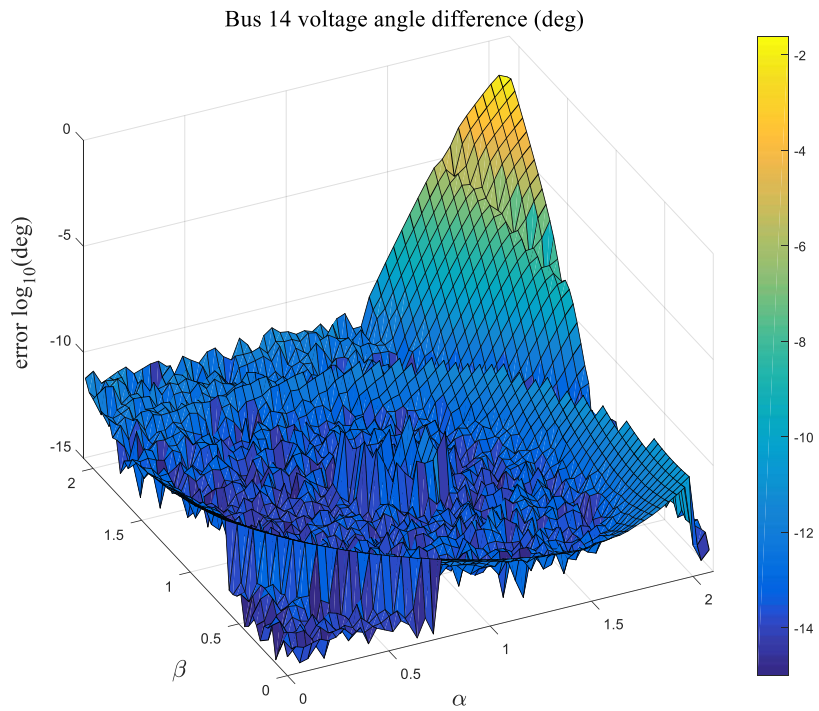
The Chisholm approximant improves the flexibility of the HEM as compared to the univariate HEM power flow. The voltage comparison (Fig. 5-3-Fig. 5-4, Fig. 5-6-Fig. 5-7) indicates that the bivariate HEM can yield accurate results with $\alpha$ and $\beta$ set to any value within the range between 0 and the SNBP if sufficient terms are used in the Chisholm approximant; however, a limitation of the bivariate HEM is that the number of variables and equations becomes large. An [$L/L$] Chisholm approximant includes $2L^2+4L$ unknown coefficients, which requires solving this same number of equations. For the same order Padé approximant, only $2L$ coefficients need to be calculated. For the three-bus- and 14-bus-system tests, at high-loading levels (80% of the SNBP), the Chisholm approximant needed to be at least of the same degree (the greatest degree of $\alpha$ or $\beta$ in the approximant) as the Padé approximant which leads to $2L^2+2L$ more coefficients. For an [$L/L$] $n$-variate Padé approximant the order of complexity of the rational function calculation is $O(L^n)$, which indicates that the number of coefficients grows exponentially with the number of embedded variables.

### 5.5.2    Conclusions

This chapter presents the study of the bivariate HEM applied to the power flow problem and the implementation of Chisholm approximants. The accuracy and the flexibility of the method is demonstrated by simulations on a three-bus and a 14-bus system. On the three-bus system, the two scaling factors allow the user to scale the loads on the two PQ buses independently. On the 14-bus system, the two parameters are used to scale the two zones

of the system. Both simulations showed that arbitrary accuracy can be obtained by allowing the number of terms in the Maclaurin-series expansion to grow. In general, the bivariate HEM allows users to change the system operating condition with two variables. This approach might be used, for example, when one wants to use one approximant while scaling residential and industrial loads independently or scaling the P and Q loads separately.

# 6 CONCLUSIONS

In this dissertation, the mathematical underpinnings of three major network-reduction techniques were developed and numerically tested: generator placement methods in dc network reduction; the OP-Ward method and the unified framework for dc network reduction; the holomorphic embedding method applied to ac network reduction.

The first problem tackled was that of generator placement methods in dc network reductions. Two new generator placement methods were proposed: the OGP method and the Min-SF method. The two new methods were tested and compared to the SED method. Results showed that the Min-SF method was the most accurate and robust.

The second problem tackled was the development of a unified framework for dc network reduction, which was validated by applying it to the large-impedance fictitious-branch elimination problem. The so-named OP-Ward reduction method replicates the conventional Ward reduction under dc assumptions using an optimization formulation which allows it to be more flexible. When applied to the large-impedance fictitious-branch elimination problem it was found to be more accurate than the threshold approach used with conventional Ward reduction. The OP-Ward formulation developed here can be regarded as a unified framework for dc network reduction.

The third major focus dealt with improving the accuracy of ac network reductions by using HE techniques. The theory behind HE reductions was developed and numerical validation of the theory presented. The simulation results showed that the HE-reduced model can match the original full-model power-flow solution very accurately if the power injection is scaled uniformly. In theory the agreement is exact. And while precision limitations and computation-time considerations limit the accuracy of the approach, the

numerical accuracy is still well beyond anything required for engineering analysis and design. If the power injections are scaled non-uniformly, the theory indicates that the reduced model is no longer theoretically exact, but an equivalent scaling parameter can be calculated that allows the HE reductions to yield more accurate results than the Ward-type and the REI methods. Finally, the conventional reduction methods ignore the external generator VAr limits which can lead to large errors in reduced-network models. The HE reduction can account for the external generator VAr limits in an approximate way leading to more accurate results than the conventional methods.

Finally, a multivariate HE method was investigated and shown to rival the univariate HE method in terms of accuracy while providing more flexibility, but the cost for this flexibility is increased computational complexity which limits it applicability.

# REFERENCES

[1]  J. B. Ward, "Equivalent Circuits for Power-Flow", *IEE Transactions,* vol.68, pp 373-pp.382, 1949

[2]  W. F. Tinney, J. M. Bright, "Adaptive Reductions for Power Flow Equivalents", *IEEE Transactions on Power Systems*, vol. WRS-2, No.2, pp. 351-360, May 1987.

[3]  F. F. Wu, A. Monticelli, "Critical review of external network modelling for online security analysis", *International Journal of Electrical Power and Energy Systems,* vol. 5, pp. 222-235, 1983

[4]  E. C. Housos,  G. Irisarri, R.M. Porter, A. M. Sasson, "Steady State Network Equivalents for Power System Planning Applications" in *IEEE Transactions on Power Apparatus and Systems*, vol. PAS-99, no. 6, pp. 2113-2120, Nov. 1980.

[5]  Monticelli, A.; Deckmann, S.; Garcia, A.; Stott, B., "Real-Time External Equivalents for Static Security Analysis," in  *IEEE Transactions on Power Apparatus and Systems*, vol.PAS-98, no.2, pp.498-508, March 1979

[6]  S. Deckmann, A. Pizzolante, A. Monticelli, B. Stott, O. Alsac, "Numerical Testing of Power System Load Flow Equivalents", *IEEE Transactions on Power Apparatus and Systems,* Vol. PAS-99, No.6, Nov/Dec 1980

[7]  Deckmann, S.; Pizzolante, A.; Monticelli, A.; Stott, B.; Alsac, O., "Studies on Power System Load Flow Equivalencing," in *IEEE Transactions on Power Apparatus and Systems,* vol.PAS-99, no.6, pp.2301-2310, Nov. 1980

[8]  P. Dimo, *Nodal analysis of power systems*, Abacus Press, UK (1975)

[9]  S.C. Savulescu, "Equivalents for Security Analysis of Power Systems", *IEEE Transactions on Power Apparatus and Systems¸*vol. PAS-100, No.5, May 1981

[10] E.C. Housos, G. Irisarri, R.M. Porter, A.M. Sasson, "Steady State Network Equivalents for Power System Planning Applications", *IEEE Transactions on Power Apparatus and Systems¸*vol. PAS-99, No.6, Nov/Dec 1980

[11] F. F. Wu, N. Narasimhamurthi "Necessary Conditions for REI Reduction to be Exact", *IEEE PES, Winter Meeting 1979*, Paper A 79065-4

[12] Oatts, M.L.; Erwin, S.R.; Hart, J.L., "Application of the REI equivalent for operations planning analysis of interchange schedules," *IEEE Transactions on in Power Systems,* vol.5, no.2, pp.547-555, May 1990

[13] S. Deckmann, A. Pizzolante, A. Monticelli, B. Stott, O. Alsac, "Numerical Testing of Power System Load Flow Equivalents", IEEE Transactions on Power Apparatus and Systems¸vol. PAS-99, No.6, Nov/Dec 1980

[14] X. Cheng, T. J. Overbye, "PTDF-Based Power System Equivalents", *IEEE Transactions on Power Systems*, vol. 20, no.4, Nov 2005

[15] H. Oh, "A New Network Reduction Methodology for Power System Planning Studies", *IEEE Transactions on Power Systems,* vol. 25, no. 2, May 2010

[16] D. Shi, D. J. Tylavsky, "An Improved Bus Aggregation Technique for Generating Network Equivalents", *2012 IEEE Power and Energy Society General Meeting*, San Diego, CA, 2012, pp. 1-8.

[17] J. Ho, B. Hobbs, P. Donohoo-Vallett, etc, (2016, Jan), *Planning Transmission for Uncertainty: Applications and Lessons for the Western Interconnection,* Available: https://www.wecc.biz/Reliability/Planning-for-Uncertainty-Final-Report.pdf

[18] B. Mao *et al.*, "The Engineering, Economic and Environmental Electricity Simulation Tool (E4ST): Description and an Illustration of Its Capability and Use as a Planning/Policy Analysis Tool," *2016 49th Hawaii International Conference on System Sciences (HICSS)*, Koloa, HI, 2016, pp. 2317-2325.

[19] M. J. Rider, A. V. Garcia and R. Romero, "Power system transmission network expansion planning using AC model," in *IET Generation, Transmission & Distribution*, vol. 1, no. 5, pp. 731-742, Sep. 2007.

[20] S. P. Torres and C. A. Castro, " Expansion planning for smart transmission grids using AC model and shunt compensation," in *IET Generation, Transmission & Distribution*, vol. 8, no. 5, pp. 966-975, May 2014

[21] D. Chattopadhyay, B.B. Chakrabarti, "Reactive power planning incorporating voltage stability", *International Journal of Electrical Power & Energy Systems*, vol. 24, issue 3, pp. 185-200, Mar. 2002

[22] B. B. Chakrabarti, D. Chattopadhyay and C. Krumble, "Voltage stability constrained VAr planning-a case study for New Zealand," *2001 Large Engineering Systems Conference on Power Engineering* , Halifax, NS, 2001, pp. 86-91.

[23] H. Liu, V. Krishnan, J. D. McCalley and A. Chowdhury, "Optimal planning of static and dynamic reactive power resources," in *IET Generation, Transmission & Distributio*n, vol. 8, no. 12, pp. 1916-1927, Dec. 2014.

[24] Xiaopeng Liu, J. Shen, A. Philip, E. Viray, Ming Jiang and D. Leon, "External WECC model reduction in on-line network applications for Alberta power grid," 2013 *IEEE Power & Energy Society General Meeting, Vancouver, BC*, 2013, pp. 1-5.

[25] H. K. Singh, S. C. Srivastava, "A Reduced Network Representation Suitable for Fast Nodal Price Calculations in Electricity Markets", *IEEE Power Engineering Society General Meeting, 2005*, 2005, pp. 2070-2077 Vol. 2.

[26] E. H. Allen, J. H. Lang, M. D. Ilic, "A Combined Equivalenced-Electric, Economic, and Market Representation of the Northeastern Power Coordinating Council U.S. Electric Power System", *IEEE Transactions on Power Systems,* vol. 23, No.3, Aug 2008

[27] Di Shi; Shawhan, D.L.; Nan Li; Tylavsky, D.J.; Taber, J.T.; Zimmerman, R.D.; Schulze, W.D., "Optimal generation investment planning: Pt. 1: network equivalents," in *North American Power Symposium (NAPS), 2012*, vol., no., pp.1-6, 9-11 Sept. 2012

[28] B. V. Cherkassky, A. V. Andrew and T. Radzik, "Shortest Paths Algorithms: Theory and Experimental Evaluation", Mathematical Programming, Ser. A 73(2), pp. 129-174, 1996

[29] Di Shi, "Power system network reduction for engineering and economic analysis", PhD Dissertation, 2012

[30] Y Zhu; D. Tylavsky, "An optimization based network reduction method with generator placement," in *North American Power Symposium (NAPS), 2015*, vol., no., pp.1-6, 4-6 Oct. 2015.

[31] H. Ma; S. M. Shahidehpour, "Unit commitment with transmission security and voltage constraints," *IEEE Transactions on Power Systems*, vol.14, no.2, pp.757,764, May 1999

[32] M. Shahidehopour; F. Yong, "Benders decomposition: applying Benders decomposition to power systems," *IEEE Power and Energy Magazine*, vol.3, no.2, pp.20,21, March-April 20

[33] Boutsidis C, Mahoney MW, Drineas P. An Improved Approximation Algorithm for the Column Subset Selection Problem. Philadelphia: *Society for Industrial and Applied Mathematics*; 2009.

[34] Golub GH, Van Loan CF. Matrix computations. 3rd ed. Baltimore: Johns Hopkins University Press; 1996.

[35] "IEEE 118-bus, 54-unit, 24-hour system" available at motor.ece.iit.edu/data/JEAS_IEEE118.doc

[36] W. F. Tinney and C. E. Hart, "Power Flow Solution by Newton's Method," in *IEEE Transactions on Power Apparatus and Systems*, vol. PAS-86, no. 11, pp. 1449-1460, Nov. 1967.

[37] B. Stott, "Decoupled Newton Load Flow," in *IEEE Transactions on Power Apparatus and Systems*, vol. PAS-91, no. 5, pp. 1955-1959, Sept. 1972.

[38] B. Stott and O. Alsac, "Fast Decoupled Load Flow," in *IEEE Transactions on Power Apparatus and Systems*, vol. PAS-93, no. 3, pp. 859-869, May 1974.

[39] B. Stott, "Review of load-flow calculation methods," in *Proceedings of the IEEE*, vol. 62, no. 7, pp. 916-929, July 1974.

[40] V. Ajjarapu and C. Christy, "The continuation power flow: a tool for steady state voltage stability analysis," in *IEEE Transactions on Power Systems*, vol. 7, no. 1, pp. 416-423, Feb 1992.

[41] C. A. Canizares and F. L. Alvarado, "Point of collapse and continuation methods for large AC/DC systems," in *IEEE Transactions on Power Systems,* vol. 8, no. 1, pp. 1-8, Feb 1993.

[42] P. Xu, X. Wang and V. Ajjarapu, "Continuation power flow with adaptive stepsize control via convergence monitor," *in IET Generation, Transmission & Distribution*, vol. 6, no. 7, pp. 673-679, July 2012.

[43] S. Rao; Y. Feng; D. J. Tylavsky; M. K. Subramanian, "The Holomorphic Embedding Method Applied to the Power-Flow Problem," *IEEE Transactions on Power Systems*, vol.PP, no.99, pp.1-13

[44] Trias, A., "The Holomorphic Embedding Load Flow method," in *Power and Energy Society General Meeting, 2012 IEEE*, vol., no., pp.1-8, 22-26 July 2012

[45] H. Stahl, "On the Convergence of Generalized Padé Approximants," *Constructive Approximation*, 1989, vol. 5, pp. 221–240.

[46] H. Stahl "The Convergence of Padé Approximants to Functions with Branch Points," *Journal of Approximation Theory*, 1997, vol. 91, no. 2, pp. 139–204.

[47] G. Baker and P. Graves-Morris, "Padé approximants," Series: Encyclopaedia of Mathematics and its applications, Cambridge University Press, New York, 1996.

[48] A. Cuyt, "Padé Approximants for Operators: Theory and Applications", Springer-Verlag, Berlin Heidelberg, New York, Tokyo, 1984

[49] Shruti D. Rao, Daniel J. Tylavsky, Yang Feng, "Estimating the saddle-node bifurcation point of static power systems using the holomorphic embedding method", *International Journal of Electrical Power & Energy Systems*, vol. 84, 2017, pp. 1-12

[50] S. Rao and D. Tylavsky, "Nonlinear network reduction for distribution networks using the holomorphic embedding method,"*2016 North American Power Symposium (NAPS)*, Denver, CO, USA, 2016, pp. 1-6.

[51] EVTA, "Transmission Atlas File ss11sum107152010," Tech. Rep., Energy Visuals, 2012 [Online]. Available: http://www.energyvisuals.com